MODELLING AND IDENTIFICATION OF PAPER MACHINE WET END CHEMISTRY

by

ROGER WILLIAM SHIRT

B.Sc.(Eng.), Queen's University, 1987
M.Sc.(Eng.), Queen's University, 1990

A THESIS SUBMITTED IN PARTIAL FULFILLMENT OF
THE REQUIREMENTS FOR THE DEGREE OF

DOCTOR OF PHILOSOPHY

in

THE FACULTY OF GRADUATE STUDIES

Department of Electrical and Computer Engineering

We accept this thesis as conforming
to the required standard

THE UNIVERSITY OF BRITISH COLUMBIA

December 1997

In presenting this thesis in partial fulfilment of the requirements for an advanced degree at the University of British Columbia, I agree that the Library shall make it freely available for reference and study. I further agree that permission for extensive copying of this thesis for scholarly purposes may be granted by the head of my department or by his or her representatives. It is understood that copying or publication of this thesis for financial gain shall not be allowed without my written permission.

Department of Electrical and Computer Engineering

The University of British Columbia
Vancouver, Canada

Date January 16, 1998

ABSTRACT

Chemicals are added in the wet end of a paper machine to control operability and/or quality measures such as retention, drainage, sheet strength, etc. Current understanding of the effects of such additives in a mill environment is generally restricted to either qualitative or empirical descriptions. This is primarily due to the large number of interacting factors present in the aqueous papermaking environment as well as variations in furnish properties. Furthermore, the existence of large time constants and recycle flows in the white water system leads to complex mixing dynamics. This inability to quantitatively predict process performance inhibits development of closed-loop control schemes.

This thesis is an attempt to bridge the gap between development of fundamental papermaking chemistry models in the laboratory and application of these models in a mill environment.. A dynamic simulation approach is used to model the interactions between chemical additives and furnish particles. Detailed descriptions of the polymer adsorption, flocculation and wire retention and drainage processes are developed. Consistencies of all furnish particles, in particular fines, are faithfully tracked throughout the wet end. The effects of operating variables such as polymer addition rates, furnish composition, degree of stock refining and applied vacuum can be directly assessed in a simulated operating environment. Results are compared against on-line data from a fine paper mill in Canada are shown to be accurate.

Identification tools are also developed as part of the overall goal of identifying a model suitable for controller design. A method is first proposed for specifying a confidence interval on the anticipated controller robustness at the identification stage. This is accomplished through optimization of a controller robustness measure with the constraint that the model parameters lie within a $(1-\alpha)\%$ confidence interval. Parametric nonlinearity is accounted for by this method

and the efficacy of the method is shown to be, in part, a function of the degree of this nonlinearity. Input test signals can be chosen which minimize this uncertainty and a method is developed for this purpose.

Identification techniques are applied to the High Molecular Weight Anionic Polymer Flowrate $\Leftrightarrow$ White Water Filler Consistency loop. Significant nonlinear behaviour is found to exist in the higher order dynamics of this pairing. While the control relevant identification techniques developed in this thesis are not effective due to the nonlinearities present the value of an accurate dynamic simulation is highlighted.

TABLE OF CONTENTS

LIST OF TABLES

LIST OF FIGURES

NOMENCLATURE

A	Area
$A(\bullet)$	Process transfer function denominator polynomial
AR	Parameter in first-order autoregressive sequence
a	Process transfer function denominator polynomial parameter
$a(\bullet)$	Unit variance white noise process
B	Basis Weight
$B(\bullet)$	Process transfer function numerator polynomial
b	Process transfer function numerator polynomial parameter
C	Consistency
C_m	Mat compaction
C_o	Concentration of polymer
$Cov(\bullet)$	Covariance function
CR	Confidence region
CSF	Canadian Standard Freeness
DF	Decay factor
d	Disturbance transfer function parameter
$d(\bullet)$	Value of distance norm
E, e	Residual error matrix, vector
F	Mass flowrate
$F_{\alpha;p,N-p}$	$(1-\alpha)$% value of F-distribution with p and N-p degrees of freedom
FPR^x	First-pass retention of component x
G	Hydrodynamic shear
G_c	Controller transfer function
G_p	Process transfer function
$\tilde{G}_p, G_\Delta$	Reduced order and unmodelled portions of process transfer function
g	Process gain
$g(\bullet)$	General nonlinear parametric function
H	Pressure head
$H(\bullet)$	Disturbance transfer function
H_m	Desired closed-loop response
i	Index
J	Jacobian matrix
J_{stab}, J_{perf}	Performance and stability controller robustness objective functions
$\tilde{J}_{Perf}$	Normalized performance controller robustness objective function
j	Index
K	Constant
k	Kozeny constant
k_{att}, k_{det}	Attachment and detachment rate constants
k_o	Smoluchowski rate constant
$l(\bullet)$	Likelihood function
M	Fisher's Information Matrix
N	Number of observations in a set of data
N_j	Number concentration of particle j

$n_o^{P/j}$	Dosage of polymer P relative to the amount required to completely cover particle j
P	Pressure
p	Number of parameters
Q	Volumetric flowrate
R	Specific filtration resistance
R(•)	Controller design polynomial
R_{xc}, R_{AC}	Cross-correlation and autocorrelation test statistics
r, r^*	Overall and one-pass refining ratios
r^i	Empirical rate constant for furnish component i
S(•)	Controller design polynomial
SS(•)	Sum of squares function
SRDP(•)	Signed root deviance profile function
T(•)	Controller design polynomial
u	Independent variable in dynamic process
Var(•)	Variance function
x	Independent variable in static processes
y	Process response variable
y_{sp}	Set-point signal
z^{-1}	Unit backward shift operator
Δ	Difference operator
Φ	Frequency spectrum
Γ^{Max}	The maximum amount of adsorbed polymer per unit surface area
α	Tail area probability level
α_{Fast}	Collision efficiency
α_v	Hydrodynamic specific volume
β	Variable parameter
β_e	Residual sequence upper bound
$\chi_{\alpha;\, p}$	(1-α)% probability level of chi-squared distribution with p degrees of freedom
ϕ	Angle
ϕ_j	Instantaneous retention of drainage element j
$\gamma^{P/j}$	Deposition efficiency of polymer P onto particle j
η	Liquid viscosity
θ	Fractional coverage on a particle surface Parameter vector
$\hat{\theta}$	Parameter vector estimated from input/output data
$\hat{\theta}_c$	Parameters yielding minimum sum of squares when constrained to lie along a particular contour, c, of a nonlinear function of the parameters
ρ	Density

ρ_u	Autocorrelation function of sequence u
σ	Specific surface area
$\tau^{P/j}$	Time constant for adsorption of polymer P onto particle j
ω	Frequency
ξ	White noise sequence
$\psi(\bullet)$	Overall less nominal controller performance residuals
∇	Gradient operator

ACKNOWLEDGMENTS

First I would like to thank my supervisors Dr. Guy Dumont and Dr. Michael Davies whose teaching I have and will follow. This thesis is a product of their encouragement and guidance. As well, my continued association with Dr. Thomas Harris, Dr. David Bacon and Shannon Quinn of Queen's University (Ontario) has, as always, been inspirational.

I am indebted to the technical expertise of Bruce Atkinson, Larry Erickson and David Barzyk of Weyerhaeuser from whom I have learned a great deal. This project would not have been possible without their time and interest.

I would like to make special mention of the generous financial support of Weyerhaeuser and Weyerhaeuser Canada. Industrial/academic cooperation such as I have enjoyed can only serve to further science and engineering. The financial support of PAPRICAN and the Natural Sciences and Engineering Research Council of Canada is also gratefully acknowledged. I would also like to thank my colleagues at Simons Technologies Inc. for technical and software support during this project.

I am very sorry to leave my friends at the Pulp and Paper Center. Deserving special mention are Jahan Ghofraniha and Tazim Rehmat who were always there with crucial technical or moral support when I needed it.

Finally, I wish to thank my family and friends who have endured my self indulgence in this undertaking over the past years. I hope to repay my debt to you in the future.

Dedication

This thesis is dedicated to the memory of my mother.

Chapter 1

Introduction

1.1 Motivation

Although the process of manufacturing paper is centuries old, experience and rules of thumb for successfully operating a papermaking process are often used rather than 'hard' rules derived from phenomenological models. This is a direct result of the number and complexity of interacting papermaking phenomena. An excellent introductory perspective of many important aspects of papermaking is given by Roberts (1996a).

This thesis concerns itself with the surface chemistry of papermaking. Chemistry phenomena are of fundamental importance to the papermaking process as they affect both final paper sheet properties and operability of the paper machine. Both the papermaking furnish, comprised of fibrous and mineral filler materials, and the surrounding aqueous medium affect this chemistry. Furthermore, chemicals are added to affect sheet properties and machine operability. Because the surface area to mass ratio of particles involved in papermaking is large, the study of chemical interactions in papermaking involves a branch of chemistry known as colloidal chemistry (Scott (1996)).

Modelling of chemical papermaking phenomena is complicated by variations in furnish properties and the surrounding aqueous environment which arise in the processing of a naturally derived raw material. As well, stringent paper machine performance requirements are placed on any model of the system as papermakers strive for higher quality products, more flexible processes and greater production rates. When coupled with the above

imprecise knowledge of many papermaking chemistry phenomena, the goal of developing models and control schemes for this system is very challenging indeed.

Kaunonen (1988) stated that there are two approaches to studying the wet end (stock preparation plus sheet forming sections) of a paper machine. The first is to conduct laboratory experiments under carefully controlled conditions and elucidate basic chemical mechanisms. The other is to measure the operating process on-line and build models and control schemes in an essentially empirical manner. Here, a possibly third distinct approach is followed. This is the application of fundamental papermaking chemistry models developed in the laboratory in a simulated operating environment. In this way the interactions between the basic chemical mechanisms and the hydrodynamics of the paper machine wet end can be explored. Hence, the present approach can be regarded as a bridge between those identified by Kaunonen. Indeed, this approach follows the suggestion of Ödberg et al. (1993) that "in mathematical dynamic simulation of paper machines, chemicals should also be included".

An additional incentive for approaching the problem in the above manner was due to the proliferation of literature describing reliable on-line measurement techniques for key wet end operating variables. These measurements provide a means for studying the dynamic behaviour of the wet end which is known to have a broad range of time constants. Furthermore, the various recycle streams present in the wet end can be easily handled in a simulation environment.

Identification of a model for prediction and eventual control of wet end chemistry phenomena must proceed in several steps. These steps reflect the state of a priori knowledge about the system and are shown in Figure 1.1. Initially, development of a first-principles simulation model is undertaken in order to be able to accurately predict

process phenomena. Both previous operating knowledge about the process and more general results reported in the literature are used in development of the simulation model. At the next stage on-line identification experiments can be performed using the knowledge gained from development of the simulation model. These experiments can be used to 'calibrate' the simulation model. Since the simulation model is not in a convenient form for design or implementation of an eventual control scheme simpler, often linear, models are identified from process input/output data generated on-line. Also at the identification step, techniques for the mathematical design of experiments can be employed to ensure that the resulting simplified model is optimal for the purposes of control. From these steps and with a suitable model, a control scheme can be design for the wet end chemistry process and implemented.

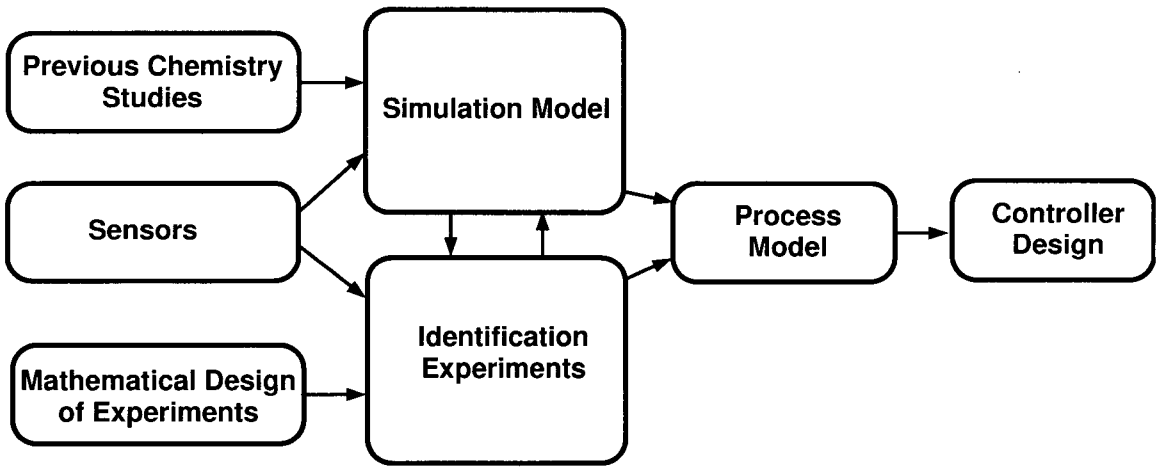

Figure 1.1: Thesis organization flow diagram

Clearly the above model building process involves a great many areas any of which could form a significant project. For this reason, and due to the fact that this approach has not been previously applied to a complete papermaking operation, emphasis has been placed on the development of a reliable simulation model. The other area of concentration is devilment of identification techniques which accurately describe and minimize the

uncertainty in models identified from noisy data. The emphasis here is on producing models which have desirable properties when they are to be used in a closed-loop control scheme.

1.2 Thesis Objectives and Approach

The main objective of this project is to produce a reliable model for prediction of first-pass retention and wire drainage effects on an operating paper machine. Furthermore, the model is required to be suitable for design of control schemes.

The layout of this thesis follows accordingly. Chapter 2 reviews some fundamental aspects of the physical and chemical interactions present in wet end chemistry. As well, the current state of on-line sensor measurement in the fine paper mill under study is discussed along with current wet end control practices. The main tool for identification of development of the wet end chemistry model in this thesis is dynamic process simulation. In Chapter 3 both the methodology of dynamic simulation in general and the specific implementation of wet end chemistry models is discussed. Details of the specific first-principles chemistry models are given here. The validity of this simulation model is demonstrated in Chapter 4 by comparison against on-line data. At this point it is assumed that the simulation model is directionally correct but may not necessarily be able to produce precise predictions of retention and drainage phenomena. Accordingly, tools are developed in Chapter 5 which characterize and minimize the uncertainty associated with conducting identification experiments using on-line data. Parameters in approximate linear (in the inputs) dynamic models derived from the first-principles simulation can be identified from such identification experiments with the resulting models used for controller design purposes. As well, by appropriate selection of applied input signals the experiments can yield models

which are most appropriate for eventual closed-loop implementation. These techniques are implemented in Chapter 6 using the verified simulation model as the 'true' process. The objectives here are two fold. First, the linear control relevant identification techniques are tested in a more challenging environment. Secondly, identification of the filler retention control loop dynamics can be carried out in a noise free environment.

1.3 Contributions of Thesis

To the knowledge of the author, this work develops the first large scale dynamic simulation of a paper machine wet end which incorporates chemical phenomena. Where possible, fundamental physical and chemical models have been employed. As part of the simulation, careful tracking of chemistries in white water recirculation loops was undertaken. It has been shown that the simulation model provides reliable predictions of retention and drainage phenomena when validated against on-line data. In addition, the fundamental nature of the simulation model allows further confirmation of these responses through observation of wet end mechanisms. Through the simulation model, quantitative rather than qualitative predictions of wet end responses can be made avoiding the limitations of empirical model building.

A technique for producing $(1-\alpha)\%$ confidence bounds on anticipated controller robustness at the identification stage is proposed. The constrained optimization solution represents application of a general technique introduced by Chen (1993). The same technique is also used to produce frequency domain bounds on the process uncertainty. A control relevant input signal design procedure is proposed which accounts for the fact that the identified model is to be used in a closed-loop control scheme. These techniques represent improvements over the existing ones for producing uncertainty bounds in that 1) they

account for parametric nonlinearity and 2) the confidence level can be explicitly specified. The above work on identification techniques for linear dynamic systems was carried out in collaboration with Dr. Tom Harris, Dr. David Bacon and Shannon Quinn of Queen's University (Ontario, Canada) whose contributions are acknowledged.

Finally, control relevant identification techniques are applied to the wet end chemistry system for the first time. While limitations of the input test signals procedure are exposed, the nonlinear behaviour of the wet end chemistry system is also elucidated.

Chapter 2

Review of Paper Machine Wet End Chemistry

This chapter provides a general overview of papermaking chemistry phenomena as well as their measurement and control. First, a description of the fine papermaking process used in this study is given. Chemical aspects of this process are then discussed with particular emphasis on retention of fine particles and drainage. The last ten years have seen the emergence of a number of sensors for on-line measurement of key wet end variables. Those that are pertinent to this project will be reviewed. Finally, the current practice of wet end chemistry control will be discussed along with the role of the present simulation model in furthering the stability of the wet end through control system improvement.

2.1 Process Description

The papermaking system is aqueous with between 0 and 12% by mass of wood fibres, which is referred to as the fibre furnish. Chemicals are normally added at a level of 0-5% by mass of the furnish while filler may comprise up to 20% by mass of the final paper sheet. The aim in the papermaking process is to transform the dilute furnish into a continuous paper web. The success of this process is dependent upon both (hydro)mechanical and chemical factors with interactions between the two. Mechanical factors such as process and equipment design will not be discussed in this thesis. In this section the physical layout of the papermaking wet end process will be discussed followed by a qualitative discussion of the effect of chemical additions.

2.1.1 Physical Process

Figure 2.1 shows a simplified flow diagram of the wet end of the fine papermaking mill at Prince Albert, Saskatchewan. This mill has been used to study and implement concepts developed in this thesis. Softwood, hardwood and machine broke at approximately 5.0% consistency (% wood fibre by mass) are combined at the mix tank. It is assumed throughout that softwood comes from never-dried slush pulp and that hardwood furnish has been repulped from bale form. In practice, the reverse could also be true. Machine broke is comprised of repulped fibres from paper machine sheet breaks and edge trimmings which, together with other internally reclaimed fibres, account for approximately 1/3 of the total incoming fibre. The ratio of hardwood to softwood is approximately 70:30 and each of these streams is individually refined. The combined stream is controlled to a consistency of approximately 4.0% and further refined in the "tickler" refiner. A tickler refiner is designed to fibrillate fibres rather than cut them.

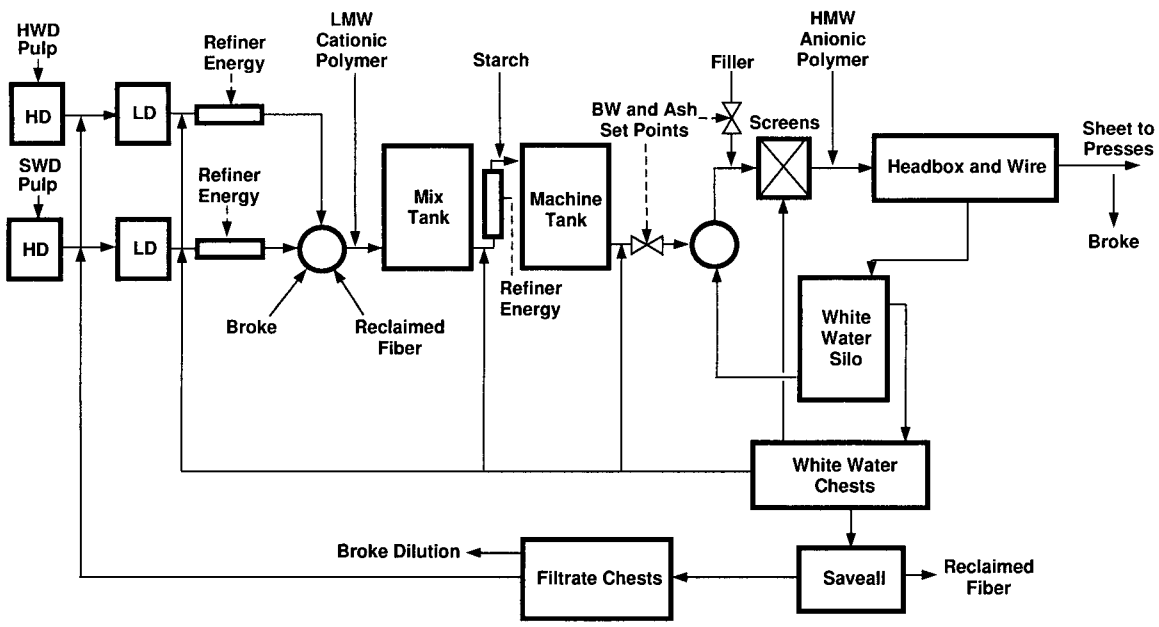

Figure 2.1: Simplified process flow diagram

This combined stream, or thick stock, is diluted to less than 1% consistency by recirculated water from the headbox. Mineral fillers, such as precipitated calcium carbonate (PCC) are added at this point. After cleaning, deaeration and screening, the thin stock is pumped at constant head to the headbox at approximately 0.65% consistency. The function of the headbox is to deliver a uniform amount of stock onto a moving mesh, called the wire, where paper fibres are retained and water is able to drain through. Most of this water is recirculated to the White Water Silo where it is used to dilute incoming stock. By the end of the wire a contiguous paper sheet has formed having approximately 20% consistency. This sheet passes through presses and steam dryers before being placed on reels for shipping or coating. The moisture content of the final sheet is approximately 5%. Primary products from the mill are copy and offset grade fine paper. There are approximately two grade changes per day.

Water which is not used for short circulation dilution of incoming stock is sent to dilution points further back in the process. This is termed long circulation and its various components are discussed by Ryti and Paulapuro (1991). It is used for consistency control at various points as well as rejects dilution water for the cleaners and screens. A saveall disk filter is installed between the white water and filtrate chests in order to capture fines particles and return them to the stock mixing area. Operation principles of saveall filters are reviewed by Doucette (1988). Cloudy filtrate from the saveall and broke thickening screens is used for dilution of stock while clean filtrate is used for machine showers.

The broke system collects discarded product and repulps furnish during a paper machine web break. The collected furnish must be diluted so that it can be pumped back to into the stock preparation area. Excess water is removed by passing the diluted broke over thickening screen with the filtrate going to the Cloudy Filtrate Tank. Since the occurrence

of breaks is discontinuous (approximately 1-2 breaks per day on the Prince Albert machine) large hold-up tanks are required, namely the Broke High and Low Density storage tanks. Broke is diluted to 4% consistency before being mixed with virgin and reclaimed fibre.

2.1.2 Chemical Processes

Chemicals are added to the papermaking furnish in order to accomplish a number of goals related to machine operability and sheet quality. Among these are:

- Better first-pass retention of fine particles in the sheet
- Faster drainage of water from the sheet
- Dry sheet strength
- Water penetration resistance (sizing)
- Biological activity control

This thesis is concerned with only the factors which affect the first two of these objectives, namely retention and drainage.

First-pass retention (FPR) is defined as,

$$FPR^x = 100\left(\frac{\text{Mass of 'x' retained in paper web}}{\text{Mass of 'x' delivered to wire}}\right) \tag{2.1}$$

Since it is easiest to measure the consistency, C, of components in the headbox stock and the white water, first-pass retention is most commonly defined as,

$$FPR^x = 100\left(1 - \frac{C^x_{WW}}{C^x_{HBX}}\right) \tag{2.2}$$

where it is assumed that the mass flowrate of stock drained from the wire is approximately equal to that in the headbox. Following Unbehend (1991), a retention aid will be defined as any chemical which is added to improve first-pass retention while a drainage aid is added

to improve sheet drainage. This section discusses general characteristics of such additives and the effect of the surrounding chemical environment on their effectiveness.

The theory behind chemical binding of particles in papermaking has received considerable attention and is described in detail elsewhere (Roberts (1996), Unbehend (1991)). In short, there are two basic chemical mechanisms by which particles may be brought together: coagulation and flocculation. The goal of each is to bind particles together so that flocs are formed which are less likely to pass through the wire.

Due to dissociation of surface acid groups during pulping, wood fibre particles are generally negatively charged at their surfaces (Roberts (1996), Lindström (1992)). Thus they have a tendency to repel one another. A tightly bound layer of positively charged ions forms next to the fibre surface and beyond this is a more diffuse region of counter-ions. This phenomenon is described by the Electrical Double layer model which has been detailed elsewhere (Roberts (1996), Eklund and Lindström (1991)). The electrical potential between the particle surface and the surrounding solution decreases as one moves away from the particle surface. Addition of positively charged species which adsorb onto the fibre surface, such as cationically charged polymers, will decrease the repulsive energy between particles thereby allowing them to approach one another more closely. Attractive van der Waal's forces also exist between particles as a the result of electrostatic interactions between electron rich and deficient regions of adjacent molecules. The net potential energy of interaction between two fibre particles is the sum of the attractive and repulsive forces. If sufficient amounts of cationic polymer retention aid are available in solution, particles may approach each other sufficiently closely and a stable net attraction will be achieved. This phenomenon is known as aggregation.

Zeta potential is defined as the net electrical potential of a particle measured at the hydrodynamic plane of shear between the bound layer of counter-ions and the solution (Roberts (1996)). Measured values of zeta potential indicate an average potential over all particles as the actual distribution of potentials has been found to be quite broad (Sanders and Schaefer (1991)). Clearly the amount and charge of adsorbed polymers directly influences the zeta potential. This quantity is generally used as an indication of the aggregation potential of particles and in this way can be related to retention and drainage phenomena.

A second mechanism whereby particles may be bonded together is flocculation. In the bridging model, long chain polymers adsorb simultaneously onto two furnish particles thereby forming an interparticle bridge (Gregory (1988)). Either cationic or anionic polymers have been used for this purpose. When a high molecular weight (HMW) anionic polymer is used in conjunction with previously added low molecular weight (LMW) cationic polymer and/or cationic starch a patch/bridge mechanism is thought to result. In it, the cationic materials are believed to form regions of positive charge which function as anchoring sites for the HMW anionic 'bridge' molecule. This process is illustrated in Figure 2.2.

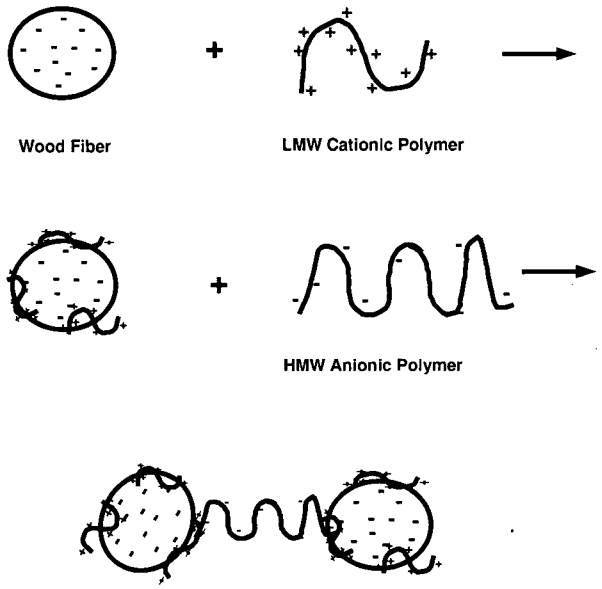

Figure 2.2: Mechanism of Dual Polymer Retention Aid System

The rate at which water drains from the fibre mat is also of critical importance as it limits the speed at which the paper machine can operate as well as affecting the structure of the sheet. Generally, the water removed is categorized into "free" and "bound" water (Unbehend (1991)). Free water is held between the individual furnish particles and is relatively easily removed by application of vacuum and pressing. Bound water is held on or within particles by capillary or osmotic forces and is primarily removed by evaporation.

The problem of draining free water is one of flow through a porous medium, specifically the forming fibre mat. Figure 2.3 illustrates this viewed as a filtration process.

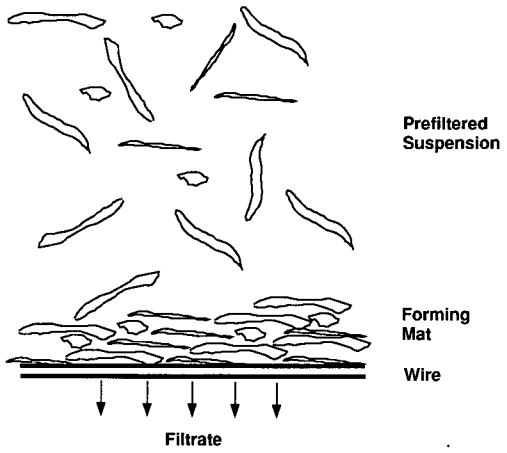

Figure 2.3: Illustration of mat formation on the wire and filtration model

With this model, the flow of water through the fibre mat can be expressed as (Branion (1978)),

$$\frac{\text{Flow Rate}}{\text{Area}} = \frac{\text{Driving Force}}{\text{Resistance to Flow}} \tag{2.3}$$

The controlling driving force is generally vacuum suction or changes in momentum applied to the sheet. The resistance to flow is a function of the mat structure and thickness, furnish particle and wire characteristics, amongst other factors. It is believed that retention of fine particles through floc formation improves drainage by immobilizing and removing fines from drainage pathways (Unbehend (1991)). Refining of fibre furnish creates fibrils and fines which retard drainage on the wire. Mathematical models for these effects will be developed in Chapter 3.

The effect of papermaking chemistry on the degree to which water is chemically bound to fibres has been recently reviewed by Lindstöm (1992). The mechanism which causes swelling of fibres is believed to be osmotic pressure resulting from the presence of counter-ions in the neighbourhood of negatively charged fibre surfaces. This is illustrated in Figure 2.4 where cations present in solution, such as Na^+ and Ca^{2+}, interact with the fibre surface creating a concentration gradient.

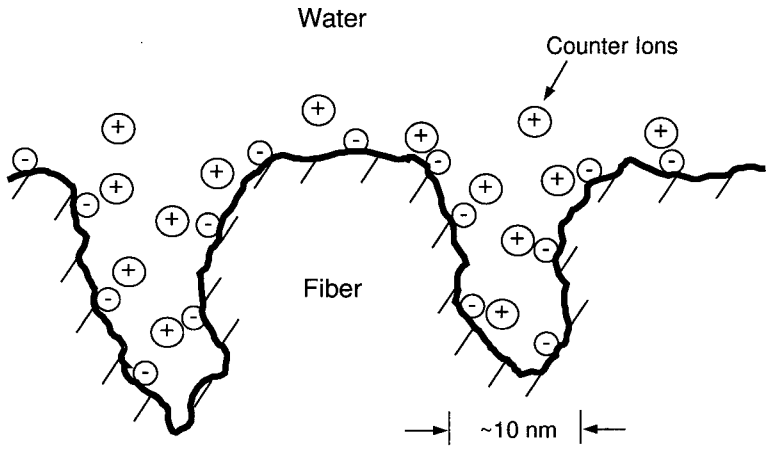

Figure 2.4: Counter-ion concentration gradient causing fibre swelling.

The amount of "bound" water associated with the furnish is a function of the furnish composition, fibre surface charge density and cell wall cohesion, number and valency of counterions in solution as well as charged substances adsorbed onto furnish surfaces. Thus degree of stock refining, pH and conductivity are variables around the paper machine which will impact on fibre swelling. Polyvalent cationic polymers will function as drainage aids in that they will adsorb onto fibre surfaces thereby displacing counter-ions (Swerin et al. (1990)). The lower concentration of these high charge density polyelectrolytes reduces the driving force for fibre swelling. Such polymers need to have sufficiently low molecular weight in order to be able to reach fibre pores. This is illustrated in Figure 2.5.

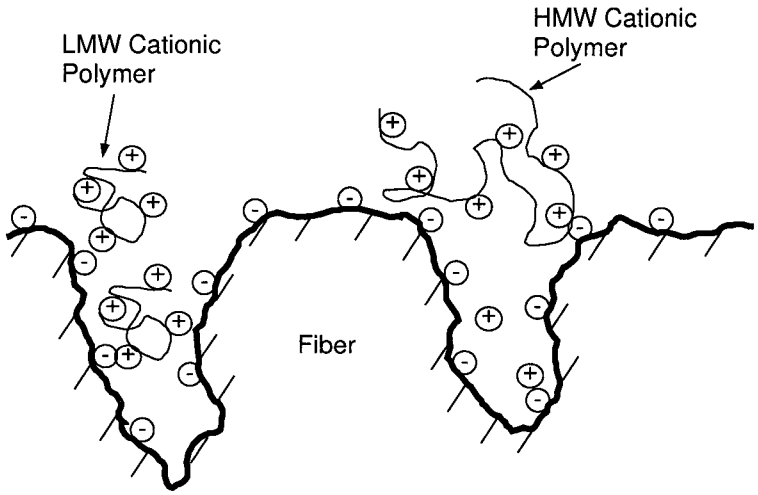

Figure 2.5: Counter-ion displacement by polyelectrolyte adsorption onto fibre surfaces

One concept that pervades the wet end chemistry literature is that of a "fines" component of the papermaking furnish which possesses properties distinct from those of larger furnish components. Fines are most often defined as the furnish fraction which passes through a 200 mesh screen (Tappi Test Methods (1996)), thereby including both fibre fines and mineral filler particles. Fines are present in incoming pulp (primary fines) and are generated through refining (secondary fines) and broke repulping (tertiary fines). As discussed by Marton (1974) the most important characteristic of fines is the disproportionately large amount of surface area per unit mass that they possess. Although fines are normally a relatively small (mass) fraction of the furnish, their large surface area has profound effects on paper machine operating variables and sheet quality. Thus, any model of chemical effects in the wet end must be capable of tracking fines variations throughout the wet end.

The presence of aqueous charged substances other than retention aids may interfere with the efficiency of the retention and mechanisms. Of note are dissolved organic substances that enter with the pulp which are commonly referred to as anionic trash (Lindström (1989)). These negatively charged substances may interact with retention/drainage aids

thereby reducing their activity. Non-organic ions such as Na^+ and Ca^{2+} may also interfere with retention aids (Eklund and Lindström (1991)). Finally, the pH of the system affects the activity of fibres, dissolved organic species and the concentration of non-organic ions which, in turn, all can affect retention.

2.2 On-line Sensors for Wet End Chemistry

Until the early part of this decade, the wet end of the paper machine lacked sensors related to chemistry with only flow and pH measurements available in most mills (Kaunonen (1989)). Over the past 15 years there has been considerable development of sensors for monitoring key papermaking chemistry variables and this activity has been reviewed by Onabe (in Roberts (1991)) and Kortelainen (1992).

On-line retention measurement appears to have received the greatest attention. This is achieved by measurement of total solids and filler consistencies at the headbox and in the wire pit. These measurements are then used in Equation 2.2 to calculate first-pass retention. Solids and filler consistencies are also measured in the top wire flume in twin wire machines. Again, the approximation assumes that the mass flowrates in the headbox and drained white water are equal. In practice a correction factor may be introduced to compensate for inaccuracies in this assumption. More detailed formulations to this equation have been proposed by Kaunonen (1988).

With the particular retention sensor system in place at the Prince Albert Paper Mill, it is possible to measure both total solids and filler consistencies between 0-1.5% and 0-0.8% respectively. The measurement principle is based on the fact that wood fibres polarize and fillers scatter light. Detailed discussions of optical consistency measurement principles can be found in Kaunonen (1988) and Kortelainen (1989). Calibration against consistencies

measured in the laboratory must be carried out on installation and at periodic intervals to maintain calibration. The most advanced models are able to operate with different furnish compositions including mechanical pulps. However, significant furnish variations would lead to measurement inaccuracies if recalibration were not performed. The Kajaani RM-200 unit is capable of providing a reading every four seconds and is thus suitable for on-line control.

Industrial application of such sensors is, by now, widespread with successful applications reported in the literature (Bernier and Begin (1994)). The experience with low consistency sensors at the Prince Albert Mill has also been generally good. They are used as monitoring tools by operators and technical staff for consistency trends but are not believed to report reliable absolute values.

Obtaining a reliable and industrially proven on-line measurement to quantitatively characterize machine drainage performance still eludes the papermaker. A traditional method commonly used by operators is to monitor the dry line on the fourdrinier section of the paper machine. This is not possible with modern twin wire machines as the dry line is not visible. Other qualitative indicators include monitoring of water released at wire direction/momentum changes and draws (i.e. sheet sagging) in the steam dryers.

To obtain a qualitative drainage indication, both direct measurements of stock on the wire and indirect indicators of stock and white water fines contents have been used. A gamma backscatter gauge has been used to monitor the mass of stock (plus forming fabric) at any point along the wire (Woodard and Wheeler (1992)). By subtracting the mass of the wire and with knowledge of the dry end basis weight, one can calculate the mass of water retained at that point. This technique is used quite often to obtain drainage "profiles" at several points along the wire. Such a profile provides a snapshot look at the performance

for each of the drainage elements. Indeed, such studies will provide the starting point for a drainage model in Chapter 3. Hawes and Buck (1992) have noted that wire wear and water trapped in the wire fabric will affect results using this technique. On-line measurement is accomplished by fixing a gamma gauge at a point along the wire. However, it is important that the gauge is in contact with the underside of the wire so that water does not collect between these two surfaces. This was thought by operations personnel at the Prince Albert mill to pose too high a risk of causing undue wear on the wire fabric at a particular point. Hence its use was discontinued.

The most commonly used on-line indicator of drainage is the 4th dryer section steam demand. This indicates the dryer work required to keep the final sheet at its moisture target of approximately 5%. While this signal does appear to respond to most expected drainage variations it suffers from two main drawbacks. First, it is a combined indication of both free and bound water drainage. A single measurement cannot separate these two effects. Secondly, it is essentially a qualitative measure as the relationship between steam demand and water drained on the wire involves complex factors in both the press and steam drying section. Despite these drawbacks, it is used as the main indicator of drainage during the course of this study.

Indirect indications of drainage potential on the wire include batch filtration type freeness analyzers on the hardwood and softwood stock lines as well as a combined stock permeability type or "drainage" sensor. General principles of these two types of sensors were reviewed by Brewster and Rogers (1985). The former measures the time to extract a given volume of filtrate at constant head (<10 psi). Permeation devices first form a pad of pulp and then measure the volume of water drained through the pad in a certain time at constant pressure (>50 psi). The measurements give indications of both the amount of fines in the stock and the degree of fibre fibrillation. However, such measurements cannot

be regarded as direct indicators of anticipated wire drainage performance as they operate at pressures much lower than those experienced on the machine and thereby underestimate compressibility of the fibre mat.

One possibility of obtaining an independent indication of drainage from the wire is by direct measurement of drained white water flows via a weir. Sensodec Ltd., a division of Valmet, has designed specialized weirs for this purpose which are sensitive to small variations in a large flow. These are inserted into the top and bottom wire flumes. Such weir based systems are also available for measuring drainage around the press section.

Several techniques exist for obtaining a measurement of the charge characteristics of pulps and these have been reviewed by Scott (1996). However, few have been reliably applied on-line. Of note are the efforts of Penniman (1993) who has developed a device based on streaming potential. The principle of measurement involved forming a pad of fibres, pumping white water through it and measuring the electrical potential across the pad. A measurement is available approximately every minute. Miyanishi (1995) has conducted several studies with on-line zeta potential instruments and observed the effects of charged polymer additions and refining in fine paper mills. Kortelainen (1992) notes that at high ionic concentrations zeta potential measurements are not representative of cationic polymer adsorption levels due to the adsorption of ions (e.g. Ca^{2+}) onto particle surfaces. Two further practical problems have prevented the use of on-line zeta potential measurement in this study. First, in prior trials, the screen on which the fibre pad formed was subject to plugging due to an inadequate backwashing cycle. Secondly, the instrument manufacturer indicated problems in replating of the silver oxide electrodes. Thus an accurate calibration could not be guaranteed.

Two other readily available on-line measurements are conductivity and pH. Conductivity indicates the total concentration of ions in the white water system and may be useful for interpreting other measurements such as zeta potential. It can also indicate the presence of non-organic carryover from pulp mill operations. pH is measured on-line in many paper mills and is fundamental to most papermaking chemistry phenomena. However, pH sensors require regular maintenance when exposed to white water systems.

2.3 Current Control Practices

Several papers have proposed schemes aimed at controlling retention or white water consistency. Early attempts to control retention found that it resulted in individual consistencies varying too much (Rantala et al. (1993)). Thus, individual consistencies are controlled separately. Industrial applications have used single input, single output (SISO) control of white water consistency through manipulation of retention aid flowrate (Bernier and Begin (1994), Rantala et al. (1994)). Significant reductions were reported in the variation of white water consistency and retention.

More advanced implementations of white water consistency control have also been reported based on MISO modelling of a number factors on a pilot scale paper machine. In Rantala et al. (1993), the significant terms in a MISO ARX model fitted to experimental data were retained indicating four significant input variables: retention aid, % chemical pulp, % groundwood pulp and % coated broke. A multivariable PID controller based on this model was designed for white water solids total consistency disturbance rejection. Open-loop and closed-loop performance were compared in the face of induced disturbances by dilution of the retention aid. Headbox total solids and filler consistencies were also controlled by manipulation of the basis weight valve and fresh filler flowrate. Set-points for each loop were provided by the basis weight and filler measurements at the reel . Reported results

showed significant improvements over open-loop operation for all three schemes. The tests were also performed in a self-tuning PID mode but slightly worse performance was observed. Scott (1996) has commented that such thin stock control systems have limitations in terms of the types of disturbances they can handle. Larger and longer term disturbances occurring due to such factors as stock fines variations, interfering anionic substances and fibre surface characteristics should be taken care of in the stock preparation area where they first appear.

Control of pH in papermaking systems has received little attention in the literature. Spriggs (1992) cites the difficulty of reliably measuring pH on-line as well as poor understanding of pH chemistry as reasons for this lack of attention. In his paper, Spriggs proposes active pH control at several points in the paper machine wet end. Conversely, for systems employing calcium carbonate as filler, the buffering effect of the carbonate ion has been noted as providing excellent stability in the pH range 7.8-8.2 (Laufmann (1992)). Indeed, the desire to avoid active pH control has been cited as a reason for conversion from acid to alkaline conditions (Casey (1981)).

Some initial work was undertaken at Island Paper Mills (New Westminister, B.C.) to determine 1) the pH sensitivity of the white water system and 2) the factors which influence pH variations. Titration curves were generated for several points in the white water system by addition of increasing amounts of sodium hydroxide and (separately) hydrochloric acid to a process sample. Figure 2.6 shows a typical curve for flume white water as well as that for the slurried PCC. Clearly the buffering in the white water system is not as strong as the PCC stream and is quite sensitive in the operating region. Since the white water system was highly closed, the same shape of titration curve was obtained for all points in the system.

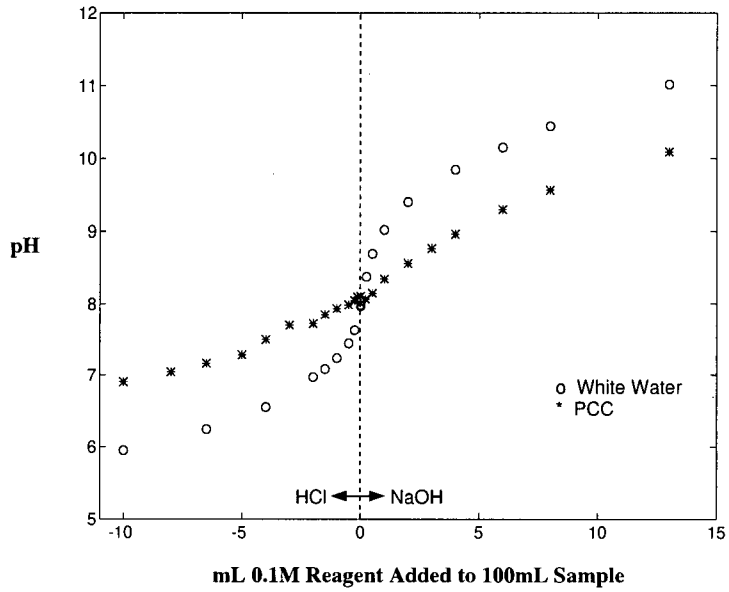

Figure 2.6: Titration curves for white water and precipitated calcium carbonate streams

Data was also gathered from two TMP newsprint mills regarding the variability of pH in incoming pulp streams. Both mills operated at pH's of approximately 4.5-4.8 and were in open-loop operation. In both cases, data showed very stable pH operation even with no closed-loop control. Laufmann (1992) reported similar pH stability for three European mills producing light, medium and high weight coated grades of paper from TMP pulps.

The conclusions from these observations were:

1. The presence of calcium carbonate in fine paper making systems does not guarantee good buffering of the white water system.
2. Good control of pH in pulp mill operations and fresh water make-up will likely ensure good pH stability in the paper machine.
3. If serious pH variations do occur in the white water system then process solutions should be found to the problem rather than compensation by on-line control.

In the Prince Albert fine paper mill, first-pass retention control is not practiced. Periodic adjustments are made in retention aid flow in order to correct large consistency deviations or during grade changes. Other chemical additives are also in open-loop operation. Dry end basis weight, sheet ash and reel moisture are all under closed-loop control. Basis weight manipulates the thick stock flow while sheet ash adjusts fresh filler flow. The reel moisture and basis weight loops are decoupled. The speed at which the white water saveall operates is controlled by the slurry level which is a function of the amount of fines present in the white water. Consistency control exists at many points throughout the wet end.

2.4 Summary

While closed-loop control of certain variables is clearly possible the impact of such control actions on other interacting variables is not yet clear. This is due to a lack of reliable models capable of predicting wet end chemistry effects. Such a lack of quantitative process information inhibits the further development of control schemes which account for the multivariable, interacting nature of the wet end. Accordingly, one of the main objectives of this project is to develop a model which will be able to predict retention and drainage responses to various operational moves and disturbances. As a minimum requirement the predictions must be directionally correct.

In order to both calibrate and validate the simulation, on-line data of process variables will be required from sensors such as those discussed above. Despite the Prince Albert mill's extensive experience with on-line sensors, in some cases problems have arisen which prevent their continuous implementation. Such problems may or may not be insurmountable but usually do require considerable time and effort on the part of mill

personnel and/or sensor suppliers for their resolution. Ultimately, the commitment required for successful implementation and maintenance of advanced sensors arises from their potential to provide information resulting in a net economic benefit to papermakers. Most often this incentive is garnered by observing the response of a single (trial) sensor and attempting to relate its response to previously unexplained variation. However, in systems which are inherently multivariable, results of such trials are often inconclusive due to interactions amongst various phenomena. Through accurate dynamic simulation of a process based on fundamental physical and chemical phenomena, improved justification for on-line measurements can be made since it becomes possible to predict exactly how the variable(s) in question affect the process. There does still exist, however, the paradox that in order to be certain of the simulation's accuracy, good process information is required. This can be partially resolved by a stage-wise approach to sensor implementation and process improvements through modelling and control.

Chapter 3

Dynamic Simulation of Wet End Chemistry

The goal of this chapter is to describe the methodology used to develop a large scale dynamic simulation of paper machine wet end chemistry. This includes both the computational techniques involved in simulation as well as the models which have been implemented. The first section reviews mathematical techniques and previous simulations of paper machine modelling. Specifics of the simulation platform used in this study are given. The physical and chemical models which are implemented in the simulation are then described in detail. Physical models include mass and momentum balances in process units such as tanks, valves, and valves as well as wire drainage and refining. Chemical effects discussed consist of adsorption of polymer additives onto furnish particles and flocculation amongst others. This separation into physical and chemical effects is for presentation purposes only; the fundamental nature of the models fully accounts for interactions between the two.

3.1 Simulation Methodology

The development of a large scale dynamic simulation usually involves two steps:

- development of a steady-state balance
- addition of dynamics

Mill wide steady state balances are usually carried out using a process simulator, although rough initial calculations can be performed by hand. A steady state balance, in turn, provides initial conditions from which the dynamic process is started. Most modern dynamic simulation

packages allow the developer to conduct steady-state balances and then expand the simulation to include dynamics on the same platform.

Both steady state and dynamic simulation use many similar mathematical techniques. The primary additional requirement placed on dynamic simulators is that of solving systems of differential equations. The success of any simulation depends on both the mathematical techniques and the quality of the process models used. The ease with which the necessary process information can be implemented and the speed at which the software performs the calculations are also critical. These issues are magnified in importance with increasing size and complexity of the process phenomena being modelled.

3.1.1 Mathematical Techniques in Process Simulation

Over the past thirty years, both steady-state and dynamic simulation techniques have found widespread application in process design and control. In the processing industries the problem consists of solving the relationships amongst numerous interconnected process units and considering inter-vessel effects, such as pipes, valves and pumps. These relationships are usually quite complex due to nonlinearities and the presence of recycle streams. For this reason, and the fact that most process simulations involve many units with potentially hundreds of stream variables, specifically designed computer simulation packages are used. Furthermore the simulation package can be specific to a particular industry (e.g. pulp and paper) reflecting the material property information and processing unit libraries required.

The mathematical techniques discussed here are of three types:

1. Numerical integration of systems of differential equations

2. Solution of systems of nonlinear equations
3. Reduction of the complexity of large sets of equations

Each of these will be discussed in turn. The purpose here is to highlight some of the main issues associated with these problems rather than to provide a comprehensive review.

Numerical Integration

Processes involving the conservation of mass, energy or momentum in a control volume are described by equations of the form,

$$\left\{\begin{array}{c}\text{Rate of Accumulation}\\ \text{of}\\ \text{Conserved Quantity}\end{array}\right\} = \left\{\begin{array}{c}\text{Rate of Conserved}\\ \text{Quantity In}\end{array}\right\} - \left\{\begin{array}{c}\text{Rate of Conserved}\\ \text{Quantity Out}\end{array}\right\} \tag{3.1}$$

Each of these conservation equations leads to either a differential or algebraic equation. However, solution of the set of (interdependent) conservation equations for a process is not generally possible by analytical means. Therefore numerical integration techniques are applied.

Consider the following first-order ordinary differential equation (ODE),

$$\frac{dy}{dt} = f(y,u,t) \tag{3.2}$$

where y is the state variable and u is the forcing function. One of the simplest methods of numerical integration is Euler's method. It is derived by first approximating the derivative in (3.2) by forward differences,

$$\frac{y_{t+\Delta t} - y_t}{\Delta t} = f(y_t,u_t,t) \tag{3.3}$$

and therefore,

$$y_{t+\Delta t} = y_t + \Delta t \bullet f(y_t,u_t,t) \tag{3.4}$$

Higher order methods, such as Runge-Kutta, use more sophisticated approximations for the derivative term. These are based on a Taylor series expansion of y(t+Δt),

$$y(t + \Delta t) \approx y(t) + \Delta t \bullet y'(t) + \frac{(\Delta t)^2}{2} \bullet y''(t) + \ldots \tag{3.5}$$

where usually the first four terms in the expansion are retained. In addition to methods which predict one time step ahead (e.g. Euler, Runge-Kutta) multistep methods make use of previous values of the state variables in order to improve predictions. Details of these methods can be found elsewhere (Boyce and DiPrima (1992)).

For a set of n first-order linear ordinary differential equations the ratio of the largest to smallest eigenvalue determines the stiffness of the system. Eigenvalues are computed as the n roots of the characteristic equation. The response of the system is given by the following equation:

$$y_t^i = b_1 e^{r_1 t} + b_2 e^{r_2 t} + \ldots + b_n e^{r_n t} + \text{forcing function terms} \tag{3.6}$$

where

y_t^i is the i^{th} state variable at time t,

b_j are parameters determined by the system and forcing function,

r_j are eigenvalues of the system.

For system stability the real parts of all the eigenvalues must be negative. The larger the magnitude of the negative real part the quicker is the decay of that term. The dominant system eigenvalue is that which controls the time it takes for the system to reach steady state. (i.e. the smallest eigenvalue).

The stiffness of the system imposes requirements on the maximum integration interval, Δt, otherwise numerical instability will result. However, a larger integration interval will obviously result in faster simulation. Consider the simple first order system,

$$\frac{dy}{dt} = ry \tag{3.7}$$

It can be shown that the values of Δt for which the numerical solution by the Euler method is stable are (Smith and Corripio (1985)),

$$\Delta t < \frac{2}{|r|} \tag{3.8}$$

More importantly, a large integration interval can also lead to inaccuracies, particularly when using low order methods such as Euler's. Thus there is an efficiency trade-off between ease of computation with low order methods and reducing the integration interval with higher order methods. It is not surprising that divergent views exist amongst practitioners (Luyben (1990), Press et al. (1988)) regarding the efficacy of Euler's method for complex integration problems.

Explicit integration schemes use only previous values of the state variables to approximate future values. Implicit schemes incorporate estimates of the current state variable into the update formula. For example, the implicit modified Euler update formula for the simple system of Equation 3.7 would be,

$$y_{t+\Delta t} = y_t + \frac{\Delta t}{2}\left[ry_t + ry_{t+\Delta t}\right] \tag{3.9}$$

or

$$y_{t+\Delta t} = \left[\frac{1+\frac{1}{2}r\Delta t}{1-\frac{1}{2}r\Delta t}\right] \tag{3.10}$$

Stability is satisfied if

$$\left[\frac{1+\frac{1}{2}r\Delta t}{1-\frac{1}{2}r\Delta t}\right] < 1 \tag{3.11}$$

which holds for all positive values of Δt when Real(r)<0. In this case, the upper bound on Δt is governed only by consideration of accuracy.

Systems of Nonlinear Equations

Systems of nonlinear equation often arise in flowsheeting problems due to application of conservation equations when there is no accumulation within the control term (i.e. dynamics). In particular, when the piping network between process units is considered in conjunction with solution of the flowsheet, the dynamics of process units may be considered slow in comparison to those of the network. This is the approach adopted by the dynamic simulator used in this work. In this way, process units serve as boundary objects during solution of the pressure/flow network. Here, a brief review of some important features of two well established algorithms is given by their application to a simple piping network example.

First, it is necessary to distinguish between two forms of the equations, *explicit* and *implicit*. If x is the set of independent variables and e is a calculated error then,

$$\begin{aligned} x^{(Calc)} &= f(x^{(Guess)}) \qquad \text{Explicit} \\ e &= g(x^{(Guess)}) \qquad \text{Implicit} \end{aligned} \tag{3.12}$$

The first type is most commonly encountered in solving recycle streams and the second occurs in solving piping networks or in process modules where conservation laws are encountered. Explicit loops have more flexibility in the way in which they may be solved as information is provided about the 'x' value(s) which can be used in the next iteration. Explicit loops may be converted to implicit form by writing,

$$e = x^{(Calc)} - x^{(Guess)} \tag{3.13}$$

Consider the piping network shown in Figure 3.1 which is taken from Jeppson (1977). There are three nodes with the head specified at Node 1 and flowrates at Nodes 2 and 3. Thus we need to solve for the heads at Nodes 2 and 3. The Hazen-Williams equation is used to calculate friction factors in an exponential head-flow relationship which gives rise to the following form of the two continuity equations:

$$e_2 = -\left(\frac{H_1 - H_2}{K_{12}}\right)^{1/n} + \left(\frac{H_2 - H_3}{K_{23}}\right)^{1/n} + 1.5$$
$$e_3 = -\left(\frac{H_2 - H_3}{K_{23}}\right)^{1/n} - \left(\frac{H_1 - H_3}{K_{13}}\right)^{1/n} + 3.0 \qquad (3.14)$$

where e_2, e_3 represent errors at nodes [2] and [3] while H_1, H_2 and H_3 are the node pressure heads. Values used for the parameters of this example are H_1=100 feet, K_{12}=1.622, K_{13}=2.432, K_{23}=0.667 and n=1.85 where the K_{ij}'s and n are experimentally determined from head loss versus flowrate experiments using water. The objective is to drive e_2 and e_3 to zero. Two different methods are now considered for solving this problem.

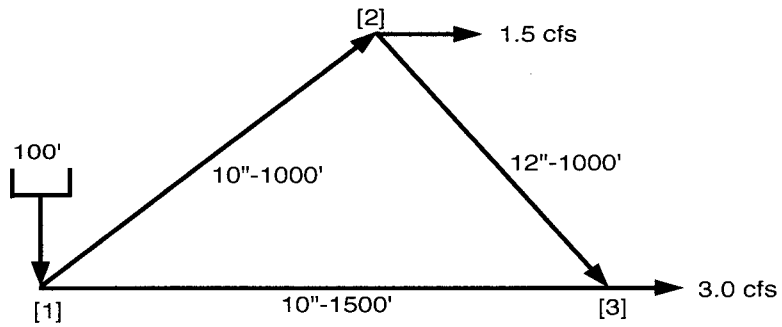

Figure 3.1: Piping network example of Jeppson (1977, p.117)

Method 1: Newton-Raphson

Consider a general nonlinear function of one variable e(x) which we want to solve by finding x such that e(x)=0. If the derivative of e(x) is available then we can take a first-order Taylor series expansion about the current point $x^{(i)}$,

$$e^*(x) \approx e(x^{(i)}) + \left(\frac{de}{dx}\right)_{x^{(i)}} (x - x^{(i)}) \qquad (3.15)$$

Since this approximate $e^*(x)$ is linear, we can find its solution $x^{(i)}$ by setting e(x)=0 resulting in,

$$x^{(i+1)} = x^{(i)} - \left(\frac{de}{dx}\right)^{-1}_{x^{(i)}} e(x^{(i)}) \tag{3.16}$$

This procedure may be generalized to the multivariable case as follows:

$$\mathbf{x}^{(i+1)} = \mathbf{x}^{(i)} - (\mathbf{J}^{(i)})^{-1}\mathbf{E}(\mathbf{x}^{(i)}) \tag{3.17}$$

where **J** is the Jacobian matrix of the error functions **E**. Iterations are continued until either $\mathbf{x}^{(i+1)} - \mathbf{x}^{(i)}$ or $\mathbf{E}(\mathbf{x}^{(i+1)})-\mathbf{E}(\mathbf{x}^{(i)})$ are sufficiently close to zero. Since it is computationally expensive to compute the inverse of a possibly large matrix **J**, a vector **z** is computed as the solution to the linear system,

$$\mathbf{J}^{(i)}\mathbf{z}^{(i)} = \mathbf{E}^{(i)} \tag{3.18}$$

and then it is subtracted from the current estimate to provide the next estimate of **x**,

$$\mathbf{x}^{(i+1)} = \mathbf{x}^{(i)} - \mathbf{z}^{(i)} \tag{3.19}$$

Given good enough initial estimates of **x** so that the solution converges, the Newton-Raphson (NR) method has quadratic convergence which means that the number of significant digits of accuracy doubles as one approaches the solution. The main requirement is the need for analytical derivatives or, alternatively, numerical determination of derivatives at each step by perturbation methods.

For the above pipe network example, analytical derivatives are supplied in Jeppson (1977) and the NR routine was implemented in MATLAB. The problem was initialized at $\mathbf{H} = [H_2 \ H_3] =$ [95 85]. Results of the first 10 iterations are shown in Table 3.1 where it is seen that the H values converged to 4 decimal place accuracy in 8 iterations. Results agreed with those given by Jeppson.

Iteration	H2	H3
0	95.0000	85.0000
1	90.6580	94.0357
2	93.5716	89.0259
3	91.0457	91.7828
4	91.9862	90.2291
5	91.3591	90.9859
6	91.4404	90.8549
7	91.4511	90.8405
8	91.4512	90.8404
9	91.4512	90.8404
10	91.4512	90.8404

Table 3.1: Newton-Raphson method iterations

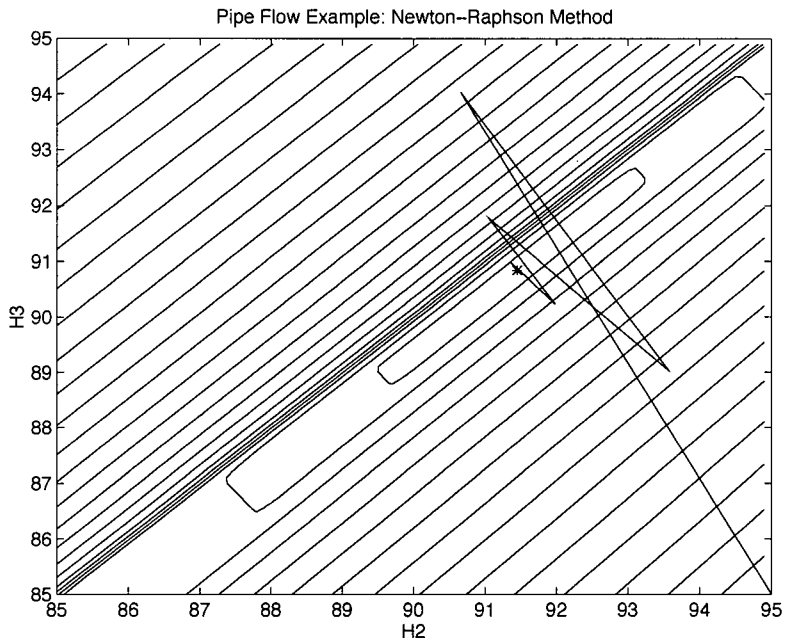

Figure 3.2: Contours of piping network showing convergence path of Newton-Raphson method.

Figure 3.2 gives a graphical representation of how the NR procedure converged. The contour lines are constant Sum([Abs(f2) Abs(f3)]), the sum of the error functions. This vector norm was chosen instead of Max([Abs(f2) Abs(f3)]) as it gave a better behaved surface, although the maximum error is often given as an indication of convergence (e.g. this is reported in the IDEAS software). Two features of this surface are worth noting. First, there is obviously a

very strong degree of interaction between H_2 and H_3 indicated by the orientation of the lines. Secondly there is a very strong nonlinearity in the surface around the point where $H_2 = H_3$. Physically this is the point where the flow from Node 2 to Node 3 changes direction. Care had to be taken in the algorithm to accommodate such changes in direction. Note that this surface does not change with the particular algorithm used to solve the equations.

The NR algorithm appears to oscillate somewhat around the converged solution (indicated by an asterix). However, the improved convergence with each step is evident. It was possible to make the algorithm diverge by selecting starting points along the $H_2 = H_3$ line but this situation was encountered with all other algorithms tried.

Method 2: Wegstein Acceleration

This is a classical method developed in 1958 by Wegstein that is used widely in flowsheeting. In it, each independent variable is updated by a one dimensional secant method thereby ignoring interactions with other variables. For this reason it is termed a "one-dimensional" method. The update formula for the j'th independent variable is given by,

$$x_j^{(i+1)} = x_j^{(i)} - \left(\frac{e_j^{(i)} - e_j^{(i-1)}}{x_j^{(i)} - x_j^{(i-1)}} \right)^{-1} e_j^{(i)} \qquad (3.20)$$

Note that two sets of initial values would be required to start the algorithm. Some thought would also have to be given to the pairing of the independent variables with the error functions. One would attempt to pair those independent variables with the function that they most strongly influence.

Table 3.2 reveals that this method does not work with the pipe network example. At iteration 22 the algorithm starts to diverge and does not recover. From Figure 7, the initial steps to get into the 'valley' appear quite effective but the algorithm then has considerable problems and oscillates from one side of the valley to another. This would appear to be the result of not being able to take the strong interactions between the variables into account. Divergence occurred with other starting values as well.

Iteration	H2	H3
0	95.0000	85.0000
1	90.0000	90.0000
2	91.1366	89.1175
3	90.6694	89.6072
4	90.5042	90.0039
5	90.5918	90.0051
6	90.7388	90.0039
7	90.7473	90.0059
8	90.7499	89.9196
9	90.7473	90.2349
10	90.7493	90.2196
11	90.7708	90.2224
12	90.9403	90.2191
13	90.9289	90.2228
14	90.9307	90.2683
15	90.9288	90.3935
16	90.9314	90.3810
17	90.9565	90.3832
18	91.0701	90.3807
19	91.0642	90.3838
20	91.0658	90.4297
21	91.0642	90.3844
22	91.5746	79.4740
23	89.5443	67.1659
24	108.8397	55.4555
25	23.8889	61.2009

Table 3.2: Wegstein Acceleration Iterations

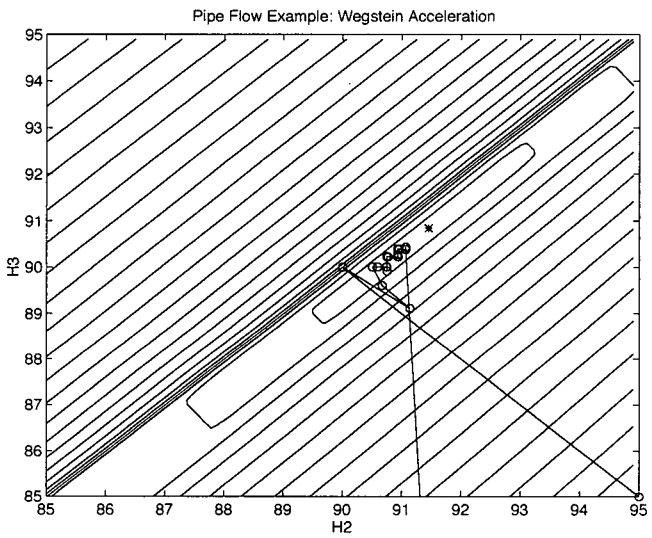

Figure 3.3: Convergence of Wegstein for piping network example

These examples emphasize the need for careful selection of the method used for solving sets of nonlinear equations. No technique is optimal for all applications and it is likely that the best approach is to use combinations of methods depending on how close one is to the optimal solution and the ease with which derivatives can be computed.

Flowsheeting and Sparse Matrix Techniques

The overall computational problem in large scale dynamic simulation involves the solution of many interconnected differential and algebraic equations. There appears to be three main approaches to solving flowsheeting problems: sequential modular, simultaneous modular and equation oriented (Westerberg et al.(1979)). In the first, rigorous mass, energy and momentum balances (possibly dynamic) are written for each processing unit/module. All input streams must be specified and calculated outputs from a module are passed to downstream modules. Recycle streams are handled by guessing values and iterating. The simulation routine will often contain algorithms identifying the order in which to calculate the modules and identify recycle streams. These procedures are called "precedence ordering" and "tearing" a flowsheet respectively. The main advantage of the sequential modular approach is the

straightforward manner in which the computations are carried out due to the requirement that all inputs be specified. In design problems, however, specifications may be placed on output streams or variables internal to the process units. These specifications are difficult to accommodate due to the usually highly complex unit models (i.e. how to map the output back to the input). Another disadvantage is that interactions between units are not considered which may lead to poor stability of the flowsheet, particularly when recycle streams are involved.

The simultaneous modular approach is similar to the sequential modular in that separate rigorous unit descriptions are written and individually solved. In addition, approximate linear multi-input, single-output models are determined by perturbation methods for each output variable of each unit. The flowsheet is then solved (i.e. all inputs and outputs of the units are determined) using the set of linear equations. The advantage here is that constraints on the output variables are easily handled. Since the set of linear equations is solved simultaneously interactions amongst processing units are accounted for.

Finally, the equation-oriented approach is arguably the most rigorous and also the most flexible of the three. The basic concept is simple: write out all equations (mostly nonlinear) describing all effects (mass and energy balances, chemical reactions, etc.) for every process unit and solve these simultaneously. Flowsheet design specifications are represented by additional equations and it is also possible to include equipment design parameters as outputs. Obviously, interactions are fully accounted for. The cost of this increased flexibility is in the computational effort required to solve this large set of equations simultaneously. Westerberg et al.(1979) report that "tearing" such a set of equations can result in a problem two to three orders of magnitude more complex than with the sequential modular approach.

The above approaches can be applied to either steady-state or dynamic simulation. The introduction of dynamics adds additional requirements for numerical integration routines. In

the case where mixed differential and algebraic equations (DAE's) are present, a large body of literature provides techniques for their solution. These techniques originated with the work of Gear (1971) and are recently reviewed by Pantelides and Barton (1993).

For any given unit or part of the flowsheet, it is usually only a small subset of the total number of variables in the flowsheet that will be involved. Thus, when setting up the solution to the flowsheet/network, the associated matrices will have a significant number of blank or zero entries. Such matrices are termed "sparse" and a review of techniques for exploiting their structure is given by Duff (1977). Here, a few of the sparse matrix techniques which are particularly useful for flowsheeting problems will be mentioned. The basic goal is to partition a potentially large set of equations into a series of smaller problems.

In order to set up an automatic procedure for partitioning, each function must be assigned exactly one "output variable". This imposes an ordering for partitioning algorithms which trace the interactions amongst the variables and equations. Such automatic "output assignment" schemes are also used for pivot selection during Gaussian elimination (Duff (1977)). The general goal in output assignment is to select the dominant variable associated with a particular equation. However, output assignments are not unique if partitions involve more than one equation.

The basis of an output assignment algorithm is to first choose the row, for a given column, which contains the fewest incidences. Then, for this chosen row, select the column with the fewest incidences. The selected variable is then assigned to the chosen function and the rows and columns are deleted. The procedure is repeated until all variables are assigned to functions. According to Duff (1977) a similar criterion, that of choosing the element with the lowest product of row and column incidences, is also widely used.

A partitioning algorithm will have to identify groups of functions whose outputs, as specified by the output assignments, are required by others in the group in order to be solved. This dependence can be represented by a *Directed Graph.* An equation is represented as a node with the output from each node assigned as the output variable for that equation. "Edges" (connections) are drawn to other nodes that require this variable for their solution. The most commonly used algorithms to carry out partitioning are due to Tarjan (1972) and Sargent and Westerberg (1964). One starts at an arbitrary node, say f_1, and traces to any other node along a path. If either 1) a node is encountered a second time or 2) a node has no outputs, then the path is terminated. For case 1) all nodes between the previous and present occurrences are placed into a partition and for case 2) the node with no outputs is placed into a partition. Once a node (or nodes) has been placed into a partition then the node itself and all associated edges are deleted from the graph. The process is reinitiated at any remaining node and continues until all nodes have been placed into partitions. Precedence ordering takes place by placing the latest partition found on top of the stack of partitions.

In certain situations it may be that partitioning and precedence ordering have failed to produce an *Incidence Matrix* in block triangular form. Often there are only a very small number of variables preventing a successive solution. In such cases, one can remove ("tear") these variables by guessing values for them and iterating. Each stage results in a bordered block triangular matrix where there are more equations than unknowns. The extra equations are regarded as error functions which can be used in any nonlinear equation solving routine to select values for the tear variables at the next iteration.

3.1.2 Dynamic Simulation in the Pulp and Paper Industry

The techniques described in the previous subsection have found wide application in the pulp and paper industry. Indeed, the large number of units as well as complex mixing and

recirculation dynamics lends itself such analysis. An excellent application oriented introduction to both steady state and dynamic simulation in the pulp and paper industry is given in Syberg and Wild (1992). In their monograph, some distinct features of pulp and paper simulators from those in other industries (the oil industry in particular) are noted:

- solids components must be included
- only small physical property data bases are available because little is known about pulp or liquor properties
- models of pulp and paper unit operations are often quite simple. In paper mills commonly only mixers, splitters and separators are used

The white water system of the paper machine has been the subject of a number of dynamic simulation studies. These have been driven by the need to reduce fresh water usage around the paper machine. As well, the complex configurations of white water systems with their many recirculation paths prohibit their analysis by analytical methods.

Recently, Harris (1995) has reviewed applications of dynamic simulation to white water systems in newsprint mills. She also developed a large scale system of an integrated TMP mill and newsprint machine white water system, calculating both mass and energy balances. Orccotoma et al. (1996) modelled the fines distribution in a newsprint mill using dynamic simulation in order to study the effect of increased broke (repulped paper) recirculation and virgin pulp fines content on paper machine operation. First-pass retention, which was modelled by a semi-empirical relationship, was found to be sensitive to such variations. Dynamic simulation for studying the effect of broke recirculation has also been carried out by Bussiere et al. (1988) and for grade changes by Miyanishi et al. (1988). None of the above studies considered chemical effects. A notable exception to this was Humphrey (1986) who simulated the retention of alum in a pilot scale paper machine using empirical models for alum uptake developed by off-machine experiments.

3.1.3 The Simons IDEAS Simulation Platform

The dynamic simulation package being used for this project is IDEAS developed by Simons Technologies Inc. (Meincer et al. (1992)). The software uses an object-oriented approach to flowsheeting with standard processing units and material properties available in libraries. The main advantages of object-oriented simulation is that connectivity of objects is not restricted by predefined notions of causality in the system (Maciejowski (1997)). This results from the use of fundamental physical and chemical laws in developing individual objects. Less formally, the phrase "plug and play" is often used to describe object-oriented simulation models.

A "Developers Kit" is available for custom programming of novel process units and was used to design modules related to papermaking chemistry. Objects described by differential equations (e.g. tanks) are solved in a sequential modular manner using an implicit Euler method for numerical integration thereby avoiding stiffness problems. An integration interval of 1 second was used throughout to ensure accuracy of results. It was also found that longer intervals led to numerical instability in the piping network. Between units which define pressure boundaries is the "pressure-flow" network consisting of pipes, valves, pumps, etc. which tracks mass, energy and momentum dynamics throughout the system. Models for each flow element result in a system of nonlinear equations which is solved independently of the above set of differential equations based on the assumption that tank dynamics are much slower than those of the pressure/flow network. Transportation times for fluids in pipes have not been accounted for in this implementation of the simulation as there was no rigorous provision for time delays in the IDEAS software. Hold-up times in tanks are generally much larger than piping transportation times in the paper machine wet end. Tank residence times range from 1-90 minutes while transportation times between these tanks do not exceed 1 minute.

The simulation was implemented on a PowerMac 8100/100 computer and required up to 40MB of RAM. A maximum speed of 3 times faster than real time was achieved. It was found that the main burden was the pressure/flow network which required approximately 75% of the computation time. Since the longest time constants involved in wet end chemistry are of the order of several hours each simulation run was of this time scale.

3.2 Physical Modelling

Simulations of the wet end of paper machines have traditionally been built up from process units describing mass hold-up as well as stream and component mixing and separation. With assumed values for variables affected by chemical effects (e.g. retention and drainage), such a model can describe very well the dynamics present. As well, this level of modelling can provide a basis for verifying the mass balance of the simulation against either process flow diagrams or laboratory data. The first part of this project was to develop such a simulation which forms the backbone onto which papermaking chemistry models were added.

Most of the models for the above level of simulation are in existing libraries provided with the software package. A model for drainage on the wire was developed based on filtration theory and incorporated into the simulation. This section discusses modelling of these two components along with stock refining and characterization of "bound" water. These effects comprise the "physical" part of the overall simulation.

3.2.1 Modelling Elements Using Existing Libraries

In order to develop an accurate model of the wet end hydrodynamics and mixing the following information was gathered from the mill:

- pertinent unit dimensions (e.g. tank capacities)
- pump curves and control valve characteristics

- current control configurations including actual (mill DCS) tunings

There are 107 process units (tanks/mixers/separators), 31 pumps, 50 control valves and 42 PI control loops in the simulation.

All tanks are considered to have perfect mixing characteristics leading to first-order dynamics. Approximate mean residence times of the major tanks in the wet end are listed in Table 3.3. Tracer studies performed on the mixing and machine chests have shown that the assumption of perfect mixing is reasonable. While the white water silo is also modelled as a well stirred tank it is believed that regions of near plug flow exist. Since the mean residence time of the silo is quite short (≅1 minute) relative to the time constants involved in wet end chemistry, such an approximation will not introduce significant error.

Process Unit	**Mean Residence Time (min)**
SWD Low Density	67
HWD Low Density	33
Mix Chest	15
Machine Chest	8
White Water Silo	1
White Water Chest - Rich Side	3
White Water Chest - Medium Side	5
White Water Chest - Lean Side	3
Cloudy Filtrate Chest	25
Broke High Density	90*
Broke Low Density	90

Table 3.3 Mean residence times of tanks in wet end at Prince Albert Mill
(*Broke HD level varies considerably)

Cleaners and screens have been modelled as static mass splitting operations based on steady-state balances obtained from original mill process flow diagrams. Since this information is normally reported as total solids fractions, it was assumed that all fibre fines and filler material passed through the cleaners and screens from which the resulting fractionation of long fibres was calculated.

The function of the saveall disc filter is to capture fine furnish particles in a mat formed from a sidestream of hardwood fibre. The operation of different types of savealls is described by Doucette (1988) and has been modelled empirically and incorporated in a dynamic simulation by St. Jacques (1982). For the present saveall model, all of the long fibre fraction was assumed to stay with the filter cake while fines and filler were assumed to be retained in a ratio equal to that found in the saveall slurry. Dynamics are not considered which did not introduce significant error into the overall white water system dynamics due to the comparatively large volume of the following filtrate chests.

The headbox model consists of delivery of an appropriate amount of stock to the wire and the recirculation of flows to the deaerator and white water silo. No attempt has been made to model the hydrodynamic characteristics as pressure pulsations occur with much shorter time constants than mixing and recirculation effects involved in wet end chemistry.

Other than added chemicals, four components are assumed to exist within the papermaking system. These are long fibres, fibre fines, filler and water. A fifth component, flocs, exists only between the headbox and the couch. Dimensions of each of the solids components used in the simulation are summarized in Table 3.4. While the fibre fines dimensions are typical of the P200 fraction from a Bauer-McNett separation (Htun and de Ruvo (1978)), it is only necessary that these dimensions lead to a proportionately large specific surface area since in reality there is a distribution of particle sizes in the furnish. These values simply provide us

with the necessary degrees of freedom to investigate the effects of variations in this particle size distribution. As well, the cylindrical geometry of the fibre fines corresponds to that observed in Htun and de Ruvo's study.

Furnish Component	Geometry	Radius (m)	Length (m)
Long Fibres	Cylindrical	$1x10^{-5}$	$1x10^{-3}$
Fibre Fines	Cylindrical	$1x10^{-7}$	$1x10^{-4}$
Filler	Spherical	$7x10^{-7}$	N/A

Table 3.4. Dimensions of furnish particles used in the present study

Sources of fibre fines are with the incoming pulp, through refining and with dry end sheet breaks and trim. Filler enters with fresh filler addition and through dry end sheet breaks and trim. Details of fines generation through refining of the softwood and hardwood pulps are described later. No attempt was made to model fines generation through repulping in the broke system and as such constant values of component consistencies arising from dry end sheet breaks and trim were assumed.

Sheet basis weight and ash controllers were approximately tuned to match plant process data from observed set-point changes. In practice, dead-time compensation is required in such loops. However, transportation time is not modelled in this study and standard PI algorithms were implemented for both basis weight and ash loops.

3.2.2 Refiner Modelling

Fibre fines are produced in the refining process by fibre shortening and complete removal of parts of the fibre wall (Page (1989)). Additional surface area is also created by external fibrils

which are still attached to long fibres. Marton (1980) has suggested that one should consider the hydrodynamic surface area as the most appropriate measure of pulp surface available for adsorption of starch. Applying this idea to other polymeric additives of sufficiently large size, the relationship between degree of refining and specific surface area needs to be determined.

To this end, studies were used which had previously examined the resulting Canadian Standard Freenesses (CSF) of both hardwood and softwood pulps for various specific energy inputs of the Prince Albert mill refiners. Since CSF testing is conducted at a low pressure drop and fines production has been shown not to affect significantly pulp compressibility (El-Hosseiny and Yan (1980), Ingmanson and Andrews (1959)), differences in freeness were attributed entirely to increased furnish surface area. From El-Hosseiny and Yan (1980), the relationship between CSF and pulp specific surface area is,

$$CSF = \frac{10^7}{10^4 + 1.11C_o\mu R} + \frac{1.11C_o\mu R}{10^4} \bullet \left[\frac{10^7}{10^4 + 1.11C_o\mu R} + 1000\ln\left(1000 - \frac{10^7}{10^4 + 1.11C_o\mu R}\right) - 6907.76\right] - 23.5 \qquad (3.21)$$

$$R = \frac{5.55\sigma^2 C_m}{(1 - \alpha C_m)^3}$$

where,

- C_o is the initial slurry consistency (g/mL)
- μ is the liquid viscosity (Poise)
- R is the specific filtration resistance (cm/g)
- C_m is the filtered pad "consistency" of El-Hosseiny and Yan (1980) or "apparent density" of Ingmanson and Andrews (1959) (g/mL)
- α is the hydrodynamic specific volume (mL/g)

- σ is the furnish specific surface area (cm^2/g)

For the purposes of the simulation model, the refining process consists of converting a portion of the long fibre fraction into fibre fines. In this way, the additional surface area created by fibrillation of the long fibre fraction is ascribed to production of fibre fines. Indeed, by comparing classified and unclassified pulps at various levels of refining, Ingmanson and Andrews (1959) concluded that differences in filtration resistance are almost entirely the result of increased fines levels rather than fibrillation of the long fibre fraction. In terms of the overall simulation, this assumption will not affect the total amount of adsorbed additives but may lead to small inaccuracies in screening and other physical separation processes. The particular case of particle retention on the wire is discussed in a later section.

For a sample consisting of only a long fibre and a fines fraction,

$$\sigma_{Whole} = \left[\frac{\sigma_{Fib}}{V_{Fib}}\left(100 - C_{Fines}\right) + \frac{\sigma_{Fin}}{V_{Fin}} C_{Fines}\right] \Big/ 100\rho \qquad (3.22)$$

where,

- σ_{Whole} is the specific surface area of the whole sample (cm^2/g)
- σ_{Fib} and σ_{Fin} are the per particle surface area of fibre and fines (cm^2/particle)
- V_{fib} and V_{fin} are the per particle volumes of fibre and fines (cm^3/particle)
- C_{fines} is the fines percentage of the solids material
- ρ is the density of the fibre and fines particles (g/cm^3)

With the assumption that both long fibres and fines particles are cylindrical then $\sigma/V = 2/R$ where R is the particle radius and C_{fines} can be found by rearrangement of Equation 3.22 to,

$$C_{Fines} = \frac{100\rho\sigma_{Whole} - \left(200/R_{Fib}\right)}{2\left(\frac{1}{R_{Fin}} - \frac{1}{R_{Fib}}\right)} \tag{3.23}$$

Values showing the fines produced against refiner specific energy input are plotted in Figures 3.4a and 3.4b for hardwood and softwood respectively. The individual points result from application of Equations 3.21 through 3.23 to CSF measurements in the original CSF vs. Refiner Energy studies. A linear regression of these points provides the implemented model in the hardwood and softwood refiners. The difference in responses to refining between slush (never-dried) and baled (previously dried) furnishes are immediately apparent. This is the result of decreased fibre swelling for previously dried pulps (Lindström (1992)).

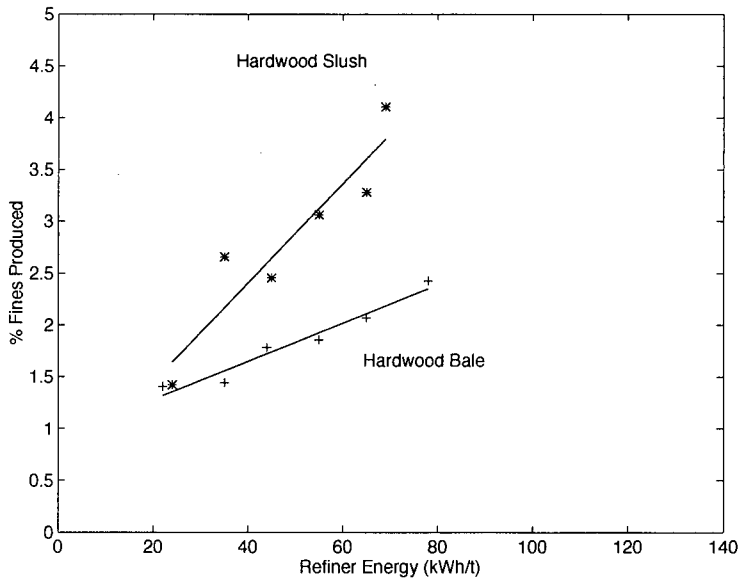

Figure 3.4a: Fines production for hardwood refiner model

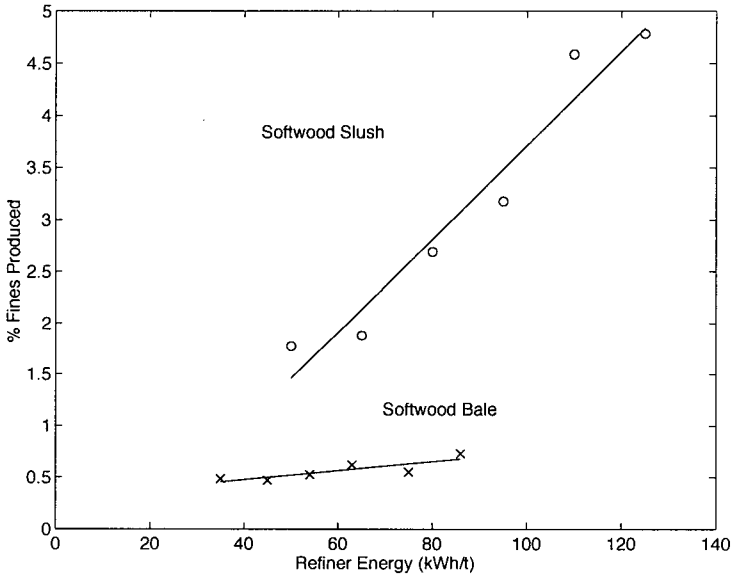

Figure 3.4b: Fines production for softwood refiner model

3.2.3 Drainage Modelling

Two types of water associated with the forming sheet on the paper machine are considered. "Free" water, which is held between individual furnish particles, is mostly removed by vacuum and gravitational forces in the forming section of the paper machine. "Bound" water, which is bound to the fibres through chemical interactions, is removed by pressing and steam drying. From first principles, a model based on filtration theory is developed for drainage of free water. Since this simulation only considers effects up to the couch, no models of pressing and steam drying operations are incorporated. However, a measure of the bound water at the couch is presented based on a semi-empirical approach. This provides a basis for drainage model validation against dryer section indicators.

Drainage on the Wire

The forming section of the paper machine, which accounts for approximately 95% of total drainage, is modelled as ten separate elements: forming board+blades, 3 individual foils, 2 multifoil boxes, 2 vacufoil boxes and a curved multifoil shoe vacuum. A schematic diagram of

the forming section is shown in Figure 3.5. Nominal drainages for each element were taken as the average measured values from several independently conducted drainage studies of the paper machine. These studies measure the mass of stock on the wire at a particular location using a nuclear backscatter technique. Drainage from flatboxes and the couch are taken as fixed percentages of the available free water based on these nominal drainages.

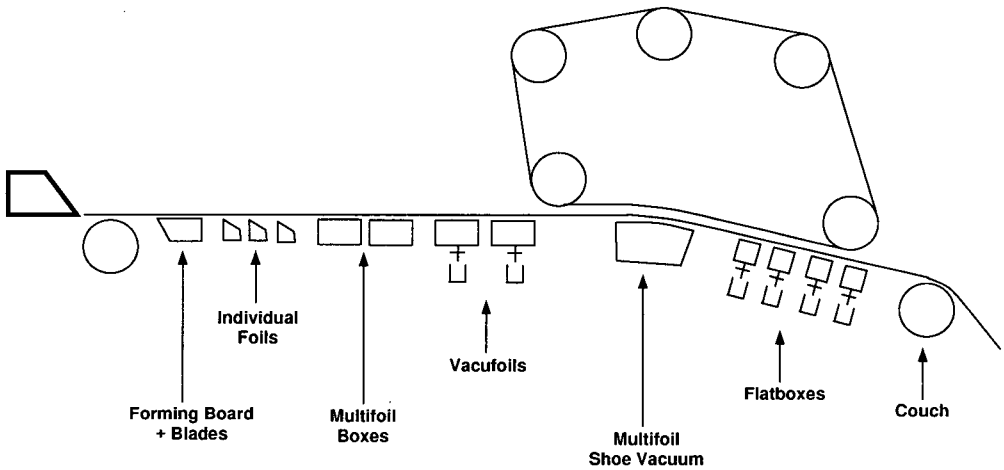

Figure 3.5: Drainage elements on wire

The following development follows directly from Branion (1978) who also discusses limitations of this theory. Darcy's equation for drainage through a porous bed is,

$$Q = \frac{A(-\Delta P)}{\mu(R_W + R_M)L} \tag{3.24}$$

where,

- Q is the volumetric flowrate through the bed (m^3/s)
- A is the cross-sectional area over which the vacuum is applied (m^2)
- μ is the viscosity of the fluid ($kg/m \bullet s$)
- ΔP is the applied vacuum (Pa)
- R_W and R_M are the specific filtration resistance of the wire and fibre mat ($1/m^2$)

- L is the depth of the porous bed (m)

While Darcy's equation ignores inertial effects of fluid flow which will certainly be present on a high speed paper machine, it provides a first-order approximation to the effects of changes in operating conditions. Equation 3.24 may be applied at each drainage element j and the total drainage from the wire determined as the sum over all Q_j's. The vacuum created by individual foils was determined by applying the analysis of Taylor (1958) and measured on-machine foil angles. The depth of the porous bed, L, is assumed equal to the mat thickness at each drainage element. Accordingly, a basis weight profile is estimated by applying a mass balance at each drainage element with instantaneous retentions, ϕ_j, calculated using the equation given in Han (1962),

$$\phi_j = 1 - (1 - \phi_j^o)\exp(\beta \bullet B_j) \tag{3.25}$$

where B_j is the basis weight at element j. The initial retention, ϕ_j^o, is estimated using the previously mentioned snapshot drainage studies. The parameter β is determined at each iteration so that the boundary conditions,

$$\begin{cases} B_0 = 0 \\ B_{10} = \text{Dry end basis weight - Small losses to flat boxes} \end{cases}$$

are satisfied. Except for the first drainage element, R_W is considered negligible compared to R_M. The mat specific filtration resistance can be evaluated by the Kozeny-Carman equation,

$$R_M = \frac{kC_M^2\sigma^2}{(1-\alpha C_M)^3} \tag{3.26}$$

where,

- the Kozeny "constant", k=5.55 (k is more rigorously a function of mat porosity)
- C_M is the mat compaction
- α is the solids specific volume (=1/ρ)

Mat compaction is used as an adjustable parameter such that an overall water mass balance is satisfied. While C_M will, in reality, vary across the drainage elements, a single, overall compaction is calculated in order to maintain numerical stability of the algorithm.

Furnish specific surface area, σ, is calculated at each time step from assumed dimensions of the individual furnish components in the fibre mat including flocs formed as a result of chemical additions. Specific surface area is one of the main factors affecting drainage performance in that a greater degree of flocculation leads to a reduction in σ which in turn enhances drainage. The total surface area of the mat to which draining water is exposed depends on how tightly the individual furnish particles are bound in the flocs. Two extremes exist. One is that individual particles are very loosely bound and so the surface area is equal to the total of all the furnish particles. The other is that the furnish particles are very tightly bound so that the flocs effectively form a sphere. A sliding scale between these two extremes can be characterized by a single parameter, the value of which was determined during calibration of the model. It was found that the best value of the parameter was very nearly toward the tightly bound extreme. This can be considered as a crude model of the sheet structure. However, further characterization of this structure and in particular its sensitivity to chemical additions would be valuable. Operator controlled effects included in the wire drainage model are summarized in the following block diagram.

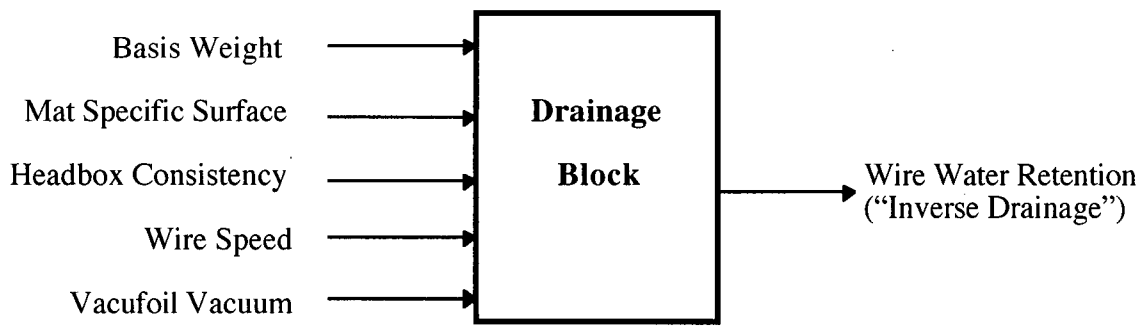

Figure 3.6: Input/outputs diagram for wire drainage model

Bound Water

Water is bound to the surface and interstices of individual cellulosic particles through both capillary and surface chemical forces (Lindström (1992)). As a result, fibres and fibre fines swell to a degree depending on the fibre/fines surface charge density, their internal pore structure and elasticity as well as the ionic strength and valency of counterions present in the surrounding aqueous medium. Fibre fines are known to retain approximately four times the amount of bound water compared with the long fibre fraction (Stone et al. (1968)). Water may also be bound to calcium carbonate surfaces through capillary forces arising from the porous nature of this filler (Brown (1996)).

Variations in the composition of the furnish components in the paper sheet lead to variations in the amount of effort required to remove this water, usually evident in the dryer steam demand. This is particularly true during grade changes and it is therefore important to be able to predict the amount of bound water leaving the couch. In the simulation environment this is accomplished by assigning specific amounts of bound water for each type of furnish particle.

The amount of water bound to furnish components can be measured experimentally by the Water Retention Value (WRV) discussed in Scallan and Carles (1972). In the present study values of 1.4 and 6.0 g water/g fibre were assigned to the long fibre and fines fractions respectively based on the data of Stone et al. (1968). To the author's knowledge, no values for WRV's for fillers have been reported in the literature. Accordingly, WRV's for PCC and chalk fillers were measured in the lab using the method of Appendix A yielding values of 0.84 ± 0.12 and 0.22 ± 0.03 g water/g filler respectively. These values, in relation to those for cellulosic particles, are consistent with the less porous and more rigid internal structure of such mineral fillers. Furthermore, as PCC has a much larger specific surface area due to its scalenohedral crystalline structure, its significantly larger WRV compared to that of chalk is

expected. We note that the four fold difference in measured WRV between PCC and chalk relates directly to their relative specific surface areas as reported by Blixt (1995). This suggests that electrostatic type interactions between water molecules and the calcium carbonate surface might play a role in determining the amount of bound water in addition to the capillary action of pores. However, further studies would have to be performed in order to confirm this mechanism.

3.3 Chemistry Modelling

The interaction between chemical and furnish components is modelled as 1) adsorption of each of the additives onto furnish components at their respective mixing points and 2) flocculation of the (partially) covered components just prior to and in the headbox. Deactivation of the adsorbed polymers is also considered. Each of these effects will be discussed in turn. Implementation of these models in the simulation environment required the establishment of a chemical process parallel to the above physical process.

3.3.1 Adsorption of Additives

Adsorption of polymers onto papermaking particles has been shown to follow Langmuir kinetics (van de Ven (1993)). In dimensionless form this can be expressed as,

$$\frac{d\theta}{dt} = k_{att}(n_o - \theta)(1 - \theta) - k_{det}\theta \qquad (3.27)$$

where,

- θ is the fractional polymer coverage of the particle surface,
- n_o is the dosage of polymer relative to the amount required to completely cover the particle surface,
- k_{att} and k_{det} are the attachment and detachment rate constants respectively.

If it is assumed that the bonds formed are sufficiently strong such that k_{det} is negligible, then as $t \rightarrow \infty$ Equation 3.27 leads to,

$$\theta = n_o \tag{3.28}$$

which is applicable to adsorption of a single polymer onto a particular furnish. In a multicomponent system, to calculate n_o for adsorption of polymer P on particle j we have,

$$n_o^{P/j} = \frac{c_o^P}{\sigma_j \bullet N_j \bullet \Gamma_{P/j}^{Max}} \tag{3.29}$$

where,

- c_o^P is the concentration of polymer (kg/m^3)
- σ_j is the surface area of an individual particle j (m^2/particle)
- N_j is the number concentration of particles j (particles/m^3)
- $\Gamma_{P/j}^{Max}$ is the maximum amount of polymer per unit surface area (kg/m^2)

The denominator in Equation 3.29 describes the total potential for adsorption of polymer P onto the surface of particle j. Therefore the polymer should distribute itself amongst the furnish components in a manner proportionately to this potential or,

$$\begin{aligned} \theta^{P/j} &= n_o^{P/j} \bullet \frac{1/n_o^{P/j}}{\sum_j \left[1/n_o^{P/j}\right]} \\ &= \frac{1}{\sum_j \left[1/n_o^{P/j}\right]} \end{aligned} \tag{3.30}$$

Thus, the fractional coverage of fibre surfaces by added polymer is equal for each furnish component. However, it is important to note that the much greater specific surface areas of fine particles means that they will adsorb a disproportionately large amount of the total polymer.

Values for $\Gamma_{P/j}^{Max}$ may be determined experimentally from polymer adsorption plateaus. It does not appear to be common practice amongst suppliers or users of these additives to conduct such experiments. However, a number of studies have appeared in the literature from which approximate values can be taken (e.g. Hedborg (1992)). The nominal values used for this study are $\Gamma_{LMW+}^{Max}=5x10^{-6}$ kg/m^2, $\Gamma_{Starch}^{Max}=1x10^{-5}$ kg/m^2 and $\Gamma_{HMW-}^{Max}=1x10^{-6}$ kg/m^2. Here Γ^{Max} associated with a particular polymer is used for each of the furnish components onto which it adsorbs. While these represent approximate values for this system any inaccuracies can be, in part, accommodated for by adjusting semi-empirical rate constants in the flocculation process model discussed in the following section. Furthermore, the effects of changing retention of a particular additive on furnish surfaces can be examined in the simulation environment by varying Γ^{Max} values.

The above implies that there is sufficient time for all the available polymer to adsorb onto particle surfaces. In order to justify this, approximate adsorption time scale calculations were performed as outlined in van de Ven (1993). For the adsorption of polymer P onto particle j the characteristic time constant, $\tau^{P/j}$, for reaching the adsorption plateau is,

$$\tau^{P/j} = \frac{1}{\gamma^{P/j}\alpha_{Fast}k_o^{P/j}N_j n_o^{P/j}} \tag{3.31}$$

where,

- $\gamma^{P/j}$ is the deposition efficiency which is dependent on the ratio of repulsive to attractive colloidal (chemistry dependent) forces
- α_{Fast} is the collision efficiency which depends on the ratio of (attractive) van der Waals forces to hydrodynamic forces
- $k_o^{P/j}$ is the Smoluchowski rate constant (m^3/s)

For the purposes of time scale calculations, it is assumed that $\gamma^{P/j} = \alpha_{Fast} = 1$ due to the (designed) high affinity of additives for furnish surfaces and the observation of van de Ven (1993) that α_{Fast} in papermaking systems is close to its maximum of 1. For collisions between a polymer molecule and a furnish particle the Smoluchowski rate constant for shear induced (othokinetic) collisions is $k_o^{P/j}=0.4G \bullet V_j$. Using an approximate hydrodynamic shear rate of $G=10^4$ (1/s) (Kamiti and van de Ven (1995)) , it was determined that time scales for all cases were of the order of 1 second or less. Thus it is reasonable to assume that complete adsorption of additives onto furnish surfaces did occur.

Part of the function of the LMW Cationic Polymer is to neutralize dissolved organic or inorganic anionic substances which interfere with the performance of the retention aid system. Such substances are present in the incoming pulp and may be released in small amounts during repulping operations in the broke handling system (Lindström (1992)). For purposes of this simulation, a given percentage of the LMW Cationic Polymer is assumed to be neutralized by such interfering substances. The effects of variations in this disturbance on the papermaking process can be investigated through this parameter.

The coverage of any furnish component by each of the three additives is tracked throughout the wet end via the parallel chemistry simulation. At stream mixing points the exit coverages for each component are calculated as the mass weighted average of the incoming stream coverages. In tanks, appropriate (first-order) lag dynamics are introduced assuming perfect mixing of the components. The nature of this parallel chemistry system can be seen in Figure 3.7 where blocks representing adsorption chemistry and mixing of stream coverages are calculated alongside standard process blocks. Information about the chemistry of a particular stream is contained in the "stream chemistry array" denoted by SCA tags on the flowsheet.

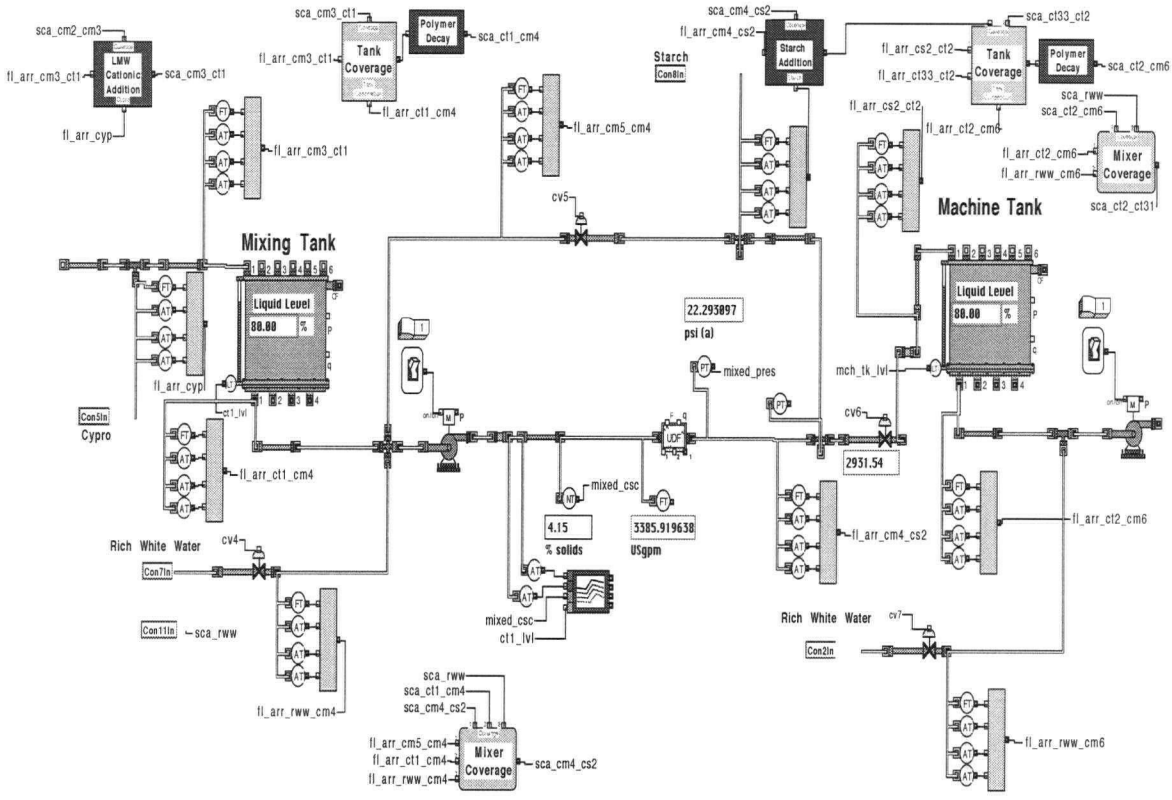

Figure 3.7. Illustration of parallel chemistry system on process flowsheet

3.3.2 Flocculation

Flocculation of the partially covered furnish components takes place immediately following the adsorption of the HMW anionic polymer. A collision theory approach is used to determine rates at which flocs are formed (van de Ven (1993)). For the purposes of this simulation, flocs are defined as a joining of any two particles. In this way, a new component is temporarily formed as all flocs delivered to the wire are assumed retained in the sheet along with all unflocculated long fibres. Only 5% of unflocculated fibre fines and 1% of unflocculated filler delivered to the wire are retained by mechanical entrapment, values which have been approximated by current mill retentions and theoretically justified by van de Ven (1984). Thus, variations in first-pass retention are realized through chemical and furnish interactions prior to the wire.

HMW anionic polymer is thought to partially adsorb onto furnish particles leaving long tails extending outward from the particle surface to a distance beyond the electrical double layer. Bridging flocculation occurs when these tails interact with another particle and a bond of sufficient strength is formed to withstand the hydrodynamic shears present (Gregory (1988)). In the standard model for bridging flocculation, based on a single polymer, effects related to the fractional polymer coverage take the mathematical form $\theta(1-\theta)$. This represents the fact that polymer adsorbed onto particles with coverage θ must interact with uncovered areas on another particle in order to form a bridge. In our multi-component system, it is envisioned that the HMW anionic polymer adsorbed onto particle i with coverage θ_i^- interacts with sites on particle j with adsorbed cationic polymer of coverage θ_i^+. Assuming detachment rates are negligible, the rate at which flocs composed of particles **i** and **j** are formed is described by the following second-order kinetic equation,

$$\frac{dC_{ij}}{dt} = k^{ij} C_i C_j \theta_i^+ \theta_j^- \left(\frac{V_i V_j}{V_i + V_j} \right) \tag{3.32}$$

where,

- k^{ij} = Flocculation rate constant for collisions between components i and j,
  $= k_o^{ij} \gamma^{ij} \alpha_{Fast}$
- C_{ij} = consistency of flocs formed from components i and j,
- C_i, C_j = consistencies of components i and j,
- V_i, V_j = volumes of individual component particles i and j
- θ_i^+ = fractional coverage of component i by cationic polymer,
- θ_j^- = fractional coverage of component i by anionic polymer.

The term involving individual particle volumes arises when transforming a differential equation in terms of rates of particle interactions to consistencies through $C_i=V_iN_i\rho$ and noting that the volume of the formed floc is V_i+V_j. As in the previous section, it will be assumed that $\alpha_{Fast}=1$. However, it may not be reasonable to assume that the $\gamma^{ij}=1$. Instead, we replace these parameters with four empirical rate constants, r^i, each associated with a furnish component (long fibre, fibre fines, filler and flocs). This gives,

$$k^{ij} = k_o^{ij} r^i r^j \tag{3.33}$$

for which the values of the r^i's can be determined such that nominal retentions and white water consistencies around the paper machine are obtained. In general, the r^i's were found to be much greater than unity (sometimes orders of magnitude) indicating the approximate nature of the furnish particle size distribution and Smoluchowski rate constants.

The result is a set of 16 differential equations describing all possible interactions amongst the four components. These are numerically integrated over the transportation time between the HMW anionic polymer addition point and delivery of the stock to the wire ($\cong$11 sec). Initial consistencies for the long fibres, fibre fines and filler are those present at the addition point while the initial floc consistency is zero. Floc consistency and radius are updated at each integration interval as aggregate quantities of all flocs formed. Floc radius is calculated as the total mass of particles in flocs divided by density. Typical component trajectories are shown in Figure 3.8. The apparently large degree of flocculation results from defining flocs as the joining of any two particles. Thus a filler particle adsorbed onto a long fibre is here defined as a floc which would not be discernible by visual techniques for determination of the degree of flocculation in a sheet.

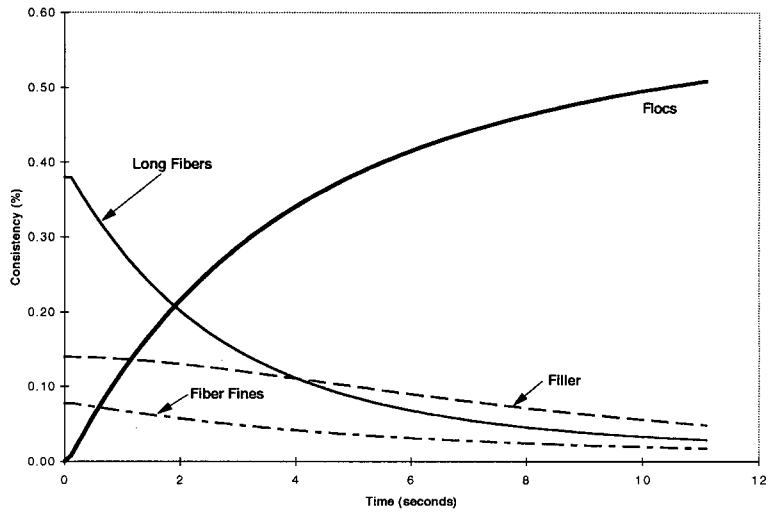

Figure 3.8: Component trajectories during flocculation process

A certain amount of flocculated stock is recirculated from the headbox to the white water silo and deaerator. Since they subsequently pass through points of high shear such as fan pumps, screens, etc., it is assumed that these "hard" flocs are destroyed. Formation of "soft" flocs through particle agglomeration, which results from adsorption of cationic additives onto negatively charged fibre surfaces, is not considered in this study. As well, flocculation due mechanical entanglement of fibres is not modelled.

3.3.3 Deactivation of Polymers

For the purposes of this simulation, coverage of particles by polymers affects retention and drainage only through the flocculation process described by Equation 3.32. Upon adsorption onto furnish surfaces polymers are believed to undergo reconformation into flat configurations and further diffusion into particle pores (Koethe and Scott (1993). The surface charge behaviour of particles over time after addition of cationically charged polymers has been studied by Koethe and Scott (1993) and for starch by Gupta and Scott (1995). It was found that addition of polymer resulted in a rapid, instantaneous increase in surface charge followed

by exponential charge decay to approximately 50% of the originally level. Time constants for this study were typically in the order of 20 minutes.

In order to implement such behaviour in the present model it was assumed that the coverage of cationic additives underwent similar behaviour. In this way their effectiveness during the flocculation process diminishes with time. This view is consistent with the electrostatically dominated flocculation mechanism put forward in the previous section. From the above mentioned studies by Scott and coworkers, charge decay data was used from the most appropriate (of several) examples which matched the current additives and furnish characteristics. For LMW cationic polymer, data from polymer P-II in Koethe and Scott (1993) was used while for starch, data from Figure 4 in Gupta and Scott (1995) was used. Corrections were made for chemical dosage rates.

At the initial, fully charged conditions, coverage was assumed to equal those values calculated by Equation 3.34. Decay in these coverages proceeded at a rate proportional to the corresponding charge decays. The resulting models for decay of LMW cationic and starch coverages are:

$$\begin{aligned} DF_{LMW+}(t) &= 0.452 + 0.548e^{-0.0416t} \\ DF_{Starch}(t) &= 0.455 + 0.546e^{-0.0357t} \end{aligned} \tag{3.34}$$

where DF is the (decay) factor by which the corresponding coverage is multiplied at any point in the wet end and t (minutes) is the time from chemical addition. In order to implement these models in the simulation, mean residence times for each process unit with capacity (e.g. tanks) were computed and the coverages updated at the exit of each.

The HMW anionic polymer is also believed to undergo similar reconformation onto the particle surface. However, this leads to greatly reduced rates of flocculation for reasons described by

Pelssers et al. (1989). Thus, particles recirculated through either the white water or broke systems are assumed to lose any active HMW anionic polymer coverage.

3.4 Summary

The models implemented into a dynamic simulation have been explained. Figure 3.9 summarizes many of the interactions present in the simulator. Other standard effects not included in this diagram are furnish composition, controller tunings and process configuration.

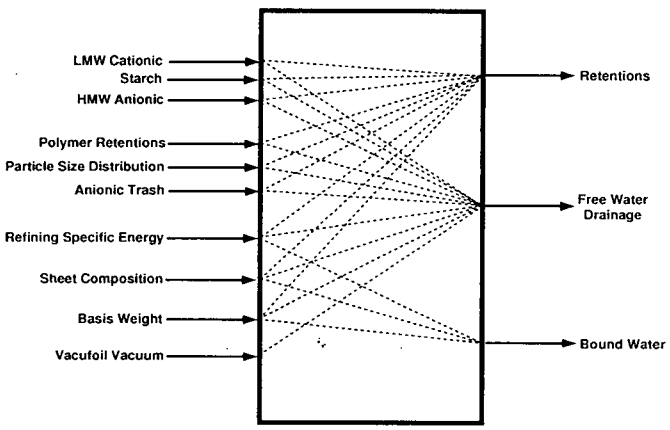

Figure 3.9: Block diagram of simulator capabilities

There may be some important chemistry phenomena missing in the above diagram. For example, part of the function of the LMW Cationic polymer is to act as a drainage aid by deswelling fibres. However, during a mill sampling campaign, no concrete relationship showing this effect could be determined and it is therefore excluded in the present simulation. The complete IDEAs process flowsheets are shown in Appendix B.

A major advantage to the modular manner in which fundamental effects are implemented in the simulation is that as further relationships are uncovered amongst process variables, they can be implemented into the simulation without affecting the existing model. Thus one can test whether certain effects are responsible for observed but unexplained variations. It is also important to emphasize that other paper machines with different wet end configurations and furnish can be modelled once the necessary process parameters have been obtained.

Chapter 4

Validation of Simulation

Development of the wet end chemistry simulation model proceeded in a stage-wise fashion with calibration and subsequent validation at each step. First, a steady-state balance was achieved from which the dynamic simulation followed. Validation was carried out using the process experience of mill personnel and on-line data. Both of these sources of information proved of great importance. This section presents these various stages of model building and tests simulation results during a number of operating scenarios.

4.1 Steady-State Material Balance

The first step in verifying the accuracy of the simulation is to obtain steady-state conditions which match those of the operating paper mill. Since numerous grades are produced on the machine typical conditions representative of one offset grade were used.

The general procedure followed to achieve the overall steady-state balance was:

1. Obtain a steady state balance from each of the 7 process and instrumentation diagrams and adjust simulation flows to match. Here, water and total solids were the only components considered. Most dynamic models (described in Chapter 3) were included along with controllers. Retention and drainage levels were assumed fixed.

2. Combine these individual worksheets to obtain an overall initial total mass balance and solids consistencies.
3. Update consistencies to match those currently observed on the paper machine. Such information was obtained from mill operating records and (previous) sampling campaigns.
4. Incorporate fiber fines and filler into the simulation. Intermediate starting values were obtained by rough hand calculations and further details of these components will be discussed shortly. The simulation was then allowed to come to steady-state with the four components.
5. The wire drainage and chemistry models were added, one at a time, allowing the simulation to reach steady-state after each. Certain drainage and chemistry parameters were adjusted in order to match the representative mill conditions. These conditions will be discussed shortly.

Most of the models for fines and filler behaviour in processing units were discussed in Chapter 3. The procedure at the refiners will now be discussed in more detail. Due to the presence of a recirculation around the refiners the fibers are exposed to multiple passes. In order to achieve an overall degree of refining this recirculation must be modelled. The degree of refining is expressed as the percentage of long fiber fraction converted into fiber fines.

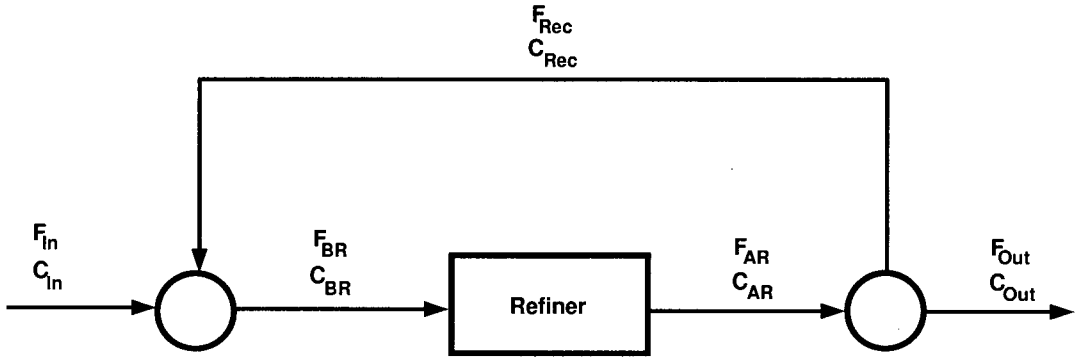

Figure 4.1: Recycle flow of fiber through refiners. F is the mass flowrate and C is the fiber consistency at any point.

Consider the refiner with recycle in Figure 4.1. A fiber balance at the input node gives

$$C_{IN}F_{IN} + C_{Rec}F_{Rec} = C_{BR}F_{BR} \tag{4.1}$$

Multiplying through by $C_{Rec}/(C_{BR}C_{In})$ gives,

$$\frac{C_{Rec}}{C_{BR}}F_{In} + \frac{C_{Rec}}{C_{In}}\frac{C_{Rec}}{C_{Br}}F_{Rec} = \frac{C_{Rec}}{C_{In}}F_{BR} \tag{4.2}$$

Noting that $C_{AR} = C_{out} = C_{rec}$ and defining,

$$R = \frac{C_{Out}}{C_{In}} \quad \text{(Overall long fiber refining ratio)}$$

$$R^* = \frac{C_{AR}}{C_{BR}} \quad \text{(One - pass long fiber refining ratio)} \tag{4.3}$$

leads to,

$$R^*F_{In} + R^*RF_{Rec} = RF_{BR} \tag{4.4}$$

Using the overall mass balance around the input node gives the desired one-pass long fiber conversion to fines in terms of the specified overall conversion and flowrates,

$$R^* = \frac{R\left(1 + \frac{F_{Rec}}{F_{In}}\right)}{1 + R\left(\frac{F_{Rec}}{F_{In}}\right)} \tag{4.5}$$

This expression can be implemented into the refiner object on the simulation process flowsheet.

The primary markers used to calibrate the steady-state simulation for a typical offset grade sheet are:

Production	34 ton/hr
Basis Weight	73 g/m^2
Sheet Ash	17%
Headbox Solids Consistency	0.60 - 0.65%
Flume Total Solids Consistency	0.1%
Flume Filler Consistency	0.06%
Couch Solids Consistency	20%
Solids Retention	85-90%
Filler Retention	65%
Cloudy Filtrate Solids Consistency	0.14%

The empirical rate constants, r_j, of Equation 3.33 were the final tuning parameters adjusted in order that the above conditions were achieved. While each r_j is associated with a particular component, adjusting any one of their values affects the flocculation of not only that component but of all others as well. This strong degree of correlation inhibits easy tuning of the system. It may be possible to determine the underlying dimensionality of this system through singular value decomposition or other chemometric techniques (Wise (1994)). From this a smaller or uncorrelated set of tuning parameters might be found. However, this was not undertaken in the present project.

The base case simulation conditions achieved were:

Basis Weight	73.0 g/m^2

Sheet Ash	17.0 %
Production	32.4 ton/hr
Hardwood/Softwood Ratio	70:30
%Broke of Total Mix	17.0%
Couch Solids Consistency	19.4%
Cloudy Filtrate Solids Consistency	0.13%
Headbox Solids/Filler/Fines Consistencies	0. 60 / 0.14 / 0.08 %
Flume Solids/Filler/Fines Consistencies	0.074 / 0.055 / 0.020 %

Results for the steady-state distribution of long fibers, fiber fines and filler throughout the wet end are shown in Figure 4.2 in the same format as in Orccotoma (1996). Note that the diagram shows proportions and not absolute quantities.

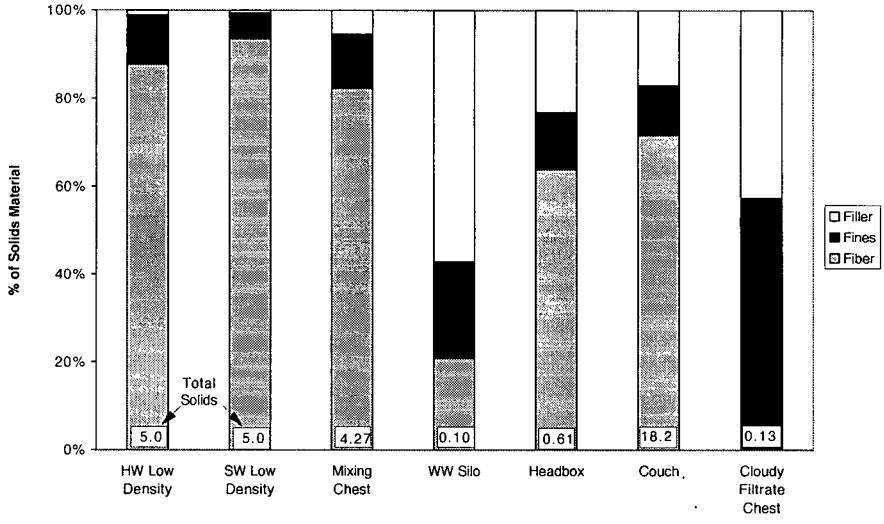

Figure 4.2: Steady-state distribution of fiber, fines and filler fractions

Initial assumed fiber fines (mass) contents of baled hardwood and slushed softwood are 10% and 5% respectively which agree roughly with values reported by Britt (1975). The presence of filler in the mixing chest illustrates fines buildup in the incoming stock line due to broke and white water recirculation. At the headbox, the total fines content is greater

than 30% of the solids material which decreases by the couch due to more favourable retention of the long fiber fraction. Filler content is a proportionately higher fraction of the fines in the white water silo due to its poorer retention. Cloudy white water, which is distributed through the long circulation to stock dilution points, is made up of roughly the same proportions of fiber fines and filler material.

4.2 Simulated Step Tests

This section implements step tests into the simulation and analyzes the response mechanisms and directionality. The validity of the simulation has been judged against process experience by both the author and Weyerhaeuser personnel. Of equal importance to the correctness of the retention and drainage responses is identification of the mechanisms by which they are achieved.

4.2.1 HMW Anionic Polymer Step Increase

A simulated 10% step increase in HMW Anionic Polymer (retention aid) was implemented in the simulation model starting from the conditions given in Section 4.1. The step occurred at t=60 minutes.

Polymer coverages on the long fiber fraction at the headbox are shown in Figure 4.3. The immediate increase in retention aid coverage is expected with some beneficial dynamics as the white water short circulation becomes cleaner. Also seen is a slight slow rise in the starch coverage as fines are cleaned out of the white water long circulation.

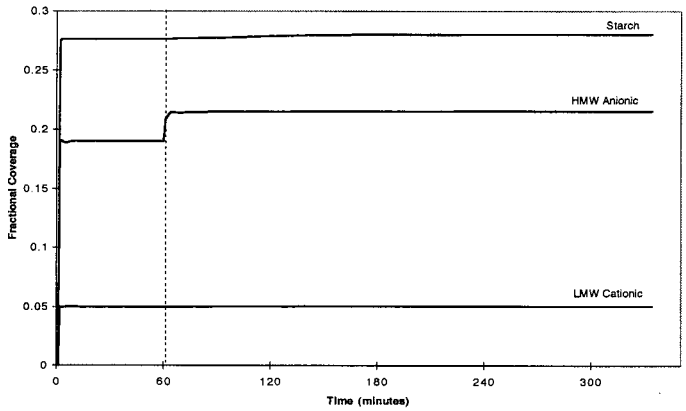

Figure 4.3: Polymer coverages on long fiber fraction for 10% HMW Anionic increase

Figure 4.4 shows the component consistencies after flocculation, i.e. of the stock delivered to the wire. The floc consistency, after some initial dry end controller dynamics, remains approximately constant. From the large, immediate drop in filler consistency it is apparent that the largest gains in flocculation are in capturing filler particles. The overall consistency of the stock on the wire drops as the retention increases.

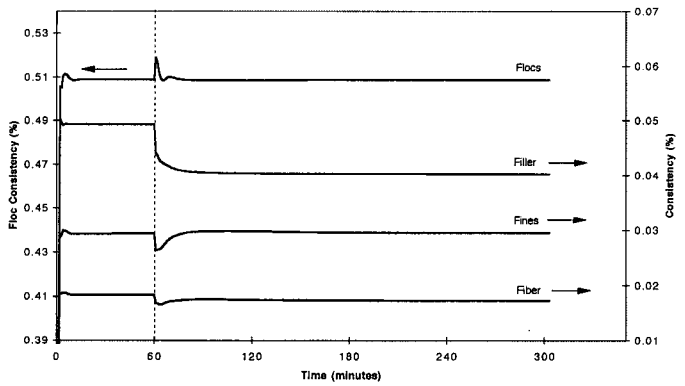

Figure 4.4: Consistencies of stock delivered to wire for 10% HMW Anionic increase

Dry end controller dynamics play an important role in the overall machine responses to wet end chemistry variations. In Figure 4.5, the basis weight shows an initial jump due to increased retention of filler. The controller responds by lowering thick stock flow. However, as seen in Figure 4.6, the increase in sheet ash causes a simultaneous decrease in fresh filler flow. The result is overshoot in the basis weight control and the short term

oscillatory response observed. Over the longer term, there is a slight decrease in thick stock demand due to decreased amounts of filler in the recirculated white water. The filler balance in the short circulation is relatively slow to recover. In addition to the long circulation dynamics mentioned above, there are also some "medium" circulation dynamics due to the silo→white water chest→cleaner dilution→headbox pathway.

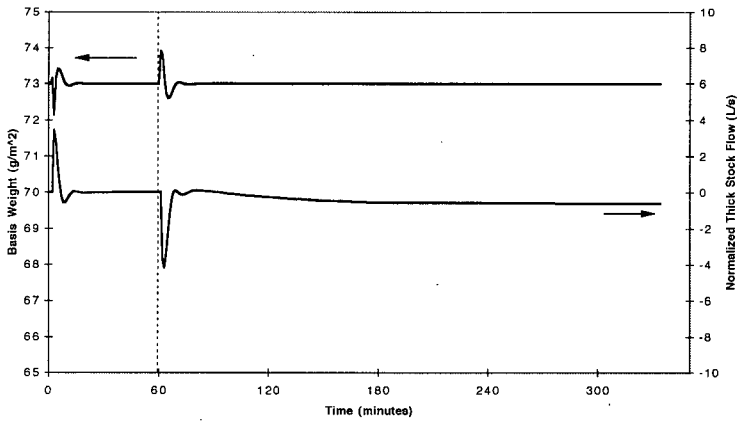

Figure 4.5: Basis weight and thick stock flow response to 10% HMW Anionic increase

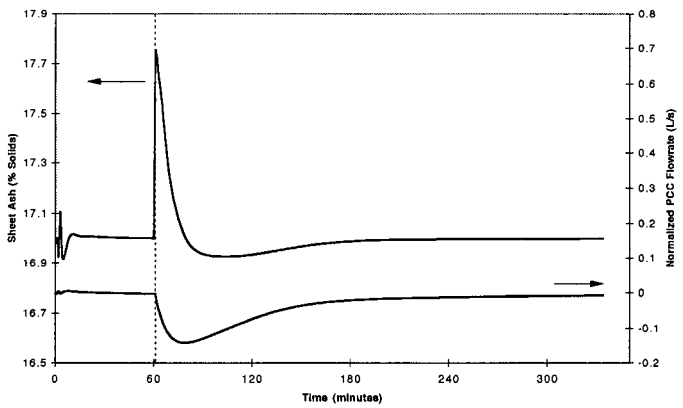

Figure 4.6: Sheet ash and fresh filler flowrate response to 10% HMW Anionic increase

Flume consistencies reflect the above phenomena as shown in Figure 4.7. The drop in flume solids is primarily the result of increased filler retention. This drop is rapid due to the combined effects of pulling filler particles into flocs and reduction of PCC flowrate from the ash controller action. Fiber fines drop initially with increased retention but recover somewhat with the basis weight loop response.

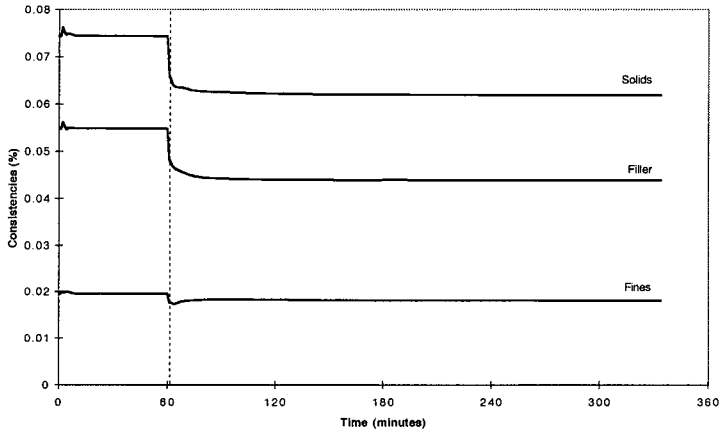

Figure 4.7: Flume consistencies for 10% HMW Anionic increase

Drainage responses are shown in Figure 4.8. Wire water retention is the fraction of water retained in the web after the multifoil shoe vacuum. It can be thought of as an inverse indicator of drainage. The rapid decrease in drainage directly follows the reduction of unflocculated filler in the stock delivered to the wire. Bound water at the couch follows the dry end controller dynamics but its steady state value remains constant.

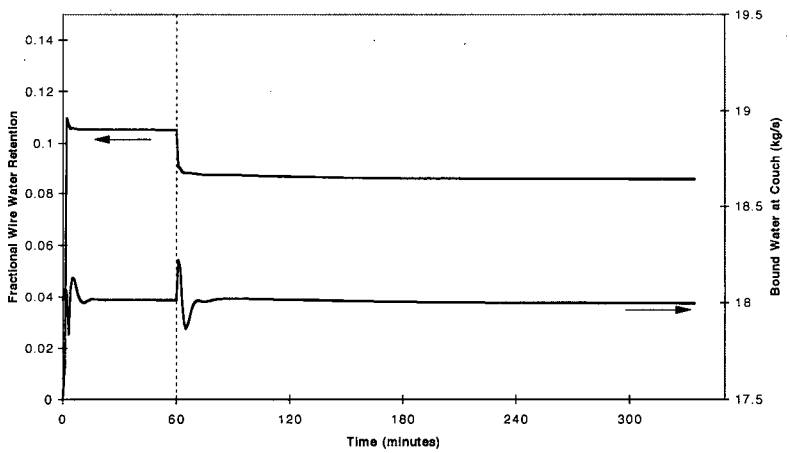

Figure 4.8: Drainage responses to 10% HMW Anionic polymer increase

Finally, cloudy filtrate consistencies are shown in Figure 4.9. In accordance with the increased filler retention, filler consistency drops. This causes the slight increase in starch

coverage seen in Figure 4.3. Fines consistency, on the other hand, shows some transient behaviour but no long term change in level. The overall impact of the retention aid change on cloudy filtrate consistencies is small.

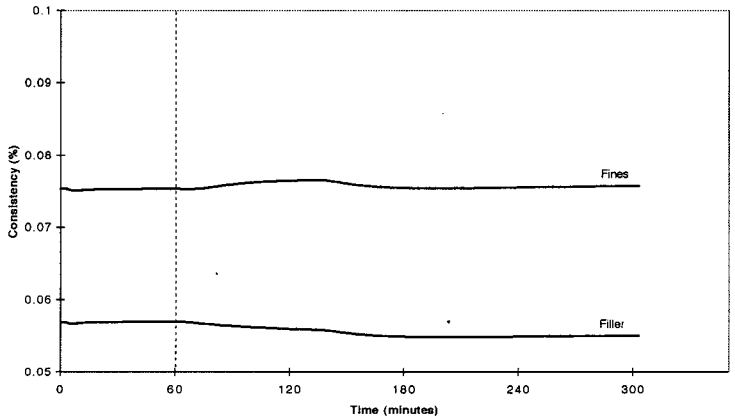

Figure 4.9: Cloudy filtrate chest consistency response to 10% HMW Anionic polymer increase.

4.2.2 LMW Cationic Polymer Step Increase

A 4% increase in LMW Cationic Polymer was implemented into the simulation in the same manner as the HMW Anionic Polymer in the previous section. The overall impact of such a change is much smaller than for the HMW Anionic but the mechanisms are similar. Because the polymer is added prior to the mix tank, the impact on retention and drainage at the wire is not immediate.

Figure 4.10 shows long fiber fraction coverages of starch and LMW Cationic polymer. The second-order dynamics induced by the mixing and machine chests are evident in the LMW Cationic coverage which is monitored at the headbox. Due to a slight decrease in stock demand with improved retention, there is a secondary increase in coverages evident in the starch.

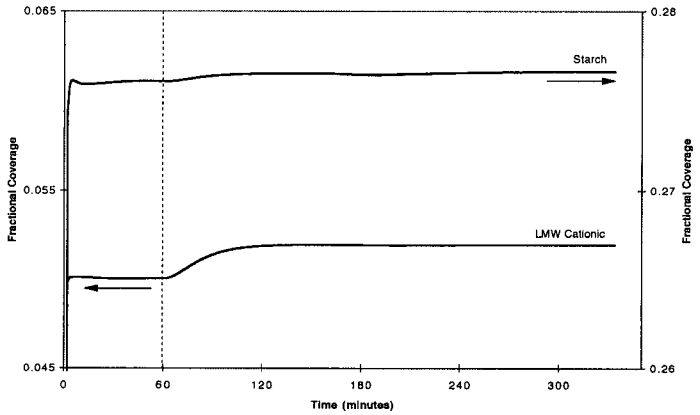

Figure 4.10: Long fiber fraction polymer coverages for LMW Cationic step increase

The filler and fines flume consistencies both decrease with the filler dominating as with the HMW Anionic polymer step. This is the result of greater flocculation of filler particles.

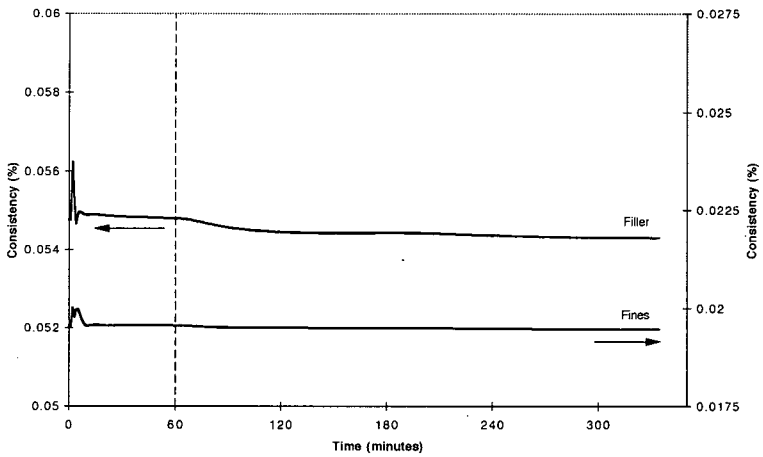

Figure 4.11: Flume consistencies for LMW Cationic step increase

The second-order dynamics are very apparent in the wire drainage response of Figure 4.12. A secondary decrease in water retention is also noticed at about 4 hours as a result of less fines present in the white water long circulation. However, no detectable effect is noticed in the coverages of Figure 4.10 from recirculation of undecayed polymer.

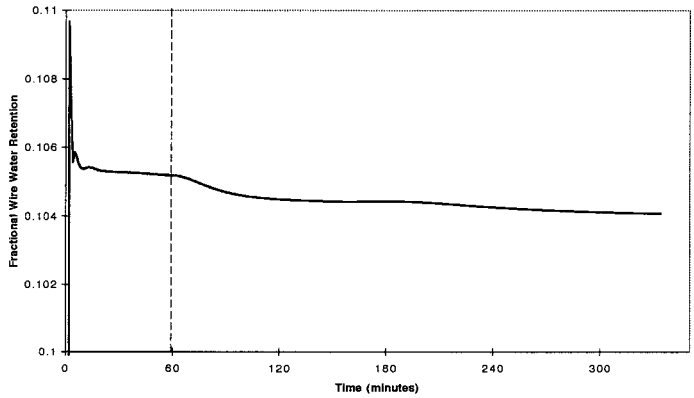

Figure 4.12: Wire drainage response for LMW Cationic step increase

4.2.3 Broke Step Increase

The effect of a step increase in broke content was simulated next. A step from the base condition of 17% broke to 30% was implemented at t=60 minutes. The most immediate effect was seen at the mix chest where the increases in fines and filler content are evident in Figure 4.13. These increases show essentially first order dynamics although there are additional effects introduced by the stock proportioning controller. The increase in filler content is dominant.

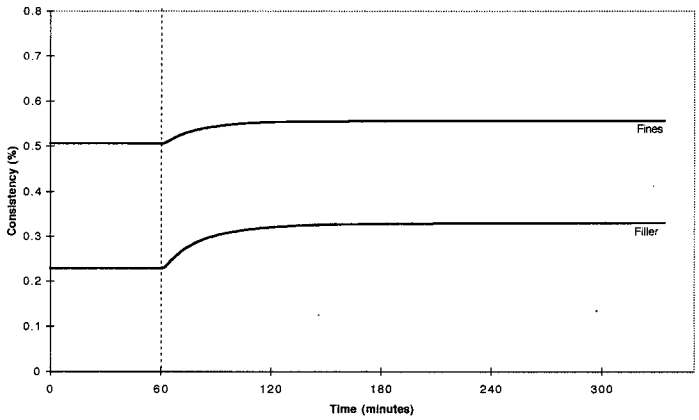

Figure 4.13: Mixing chest consistencies for broke step increase

As a result of the increased levels of fine particles in the system, polymer coverages decrease on the long fiber fraction as seen in Figure 4.14. However, as seen in Figure 4.15, the same is not true for the filler fraction. In this case the coverages of cationic materials increases with increasing broke due to the recirculation of partially covered furnish particles through the broke system. This effect overwhelms that due to replacement of previously uncovered virgin stock with more fine material. Coverage of HMW anionic polymer decreases on all furnish fractions due to the increased fines levels in the system. It is recalled that the model assumes complete deactivation of HMW anionic polymer activity as far as its role in the flocculation process.

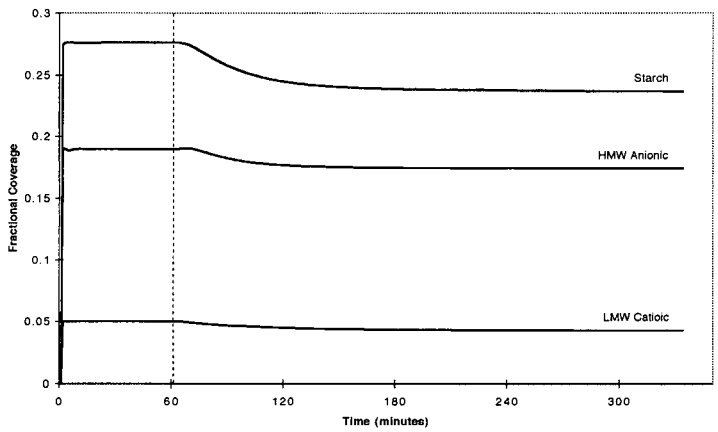

Figure 4.14: Additive coverages on long fiber fraction for broke step increase

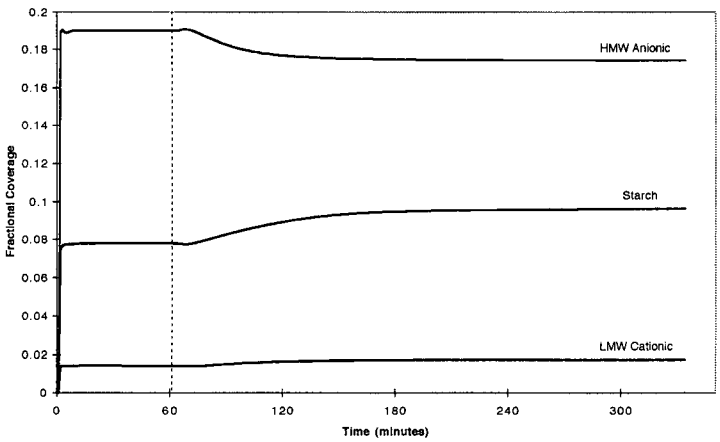

Figure 4.15: Additive coverages on filler for broke step increase

The transient sheet ash and fresh filler flowrate responses of Figure 4.16 are expected from the previous figures. As more filler enters into the system through the broke stream and this filler is preferentially coated with polymer, more of it will be incorporated into the sheet. Hence the transient rise in sheet ash content before regaining the set-point. With the higher filler recirculation, fresh filler demand is reduced.

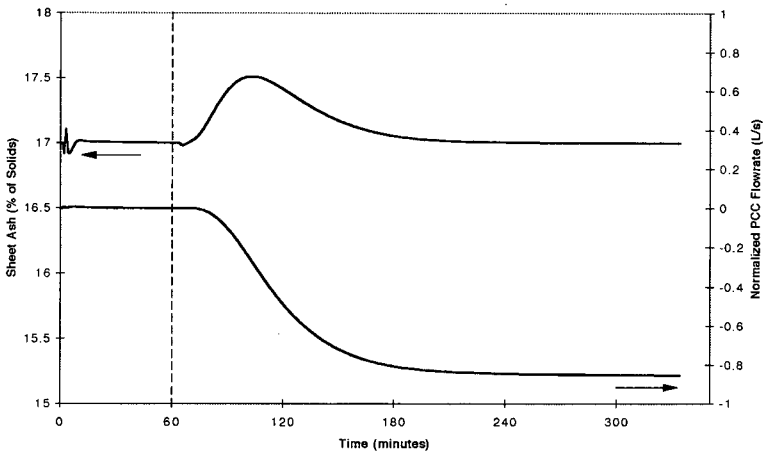

Figure 4.16: Sheet ash and fresh filler flowrate responses to broke step increase

Basis weight response (Figure 4.17) is more stable but does exhibit a short initial transient which is also visible in the sheet ash response. This short term transient is the result of reduced hardwood and softwood stock demand from the low density chests and a corresponding reduction in dilution water demand from the rich white water chest. The rich white water chest operates at constant head and also supplies dilution water to the primary cleaner rejects in the standpipe. With the stock dilution water decrease, additional water is sent to the standpipe creating increased stock flow through the cleaners. This manifests itself as an increase in accepts consistency as seen in Figure 4.18. This consistency variation transmits through to the primary fan pump discharge and onto the wire. While this effect is quickly compensated for by the basis weight controller it does serve to illustrate the fidelity of the simulation model. The thick stock flow experiences a

longer term increase to compensate for the lower proportion of fibrous material in the white water recirculation. It would appear from Figures 4.16 and 4.17 that the basis weight and ash controllers are fighting one another in order to respond to the changing furnish mix. Decoupling of these control loops should alleviate such problems.

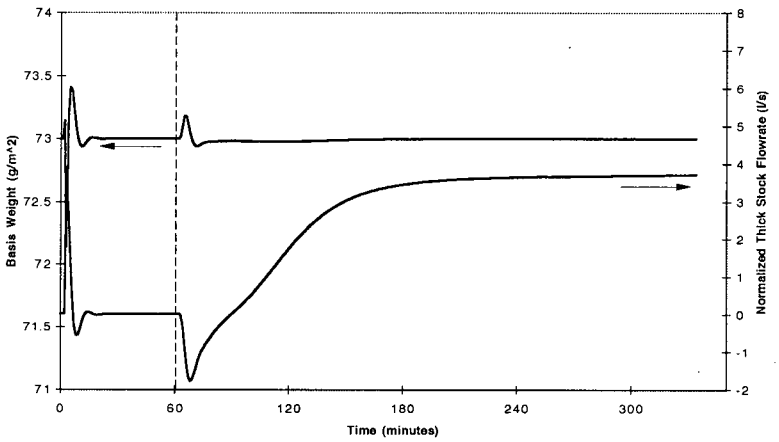

Figure 4.17: Basis weight and thick stock flow responses to broke step increase

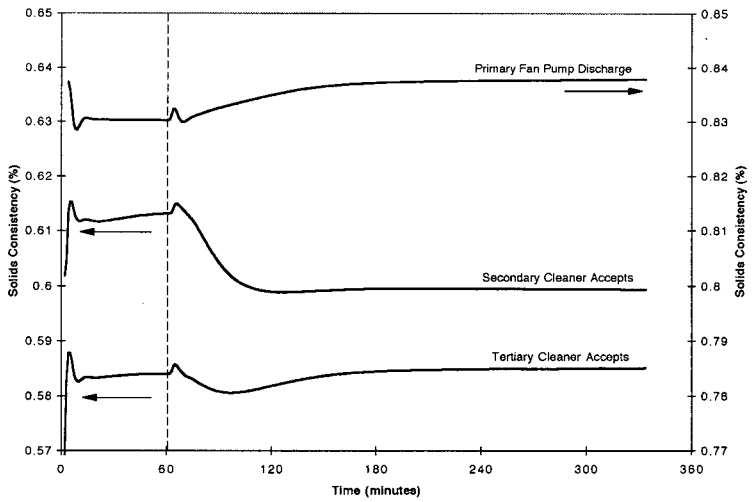

Figure 4.18: Effect of reduced hardwood and softwood stock demand through cleaner dilution circuit.

The initial drop in flume consistency seen in Figure 4.19 is due to the short term basis weight fluctuation noted above. The second-order dynamics are evident in the responses. The direction of the responses indicates that the overall increase in fines level and the

reduction in HMW Anionic polymer coverage are the dominant effect, although it is tempered by the increased cationic coverage noted in Figure 4.15.

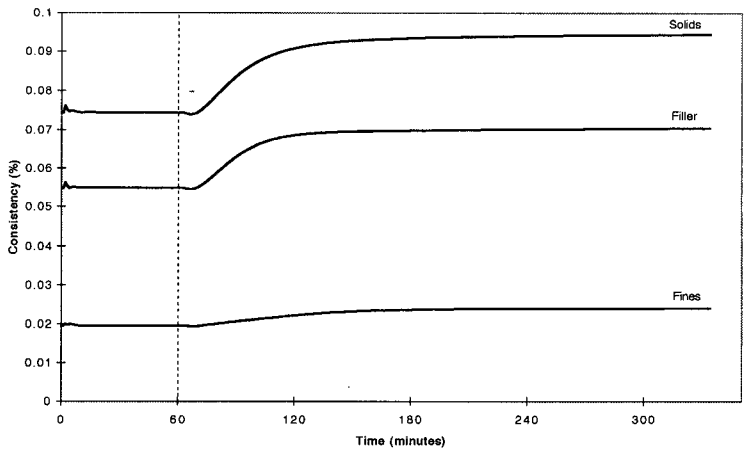

Figure 4.19: Flume consistency responses to broke step increase

Retentions are seen in Figure 4.20 to fall uniformly with filler being the most sensitive. Again this shows that the loss of HMW Anionic coverage on filler dominates over the gain in cationic coverage.

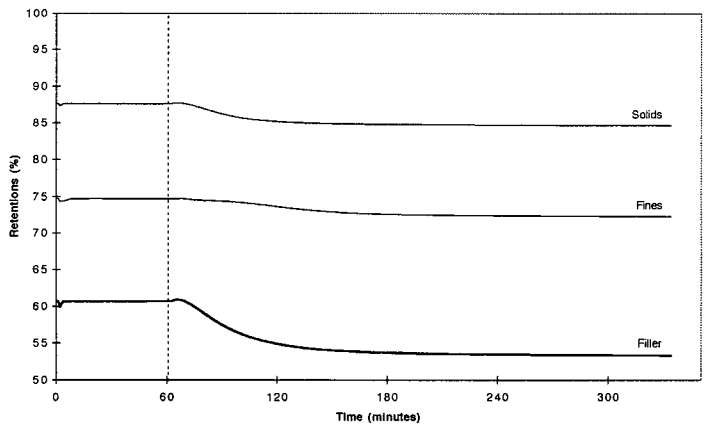

Figure 4.20: Retention responses to broke step increase

Finally, both the free and bound drainage responses of Figure 4.21 indicate a wetter sheet leaving the couch which corresponds to experience. The increased water retention on the

wire is due to a decreased level of flocculation and more free fine material. Bound water increases as fines make up a larger portion of the fibrous material. Generally second order dynamics are observed which is consistent with the broke addition point prior to the mix chest.

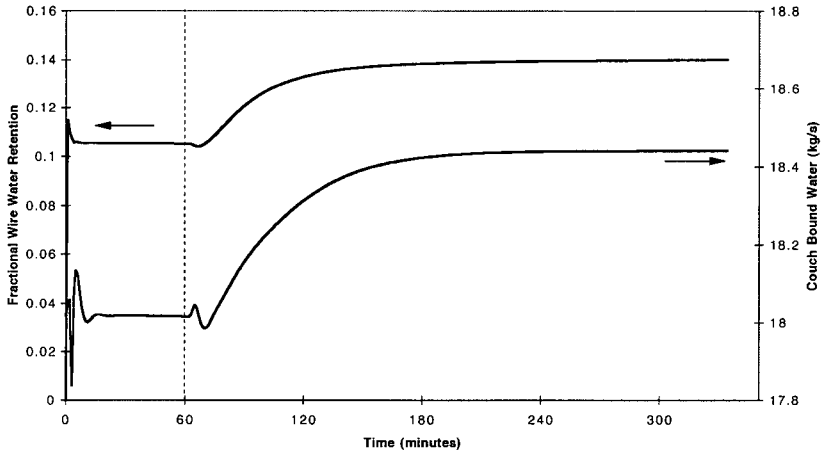

Figure 4.21 Drainage responses to broke step increase

4.3 On-machine Retention Aid Step Test

In order to test the validity of the model against machine data, an independent decrease in the retention aid level was implemented during a routine operating period. The actual form of the input signal was a ramp rather than a step as such sudden changes in the web structure and wetness might otherwise cause a sheet break. A ramp will excite fewer of the high frequency modes than a step but a good indication of the slower dynamics and gain will be available nevertheless.

A 30% ramped decrease in HMW anionic retention aid was simulated with the machine producing a 73 g/m^2 sheet at 17% filler content. Problems with the consistency sensor steady-state calibration were experienced during this time period but it is assumed that the dynamic response reflects actual conditions. Since the total solids bottom flume

consistency was often out of range, the filler consistency along with other signals were used to judge the validity of the retention dynamics.

A number of cases were simulated in order to demonstrate the effects of adjusting various parameters. These are summarized in Table 4.1.

Case	Γ_{Filler}^{Max} (kg/m^2)	Ash Controller Gain
1	1.0×10^{-6}	0.1
2	1.5×10^{-6}	0.1
3	2.0×10^{-6}	0.1
4	2.0×10^{-6}	0.5

Table 4.1: Parameters for HMW retention aid ramp increase.

Figure 4.22 shows the white water silo filler consistency responses to these changes. Cases 1 through 3 show the effect of increasing the maximum amount of HMW retention aid that adsorbs onto filler, Γ_{Filler}^{Max}, from Equation 3.29. As this quantity increases from its nominal value of 1×10^{-6} g (polymer)/m^2, the coverage of retention aid on the furnish particles decreases. This, in turn, leads to decreased retention and greater filler loadings in the white water. The interaction between filler level and retention aid dosage is evident on the response gains with higher filler loadings leading to higher gains. Thus the gain sensitivity to changes in the number of collisions between filler and other particles overwhelms sensitivity to changes in retention aid coverage.

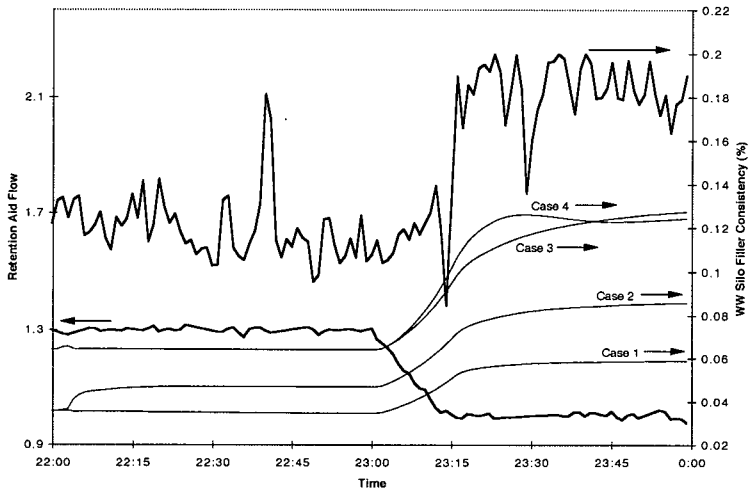

Figure 4.22: White water silo filler consistency responses to ramped retention aid decrease.

While the gain for Case 3 is close to the measured response the dynamics are somewhat slow. In Case 4 we have increased the sheet ash controller gain from 0.1 to 0.5 with other conditions as in Case 3. The result is a faster response with a slight overshoot. This matches very closely with the response measured in the silo. Part of the motivation for adjusting the controller gain arose due to the observed fresh filler flowrate dynamics. Figure 4.23 shows that the controller response of Case 4 to be very close to the actual. The large overshoot in the controller action demonstrates the tight tuning and interaction with the basis weight loop as noted in the step responses of Section 4.2.

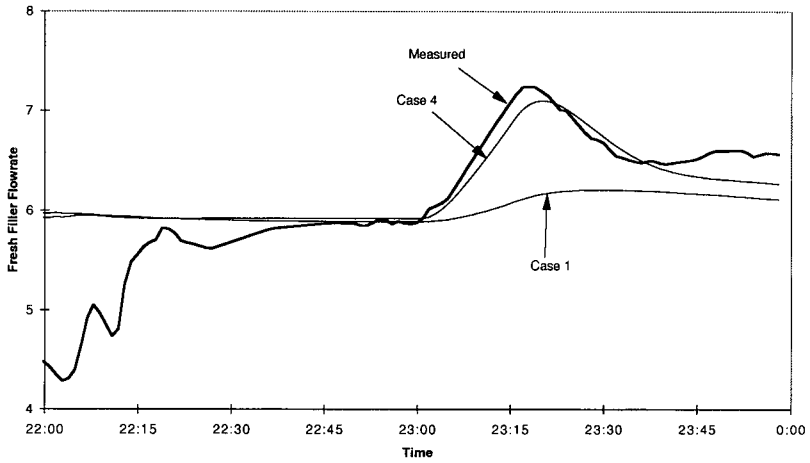

Figure 4.23: Fresh filler flowrate closed-loop response to HMW retention aid decrease

The 4th section dryer steam demand and wire water retention drainage responses are shown in Figure 4.24. The grade change slightly before 22:00 is evident as the dryer response is still reaching its new level. Although it is not completely stable at this new level, the large increase after the HMW decrease is evident albeit slightly delayed from the predicted wire water retention increase. This is partly due to the combined effects of the moisture loop dynamics, sampling/reporting delay and short transportation time between the forming section and the 4th dryer section. Perhaps more importantly is the fact that the basis weight dynamics are not accounted for in the wire drainage model for model stability reasons (although set-point changes are accounted for). In Figure 4.25 the simulation results show a short decrease in basis weight as the retention aid is first decreased and the basis weight controller has not yet compensated for this fact. The drop in basis weight is not significant enough to be visible in the noisy dry end sensor data. However, this effect implies that there is temporarily less stock and hence less bound water in the sheet going to the dryers. The short initial drop in dryer steam demand seen in Figure 4.24 is an artifact of the above effect.

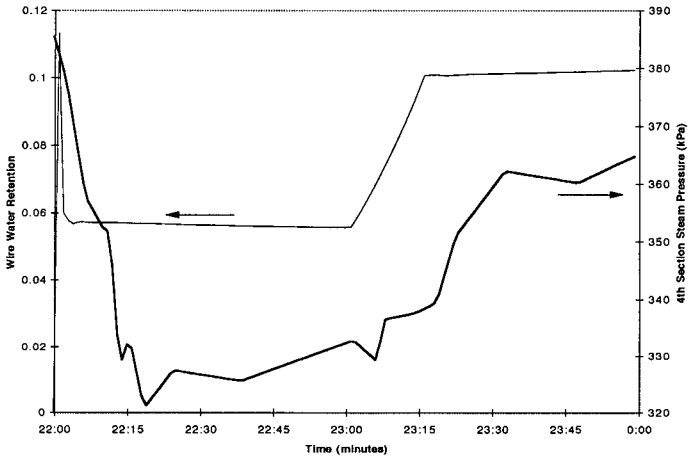

Figure 4.24: Measured 4th section dryer steam demand and simulated wire water retention for HMW Anionic retention aid ramp increase

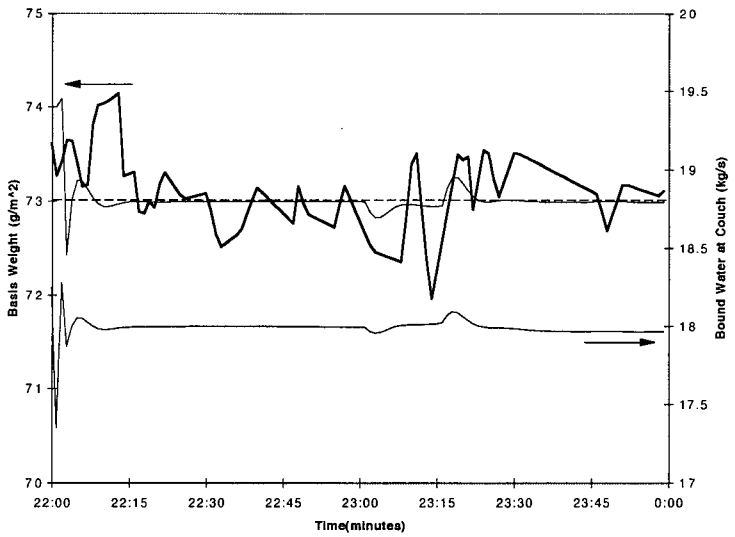

Figure 4.25: Simulated (thin lines) and measured (thick line) basis weights and couch bound water responses to HMW Anionic ramp increase

4.4 Grade Change

The simulated response of the system was compared against process data during a grade change. There were two operator moves during this time:

- A 5% increase in the sheet ash set point
- A 1 g/m^2 decrease in the basis weight

Simulation results are based on the parameters used in Case 4 from the previous section. The sheet ash set-point changes were implemented in two steps; first from 12 -15% and then from 15 - 17%. This was done in order to approximate the operator's moves during the grade change as an exact record was not available.

Figure 4.26 shows the closed-loop response of the sheet ash controller to the grade change. A dry end sheet break occurred during this period during which the signal was lost. Also evident is the staged nature of the set-point increase to avoid the possibility of a sheet break. The simulation approximates the sheet ash dynamics very well. The PCC flowrate, shown in Figure 4.27, demonstrates that the filler mass balance is quite good in that the gains of the actual and simulated PCC-sheet ash loop agree. However, some overshoot in the simulated control action is evident indicating that the sheet ash loop tuning is not accurate.

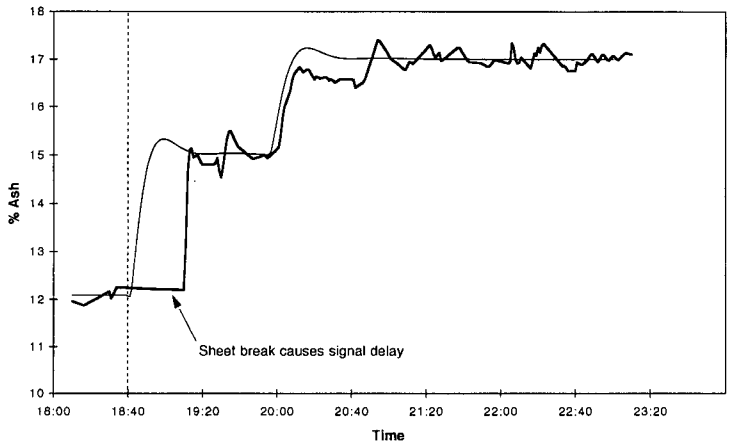

Figure 4.26: Closed-loop sheet ash response to grade change. Simulated (thin line), Measured (thick line).

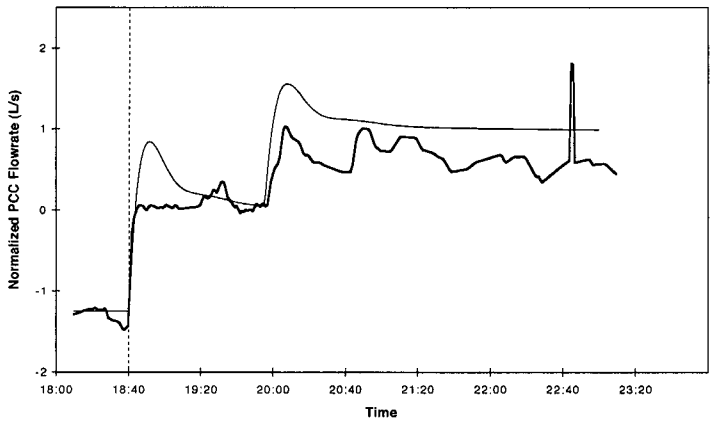

Figure 4.27: Closed-loop filler flowrate response to grade change. Simulated (thin line), Measured (thick line).

Simulated polymer coverages on the headbox long fiber fraction are shown in Figure 4.28. With the increased filler loading in the white water there is a drop in the HMW anionic polymer coverage which closely follows the sheet ash controller dynamics. As the filler content of the sheet rises together with the small decrease in basis weight, there is less thick stock demand. Since polymers are added at constant flowrates, coverage of LMW cationic polymer and starch (not shown) increase after lags corresponding to the hold-up times in the mix and machine chests. This has a positive benefit on first-pass retentions

leading to a cleaner short circulation and reverses the decline in HMW retention aid coverage to a certain degree.

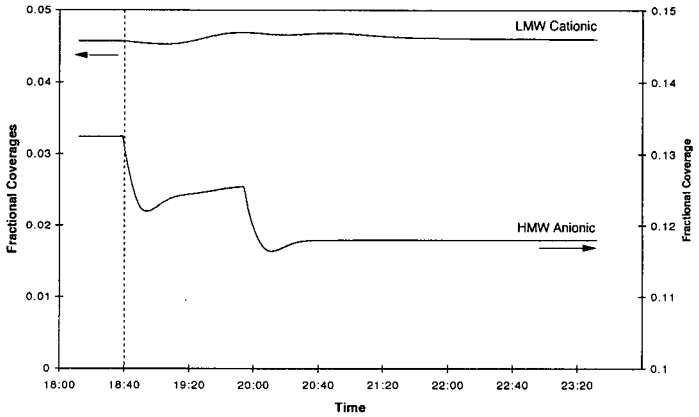

Figure 4.28: Simulated polymer coverages on the long fiber fraction during grade change.

The white water silo filler consistency during this grade change is shown in Figure 4.29. It is both directionally correct and matches the gain very well. The simulated dynamics appear to be faster than the measured again due to inaccurate sheet ash loop tuning.

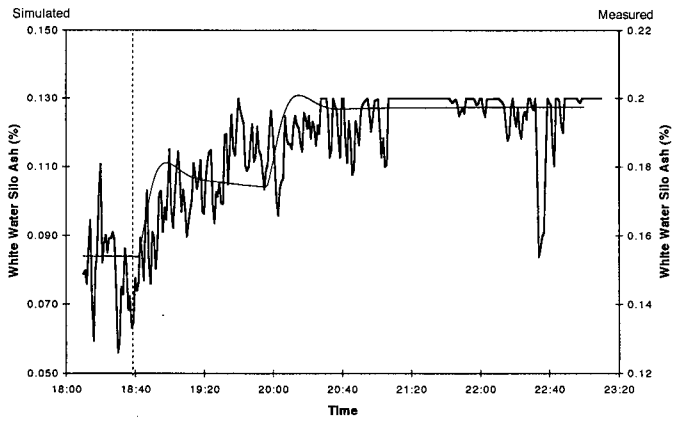

Figure 4.29: Simulated and measured white water silo filler consistencies for grade change.

Finally, Figure 4.30 compares drainage responses during the grade change. Bound water from the simulation has been scaled to fit the simulated wire water retention axis. Both free and bound water drainage indicators agree directionally with the overall decrease in dryer

steam demand. Free drainage improves from the first set-point change due to increased filler flocculation. This results from the greater number of particle collisions outweighing effects due to reduced polymer coverage. The reverse is true for the second sheet ash set-point change. Bound water is reduced during the grade change due to replacement of fibers and fiber fines with filler.

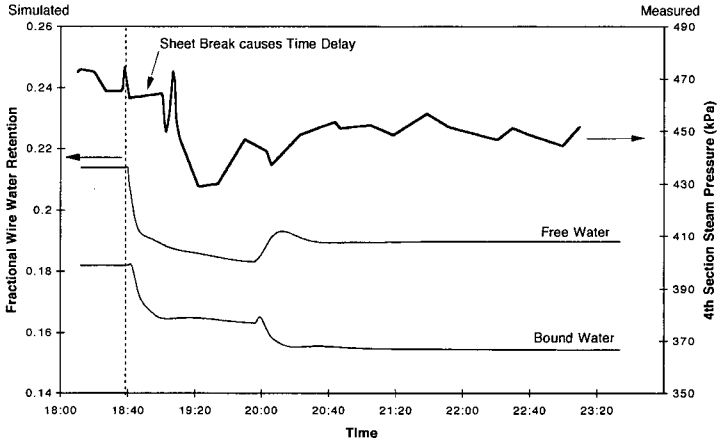

Figure 4.30: Drainage responses for grade change

4.4 Summary

This chapter has demonstrated many of the capabilities and limitations of the wet end chemistry simulation model. In general it is able to predict retention and drainage responses in both a directionally correct and, in most cases, accurate manner. Most importantly, the fundamental nature of the model allows one to interpret the responses in terms of the underlying chemical mechanisms. If an incorrect model response is encountered, the faulty or missing part of the model can be corrected without affecting the rest of the model.

Most of the attention in both the modelling, calibration and validation stages has been placed on the paper machine and short circulations. Here the dynamic effects are most

pronounced and the model performed well. Since the variations during these periods affected the white water long circulation to a lesser degree, it is difficult to characterize the success of the model for this part of the process. However, it is clear that additional disturbances not present in the model are impacting on the white water, in particular on the cloudy filtrate chest. These disturbances likely originate in the broke system and enter via the broke thickening screens.

Chapter 5

Control Relevant Identification

One objective in developing process models is to design model-based feedback control schemes for key operating variables. While a simulation may provide accurate predictions of the process, the problem of "inverting" this model to determine appropriate control actions remains. Simpler transfer function models are often used to approximate process behaviour and are of a form which facilitates controller design. These models are usually identified from input/output data after application of a perturbation to the process. Due to the approximate nature of empirical transfer function models and the noise present in input/output data, there remain uncertainties associated with the model once identification has been carried out. Such uncertainty needs to be quantified as it impacts on the robustness of the implemented controller. This chapter addresses the need to quantify these model uncertainties and that of reducing their magnitude at those frequencies most relevant to the eventual closed-loop control.

The role that the simulation model plays in the model identification process is highlighted through application to the wet end chemistry control problem. Often there is the paradoxical situation that in order to design optimal experiments for process identification one needs good knowledge of the process (Goodwin and Payne (1977)). The availability of a preliminary mechanistic process simulation helps to alleviate this situation. More importantly, the simulation model can serve as a testing ground for designed control schemes based on simplified linear process models.

5.1 Motivation for Uncertainty Bounds Based on Stochastic Theory

This section is concerned with describing and minimizing the uncertainty associated with a linear, dynamic process model estimated from input-output data generated in open-loop. Most commonly, current application of "classical" statistical methods for specifying model uncertainty involves linear approximations to nonlinear parameter confidence regions (Ljung (1987)). It is known, however, that such approximations can produce confidence regions which are severely in error in static nonlinear regression situations (Bates and Watts (1987)). Other methods, such as evaluation of the conditional likelihood function, can provide joint confidence regions for the model parameters which are exact in shape but approximate in confidence level. However, we are ultimately interested in anticipating how such parametric variability will affect closed-loop controller robustness, which is itself a nonlinear function of the model parameters. The main computational problem addressed here is that of finding the maximal closed-loop controller robustness subject to the parameters belonging to a $(1-\alpha)\%$ confidence region. This will be formulated as a constrained optimization problem (Chen (1991)).

As a measure of the efficacy of the confidence bounds formed from a dataset y, we will evaluate the "coverage"[1],

$$\text{Prob}\left(J \in \text{CR}(y)\right) = 1 - \alpha \tag{5.1}$$

that our nonlinear confidence regions, CR(y), afford. By specification of different levels of confidence, the degree of conservatism of these confidence bounds can be controlled. This is in contrast to "worst-case" strategies where uncertainty bounds encompass the true system dynamics with probability 1 (e.g. Helmicki et al. (1990)).

[1] The statistical notion of "coverage" used in this chapter is not to be confused with that used in previous chapters related to polymer coverage on papermaking furnish particles.

Once a method for accurately describing the potential uncertainty of the closed-loop system has been proposed, control relevant methods for minimizing this uncertainty will be discussed. The basis of control relevant identification is evaluation of a closed-loop objective function in terms of identification variables. In this way, identification experiments can be tailored to match closed-loop objectives.

First, consider the linear, dynamic process $G_p(\theta)$ with parameter vector θ. A controller for this plant designed from the estimated model $G_p(\hat{\theta})$ will be denoted $G_c(\hat{\theta})$. It will be assumed throughout this chapter that the estimated model has the same form as the true model. The closed-loop servo transfer function for the implemented controller is then,

$$\frac{y(t,\hat{\theta})}{y_{sp}(t)} = \frac{G_p(\theta)G_c(\hat{\theta})}{1+G_p(\theta)G_c(\hat{\theta})} \tag{5.2}$$

where y and y_{sp} denote the system response and set-point respectively. It is important to note that upon implementation of a model-based control scheme uncertainty arising from the identification stage manifests itself through the implemented controller and not through the process.

If we had access to the true parameter values θ then a controller $G_c(\theta)$ could also be determined which represents the best controller achievable for the particular design method used. In this idealized situation the closed-loop transfer function is,

$$\frac{y(t,\theta)}{y_{sp}(t)} = \frac{G_p(\theta)G_c(\theta)}{1+G_p(\theta)G_c(\theta)} \tag{5.3}$$

Note that there is no dependence upon the identification process.

The closed-loop tracking error, e_{H_2}, of an implemented controller follows from Equation 5.2,

$$\begin{aligned} e_{H_2}(t,\hat{\theta}) &= y(t,\hat{\theta}) - y_{sp}(t) \\ &= \frac{-y_{sp}(t)}{1 + G_p(\theta)G_c(\hat{\theta})} \end{aligned} \tag{5.4}$$

which gives rise to the following quadratic measure of closed-loop performance degradation arising from the use of identified parameters rather than the (unknown) true parameters,

$$\begin{aligned} J_{Perf} &= \sum \left(e_{H_2}(t,\theta) - e_{H_2}(t,\hat{\theta}) \right)^2 \\ &= \left\| \frac{y_{sp}}{1 + G_p(\theta)G_c(\hat{\theta})} - \frac{y_{sp}}{1 + G_P(\theta)G_c(\theta)} \right\|_2 \end{aligned} \tag{5.5}$$

The stability robustness of the closed-loop control scheme is also affected through the quality of the identified model. A measure of stability robustness arises from consideration of the denominator of the closed-loop transfer function in Equation 5.2,

$$J_{Stab} = \left\| 1 + G_p(\theta)G_c(\hat{\theta}) \right\|_\infty \tag{5.6}$$

Equations 5.5 and 5.6 will be used as criteria expressing closed-loop requirements in the identification process. The use of closed-loop identification criteria, including other possible cost functions, has been reviewed by Van den Hof and Schrama (1995) in the context of iterative closed-loop identification. Control-relevant concepts can be applied to situations requiring open-loop experimentation by employing frequency weighing functions derived from the above closed-loop criteria.

"Classical" statistical methods of specifying such uncertainty assume that the process model is an accurate description of the true underlying process (Box and Jenkins (1976)). It is this assumption which has prompted researchers to develop alternative methods for describing model uncertainty often abandoning the traditional stochastic description of process disturbances. According to Ninness and Goodwin (1995) the main justification for abandoning the "classical" statistical identification framework is that a process model, in particular a linear model, can never capture the true process dynamics. This has led to the recognition of both unmodelled effects and process disturbances as components of the modelling residuals (Hjalmarson and Ljung (1994)). However, if an identified model passes various validation tests, then the data does not contain evidence to suggest either an inadequate process model form or that the assumptions regarding the process disturbance model are invalid (Lee and Poola (1994), Box and Jenkins (1976)). These tests include checking the cross-correlation between input and residuals as well as autocorrelation and distributional checks of the residuals themselves. Is the fact that we have a validated model enough to guarantee that one can construct uncertainty regions with good coverage properties? This question will be explored in the context of various methodologies for determining bounds on the modelling errors when reduced order models have been fit.

A common theme throughout the chapter will be a graphical presentation which highlights the connection between the identification and control problems. By comparing parameter likelihood contours with robustness contours in parameter space, it is possible to gain insight into the impact of choices during the identification stage such as the form of the input test signal. Mapping of contour regions into the Nyquist plane will also be carried out in order to provide frequency domain bounds suitable for robust controller design.

5.2 Development of Control Relevant Identification Criteria

In this section the theory and computational methods for constructing confidence intervals of closed-loop criteria based on identification data will be presented, followed by an algorithm for translation of these uncertainty regions into the frequency domain. Corresponding techniques based on linear approximations to the (generally) nonlinear problem are next reviewed. From this, a control relevant experimental design procedure is developed. Finally, a graphical method for presentation of the overall control relevant problem in parameter space is given.

5.2.1 Confidence Intervals for Nonlinear Parametric Functions

Consider a single input/single output (SISO) linear time invariant dynamic system where the actual plant dynamics are described by,

$$y(t) = G_p(z^{-1},\theta)u(t) + H(z^{-1},\theta)\xi(t) \tag{5.7}$$

In Equation 5.7, y(t) and u(t) are the measured process output and inputs at time t, G_p and H are the process and additive disturbance transfer functions and z^{-1} is the unit backwards shift operator. The additive disturbance is driven by a normally distributed white noise sequence, $\xi(t)$, with zero mean and variance σ_ξ^2. The (px1) column vector of the parameters associated with $G_p(z,\theta)$ and $H(z, \theta)$ is θ, and estimates of θ obtained from N observations of input-output data from the process are denoted by $\hat{\theta}$. Defining the model residuals (one-step ahead prediction errors) as $e(t,\hat{\theta})$ we have,

$$y(t) = G_p(z^{-1},\hat{\theta})u(t) + H(z^{-1},\hat{\theta})e(t,\hat{\theta}) \tag{5.8}$$

or

$$e(t,\hat{\theta}) = H^{-1}(z^{-1},\hat{\theta})\left[G_p(z^{-1},\theta) - G_p(z^{-1},\hat{\theta})\right]u(t) + H^{-1}(z^{-1},\hat{\theta})H(z^{-1},\theta)\xi(t) \tag{5.9}$$

The likelihood function is given by,

$$l(\hat{\theta} \mid y) \propto \sigma_{\xi}^{-N} \exp\left(\frac{-\sum_{t=1}^{N} e(t,\hat{\theta})^2}{2\sigma_{\xi}^2} \right) \tag{5.10}$$

and describes the ability of the parameter estimates of θ to describe the observed data y. Minimization of the sum of squared residuals,

$$S(\hat{\theta}) = \sum_{t=1}^{N} e^2(t,\hat{\theta}) \tag{5.10}$$

leads to the maximum likelihood estimates of θ under normality (Box and Jenkins (1976)). Contours of the sum of squares function provide a means for constructing confidence regions for the parameters. By analogy to the linear (wrt θ) estimation situation $(1-\alpha)\%$ confidence intervals for the parameters are formed for all θ such that,

$$\frac{S(\theta) - S(\hat{\theta})}{S(\hat{\theta})} \leq \frac{p}{N-p} F_{\alpha;p,N-p} \tag{5.11}$$

where $F_{\alpha;\, p,\, N-p}$ is the value of the F-distribution with p and N-p degrees of freedom (Bates and Watts (1987)). Comparison against the F-distribution results from the fact that $(S(\theta) - S(\hat{\theta}))/p$ and $S(\hat{\theta})/(N-p)$ are independent chi-squared variables since the $e(t,\theta)$ in Equation 5.10 are independently normally distributed random variables. If the $e(t,\theta)$ are not independent then Equation 5.11 is not applicable. This would be the case if a different sampling interval or k-step ahead prediction were used to estimate the parameters (see Ljung (1987), Equation 3.33). To the author's knowledge, techniques for constructing confidence intervals in such cases are not readily available. Results in this work are therefore restricted to maximum likelihood identification.

A sum of squares surface based on a two parameter example discussed further in Section 5.3 is shown in Figure 5.1. The 95% confidence contour for the parameters 'a' and 'b' is highlighted. The interpretation is that the true parameter pair has a 95% probability of lying within this confidence contour.

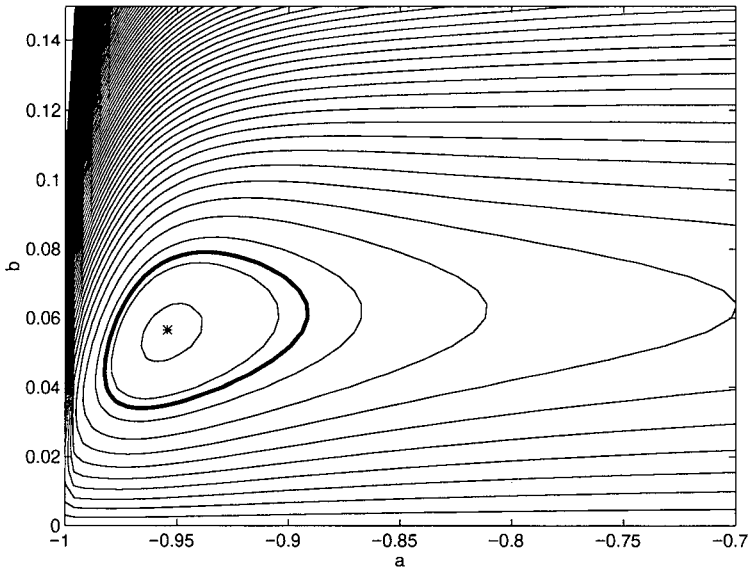

Figure 5.1: Sum of squares surface for first-order model of Section 5.3. The thick line is the 95% confidence contour.

We are interested in constructing confidence intervals for nonlinear functions of the model parameters such as those given by Equations 5.5 and 5.6. The functions considered are scalar and so lead to intervals on a line. In fact, in most cases only one bound exists or is of interest. For example, the performance robustness criterion given by Equation 5.5 has a lower bound of zero which occurs when model parameters match the true parameters. In such a case we are only interested in assessing a maximal bound on the performance robustness.

In order to see the relationship between the identification and control problems it is also possible to construct contours of the control objectives in parameter space. As an example, consider the control objective J_{Perf} expressed by Equation 5.5. First, denote assumed true values of the parameters by θ^* and use the current parameter estimates for their values. Normalizing J_{Perf} by the nominal controller performance and upon application of Parsevall's theorem we obtain,

$$\tilde{J}_{Perf}(\theta) = \frac{\frac{1}{2\pi}\int_{-\pi}^{\pi}\left|\frac{1}{1+G_P(e^{j\omega},\theta^*)G_C(e^{j\omega},\theta)} - \frac{1}{1+G_P(e^{j\omega},\theta^*)G_C(e^{j\omega},\theta^*)}\right|^2 \Phi_{y_{sp}}(\omega)d\omega}{\frac{1}{2\pi}\int_{-\pi}^{\pi}\left|\frac{1}{1+G_P(e^{j\omega},\theta^*)G_C(e^{j\omega},\theta^*)}\right|^2 \Phi_{y_{sp}}(\omega)d\omega} \tag{5.12}$$

This expression may be evaluated for a grid of points θ around θ^* applying contouring techniques to produce the parametric robust performance surface. An example plot for the two parameter example is shown in Figure 5.2 where the '*' point again denotes the location of the true parameters. Also shown is the 95% likelihood contour from Figure 5.1 which arises from the identification stage. At some point along the 95% parameter confidence contour the maximal value of $\tilde{J}_{Perf}(\theta)$ occurs. This point represents an upper bound for the expected (normalized) controller performance degradation due to parametric deviations. The next section formulates the computation of this point as a constrained optimization problem. Such a picture also allows one to compare the required size and orientation of the likelihood contours from the identification stage in order to meet a performance specification. Clearly this visual method is restricted to two dimensions but can also be applied to parameter pairs for higher dimensional problems.

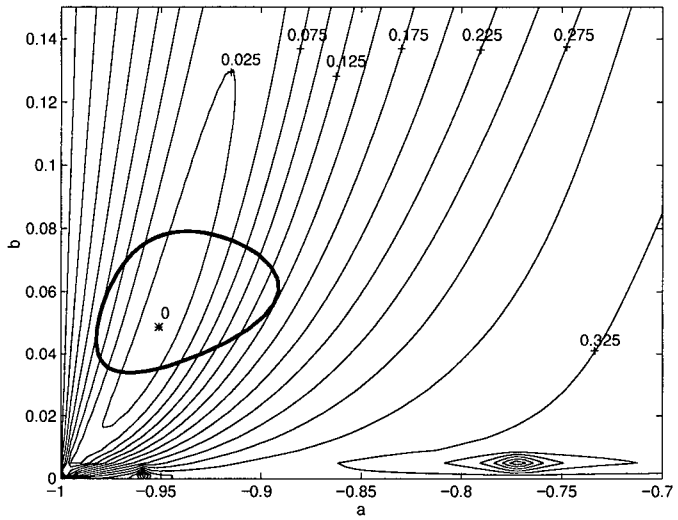

Figure 5.2: Contours of $\tilde{J}_{Perf}(\theta)$ (thin lines) for the two parameter example with the 95% confidence contour superimposed (thick line)

5.2.2 Computational Method

Denote an arbitrary nonlinear function of the parameters by $g(\theta)$ and assume it to be twice differentiable wrt θ. Such a function could include J_{perf} or J_{stab}. For any fixed value of this nonlinear function, c, denote

$$\hat{\theta}_c = \arg \min_{\theta} \{S(\theta) : g(\theta) = c\} \tag{5.13}$$

Using the example shown in Figure 5.2, $\hat{\theta}_c$ represents the location along an arbitrary contour of $\tilde{J}_{Perf}(\theta)$=c at which the corresponding sum of squares surface (shown in Figure 5.1) is a minimum.

From Chen (1991), a (1-α)% confidence region for $g(\theta)$ follows from application of the likelihood ratio test for the hypothesis $g(\theta)$=c, or:

$$CR_g(y) = \left\{ c : \frac{S(\hat{\theta}_c) - S(\hat{\theta})}{S(\hat{\theta})}(N - p) \le F_{\alpha;1,N-p} \right\} \tag{5.14}$$

where $F_{\alpha;1,N-p}$ is the value of the F-distribution at the $(1-\alpha)$ level of significance with 1 and N-p degrees of freedom. Some comments on Equation 5.14 are appropriate:

- The confidence region is dependent on the observed data. It is expected that the 'true' value of $g(\theta)$ will be encompassed by $(1-\alpha)\%$ of the confidence regions so formed.
- One degree of freedom is associated with the difference $S(\hat{\theta}_c) - S(\hat{\theta})$ as one constraint $g(\theta)=c$ is imposed on θ in the hypothesis test (see Gallant (1987)).
- Equation 5.14 is exact when $S(\theta)$ and $g(\theta)$ are linear. Otherwise it is approximate in the confidence level, due to the nonlinearity in the estimation.

Alternative methods of constructing confidence intervals for $g(\theta)$ based on linearization of $g(\theta)$ and a score test are discussed by Chen (1991). The likelihood method was found to be the most effective and algorithms were constructed based on it.

The computational problem is then:

$$\begin{aligned} &\text{Maximize} \quad g(\theta) \\ &\text{Subject to} \quad \left[\frac{S(\theta) - S(\hat{\theta})}{S(\hat{\theta})}\right](N - p) \le F_{\alpha;1,N-p} \end{aligned} \tag{5.15}$$

for determination of the upper confidence limit and minimization of $g(\theta)$ for determination of the lower confidence limit. This procedure amounts to locating the maxima and minima of the function $g(\theta)$ over the p-dimensional confidence region for θ, a problem which can be handled by any number of general constrained optimization algorithms. Here the 'constr' function provided in the MATLAB Optimization Toolbox (The Mathworks (1995)) has been used. It employs a Sequential Quadratic Programming approach.

The formulation given in Equation 5.15 involves an inequality constraint. Chen (1991) makes the simplifying assumption that the solution lies on a boundary point of the parameter confidence region and thereby transforms the inequality to an equality constraint. Justification for this simplification was based on experience, but no proof was given of its validity. For the examples tried involving robust control objective functions it has always been the case that the solution lies on the boundary of the parameter confidence region.

5.2.3 Frequency Domain Representation of Uncertainty Regions

For robust controller design using frequency domain techniques, a description of the uncertainty associated with $G_p(e^{j\omega},\hat{\theta})$ is necessary. At any ω, we would like to assess the region in the complex plane, $\mathscr{C}$, corresponding to the parametric uncertainty described by the $(1-\alpha)\%$ likelihood region in $\Re^p$.

To accomplish this, first transform the complex number $G_p(e^{j\omega},\theta) - G_p(e^{j\omega},\hat{\theta})$ to radial coordinates d and ϕ where,

$$\begin{aligned} d(\theta) &= \left\| G_p(e^{j\omega},\theta) - G_p(e^{j\omega},\hat{\theta}) \right\| \\ \phi &= \angle\left| G_p(e^{j\omega},\theta) - G_p(e^{j\omega},\hat{\theta}) \right| \end{aligned} \tag{5.16}$$

Fix ϕ at a point in the interval $[0\ 2\pi]$ so that $d(\theta,\phi,\omega)$ becomes a nonlinear function of θ only. Hence, a constrained optimization problem of the nonlinear function $d(\theta,\phi,\omega)$ results and the algorithm described in Section 5.2.2 can be applied repeatedly for successive ϕ and ω. That is, for fixed ϕ and ω,

$$\begin{aligned} &\text{Maximize} \quad d(\theta,\phi,\omega) \\ &\text{Subject to} \quad \left[\frac{S(\theta) - S(\hat{\theta})}{S(\hat{\theta})}\right](N-p) \le F_{\alpha;1,N-p} \\ &\qquad\qquad \angle\left| G_p(e^{j\omega},\theta) - G_p(e^{j\omega},\hat{\theta}) \right| = \phi \end{aligned} \tag{5.17}$$

The extremal values for $d(\theta,\phi,\omega)$ may be evaluated at a number of values of ϕ and an interpolation routine can then be applied to produce a continuous uncertainty region.

5.2.4 Linear Approximation Procedures

Linear approximations can be derived to the nonlinear closed-loop criteria and procedures for both inference and experimental design then follow. The derivation given is similar to that of Ljung (1987) although we note that parametric uncertainty is associated with the controller transfer function rather than with the process. The J_{Perf} criterion given by Equation 5.5 will be used as an example for development of the linearized criterion.

Consider again the set-point tracking error, e_{H_2}, of Equation 5.4. Taking a first-order Taylor series expansion about the true parameter values θ^* with $\nabla_\theta G_c(z^{-1},\hat{\theta})$ representing the (px1) gradient vector of $G_c(z^{-1},\hat{\theta})$ gives,

$$e_{H_2}(t,\hat{\theta}) \approx y_{sp}(t)\left[\left(\frac{1}{1+G_P(z^{-1},\theta)G_C(z^{-1},\hat{\theta})}\right)_{\hat{\theta}=\theta^*} - \left(\frac{G_p(z^{-1},\theta)\nabla_\theta G_C(z^{-1},\hat{\theta})}{\left(1+G_P(z^{-1},\theta)G_C(z^{-1},\hat{\theta})\right)^2}\right)\left(\theta-\theta^*\right)\right] \quad (5.18)$$

The first of these two terms, say $\bar{e}_{H_2}(t,\theta^*)$, is the nominal closed-loop tracking error for the controller and is not a function of the model identification. The second term gives a linear measure of the transmission of identification uncertainty to controller performance. By first subtracting the nominal controller error from the overall error we have,

$$\psi(t,\hat{\theta}) = e_{H_2}(t,\hat{\theta}) - \bar{e}_{H_2}(t,\theta^*) \quad (5.19)$$

A linear performance degradation criterion, denoted $\Delta Perf(\hat{\theta})$, is then found by taking the expectation wrt θ,

$$E_\theta\left[\Delta Perf\left(\hat{\theta}\right)\right] = \frac{1}{2\pi}\int_{-\pi}^{\pi}\Psi\left(e^{j\omega},\theta^*\right)Cov\left(\hat{\theta}\right)\Psi^T\left(e^{-j\omega},\theta^*\right)d\omega \quad (5.20)$$

where

$$\Psi(e^{u\omega},\hat{\theta}) = -y_{sp}(e^{j\omega})\frac{G_P(e^{j\omega},\theta)\nabla_\theta G_C(e^{j\omega},\hat{\theta})}{\left|1+G_P(e^{j\omega},\theta)G_C(e^{j\omega},\hat{\theta})\right|^2} \tag{5.21}$$

Here G_p is evaluated at $\theta=\hat{\theta}$ and E_θ denotes the statistical expectation wrt θ. This is the expression given by Equation 33 in Shirt et al. (1994). It is important to note that subtraction of the mean controller error, $\bar{e}_{H_2}$, removes the effects of the nominal controller performance from $\Delta\text{Perf}(\hat{\theta})$.

Linear characteristics about the precision of the estimated parameters are contained in $\text{Cov}(\hat{\theta})$, the pxp variance-covariance matrix. For experimental design purposes, Fisher's Information Matrix, M, is often used to approximate $\text{Cov}(\hat{\theta})$ before input-output data is generated by use of *a priori* parameter estimates. An exact definition of M is given elsewhere (Goodwin and Payne (1977)).

Inference: In order to develop a confidence interval for $\Delta\text{Perf}(\theta)$ we note that it is asymptotically distributed as a weighted sum of χ^2 variables due to the normality of $\hat{\theta}$. The critical value against which $\Delta\text{Perf}(\theta)$ should be compared can be determined using the procedure given in Appendix A of MacGregor and Harris (1993). This procedure uses an approximation to the weighted χ^2 distribution introduced by Box (1954).

A common method of producing confidence intervals for nonlinear functions of parameters is the Wald or linearization method explained in Chen (1993). In it, the variance of $g(\theta)$ is estimated using a first-order Taylor series expansion of $g(\theta)$ directly, resulting in $\text{Var}(g(\theta)) = \nabla_\theta g(\theta) \bullet \text{Cov}(\theta) \bullet \nabla_\theta^T g(\theta)$ which is evaluated at $\hat{\theta}$. However, for the case where $g(\theta) = J_{Perf}(\theta)$, $\nabla_\theta g(\hat{\theta}) = 0$ and the Wald method fails[2]. Thus, the linear

[2] This result is due to S. Quinn of Queen's University, Department of Chemical Engineering (personal correspondence)

approximation method developed above provides an alternative for cost functions of this type.

Experimental Design: The experimental design problem is to minimize the criterion given by Equation 5.20 wrt some function of the input signal frequency characteristics. It is noted that use of this criterion results in minimization of a weighted trace of the information matrix and leads to an A-optimal experimental design (Goodwin and Payne (1977)). The choice of input signal form is arbitrary as long as persistency of excitation conditions are met (Ljung (1987)). Examples of input signal forms used are:

- Low-order autoregressive sequences of filtered white noise; the performance criterion is minimized wrt the time series parameter(s).
- Pseudo-random binary sequences (Godfrey (1993)) or generalized binary noise (Tulleken (1990)). Here the performance criterion is minimized wrt the basic sampling interval or switching probability.
- A square wave; the performance criterion is minimized wrt the fundamental frequency.
- Weighted sums of sinusoids; the performance criterion is minimized wrt the frequencies of the sinusoids as well as their respective weights (Goodwin and Payne (1977)).

The minimization can, in many instances, be cast in terms of a small number of parameters. Some efficiencies in the optimization problems can be realized with particular input signal forms and these are discussed in the references cited above.

In the case of test signals in the form of filtered white noise, it is often desirable to implement the input signal as a binary sequence. For a stationary signal, u(t), which is continuous in level with mean $\bar{u}$, the following clipping may be applied:

$$u^C(t) = \begin{cases} A & \text{if } u(t) - \bar{u} \geq 0 \\ -A & \text{if } u(t) - \bar{u} < 0 \end{cases} \tag{5.22}$$

The spectrum of the clipped series, in terms of the original (stationary) series spectrum $\Phi_u(\omega)$, is (Kedem (1980))

$$\Phi_u^c(\omega) = \frac{2}{\pi^2}\left[\Phi_u(\omega) + \frac{1}{2\bullet 3}\left(\frac{2}{\pi}\right)^2 \sum_{\tau=0}^{\infty} e^{-j\tau\omega}\rho_u^3(\tau) + \frac{1\bullet 3}{2\bullet 4\bullet 5}\left(\frac{2}{\pi}\right)^4 \sum_{\tau=0}^{\infty} e^{-j\tau\omega}\rho_u^5(\tau) + \ldots\right] \tag{5.23}$$

where ρ_u is the autocorrelation function of the signal u(t). As an example, consider the first-order autoregressive series,

$$u(t) = -AR \bullet u(t-1) + \xi(t) \tag{5.24}$$

Denoting its spectrum $\Phi_u(\omega, AR)$, on clipping according to Equation 22, we have:

$$\Phi_u^c(\omega, AR) = \frac{2}{\pi^2}\left[\Phi_u(\omega, AR) + \frac{1}{6}\left(\frac{2}{\pi}\right)^2 \Phi_u(\omega, AR^3) + \frac{3}{40}\left(\frac{2}{\pi}\right)^4 \Phi_u(\omega, AR^5) + \ldots\right] \tag{5.25}$$

For slow processes (AR<0) typically required of input signals, clipping results in addition of higher frequency components to the original signal. However, the coefficients associated with these higher frequency terms are quite small (<5%) so the spectral features of the original signal remain dominant. Thus, the simplifications introduced by using the spectrum of the unclipped series for purposes of experimental design calculations would seem to not introduce significant errors into the properties of the final test signal.

To summarize, the input design procedure suggested above is:

- Specify: Process model, $G_p(e^{j\omega},\hat{\theta})$

  Information matrix, $M\left(\hat{\theta},\Phi_u(\omega)\right)$

  Closed-loop set point signal, $y_{sp}(\omega)$

  Closed-loop controller transfer function, $G_c(e^{j\omega},\hat{\theta})$

- Minimize $\Delta Perf\left(\hat{\theta},G_p,G_c,M,y_{sp}\right)$ wrt AR
- Use the value of the parameter AR to generate a realization of a 1st order autoregressive sequence according to Equation 5.24
- Clip the sequence according to Equation 5.22.

The process model, G_p, can be identified using a simulation model if available. An example demonstrating the effectiveness of this procedure will be given in the following section.

5.3 Numerical Illustration of Methods

Consider the following first-order linear system:

$$y(t) = \frac{bz^{-1}}{1+az^{-1}}u(t) + \frac{\xi(t)}{1+dz^{-1}} \tag{5.26}$$

with a=-0.9512, b=0.0488, d=-0.98 and $\xi(t) \sim N(0,0.2)$. We wish to apply a set-point tracking controller to this system and will examine the resulting closed-loop robustness in the sense of Equations 5.5 and 5.6. The applied controller transfer function is:

$$G_c(z,\theta) = \frac{1}{g - G_p(z^{-1},\theta)} \tag{5.27}$$

where g is the open-loop gain. This represents a model following controller with the desired closed-loop response equal to that of the open-loop process. The performance of the closed-loop scheme is tested by application of a command signal, $y_{sp}(t)$, which is a square wave with fundamental frequency ω_{sp}=0.008.

Based on the above information, two different input sequences were generated and their results compared. Both sequences are clipped (±3) realizations of white noise to which a first-order autoregressive input was applied as in Equations 5.22 and 5.24. The sequences differ in the single parameter, AR, of the 1st-order filter. The first input sequence was generated according to the optimal control relevant procedure outlined at the end of Section 5.2.4 using Equation 5.5 as the performance robustness criterion. The resulting input signal time series parameter for this sequence was found to be AR=-0.965. Figure 5.3 shows realizations of the optimal (AR=-0.965) and non-optimal (AR=-0.8) clipped input sequences respectively. Note that because the signals are binary (±3) they have equal variance.

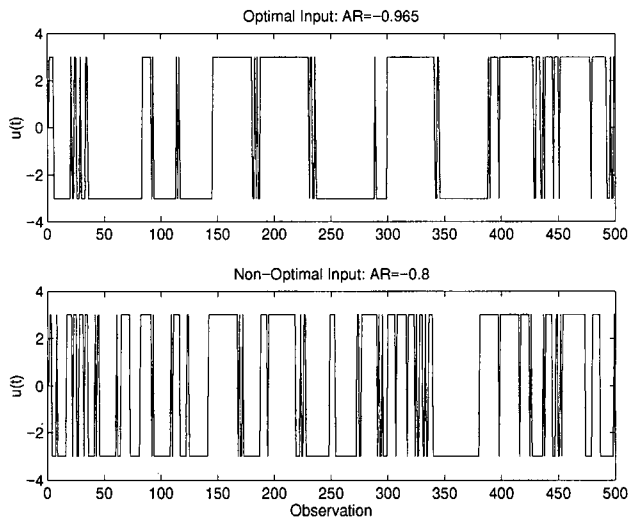

Figure 5.3: Optimal and sub-optimal input sequences for first-order example

First-order models plus disturbances were identified from N=500 input/output data points generated by applying the above two input sequences to the system of Equation 5.26. The model was of the same structure as the 'true' system. Parameter estimation was accomplished using the method of maximum likelihood and 95% joint confidence regions for the parameters 'a' and 'b' were computed. The above information is shown in Figure 5.4 along with contours of $\tilde{J}_{Perf}$ calculated according to Equation 5.12.

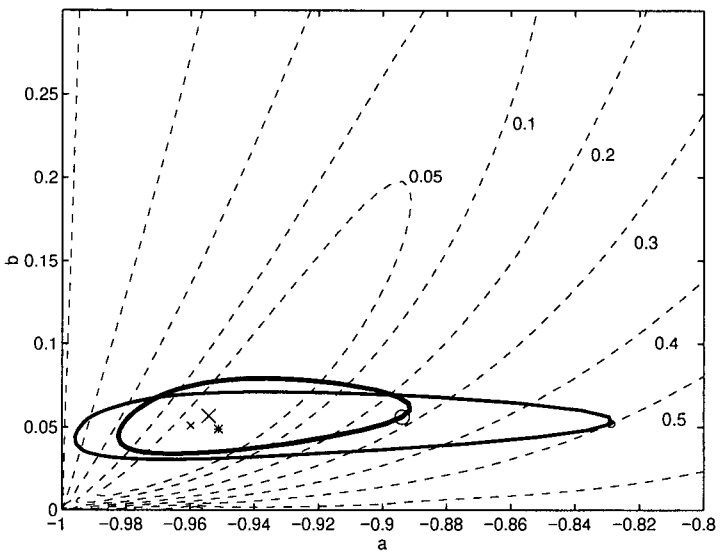

Figure 5.4: Comparison of 95% confidence contours and $\tilde{J}_{Perf}$ contours for the first-order example.

- Thick solid contour = 95% confidence region from optimal input,
- Thin solid contour = 95% confidence region from non-optimal input,
- Dashed contours = Normalized J_{perf} (levels indicated),
- x's = Parameter estimates (large=optimal, small=non-optimal),
- o's = Maximal J_{perf} within parameter confidence region,
- * = true parameter values.

Table 5.1 summarizes parameter estimates and maximal values of $\tilde{J}_{Perf}$ for the two cases. For this example, $\tilde{J}_{Perf}$ contours exhibit a severe elongation along their principle axis and highly non-uniform spacing in between. Regions leading to unstable closed-loop

performance are indicated by increasingly close spacing of contours. This occurs when the gain reverses sign (i.e. b<0) and for regions beyond a<-1.

Case	Parameter Estimates $\hat{a}$	$\hat{b}$	Maximal $\tilde{J}_{Perf}$
Optimal Input	-0.9543	0.0566	0.2727
Non-optimal Input	-0.9599	0.0509	0.5001

Table 5.1: Parameter estimates and maximal $\tilde{J}_{Perf}$ for first-order example.

The parameter confidence regions exhibit nonlinear effects but in a different manner than those of $\tilde{J}_{Perf}$. The underlying likelihood regions are seen to have considerable nonlinearity in the 'a' parameter. Clearly, the optimal and non-optimal inputs differ greatly in their ability to precisely estimate this parameter. As well, a slight rotation of the underlying likelihood surface is evident in a direction consistent with the $\tilde{J}_{Perf}$ contours. In this and other examples, application of control relevant input sequences has shown that both size and orientation of the resulting contours are important in achieving maximal robustness.

If a specification on the maximum robustness exists then the above gives a graphical interpretation of how this specification can be achieved. For example, a typical specification might be that $\tilde{J}_{Perf} < 0.1$ so that the robust performance degradation is much less than the nominal performance. In the above example, it was found that with application of the control relevant binary input signal over 500 sampling periods, $\tilde{J}_{Perf}$ = 0.2727 was achieved. Thus further experimentation would need to be performed in order to meet the performance specification.

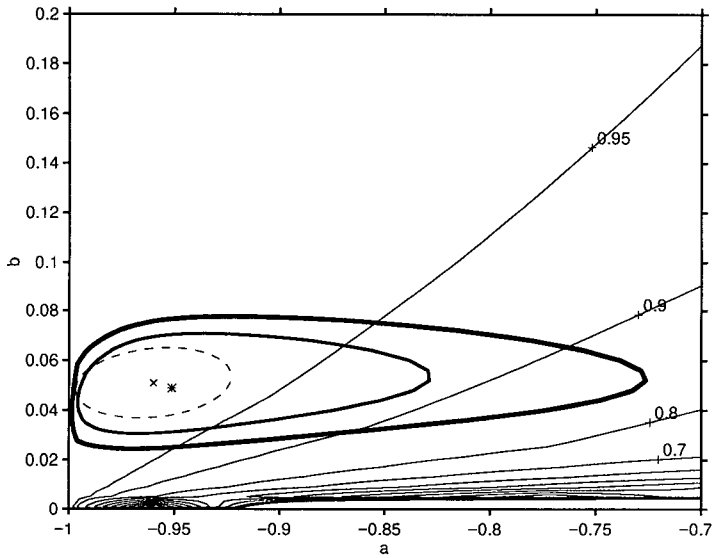

Figure 5.5: Comparison of robust stability (Equation 5.6) contours (thin solid lines), 95% and 99% nonlinear confidence regions (thick solid lines) and 95% linear confidence region (dotted ellipse) based on non-optimal input sequence (AR=-0.8). Also shown are the maximum likelihood parameter estimates (x) and true parameter values (*) for this example.

In Figure 5.5 contours of robust stability, J_{Stab}, are shown generated according to Equation 5.6. The region of instability coincides with reversal in the sign of the process model gain and is indicated by increasingly closely spaced contours. Most of the 95% likelihood confidence region is relatively far from such instability. Two issues are of note here. First, we see that the 95% confidence ellipse based on a linear approximation to the likelihood surface gives overly optimistic results mainly due to its inability to capture the asymmetric centering of the parametric uncertainty. For slowly sampled systems, common in the processing industries, a system will often be operating near stability constraints leading to such asymmetry. A more detailed comparison between the linear controller robustness bound developed in Section 5.2.4 and the nonlinear bound will be given later. Secondly, the 99% confidence region extends considerably further along the 'a' axis with

an accompanying loss in minimal robustness. For this example, use of the 95% bound would lead to a small loss (approximately 10%) in stability robustness but may not be a reasonable trade-off against the extra conservatism introduced into the controller design. The graphical procedure clearly illustrates such trade-offs.

The 95% parameter confidence region based on the optimal input was mapped into the Nyquist plane by the method of Section 5.2.3 with the resulting contours shown in Figure 5.6. For comparison, Nyquist regions based on 95% linear parameter CR's are shown as well. We note the following:

- The regions are non-circular and non-elliptical. They are also eccentrically positioned about the nominal Nyquist point.
- Orientations of the regions vary.
- The linear approximation does not accurately represent the uncertainty associated with $G_p(e^{j\omega},\hat{\theta})$, particularly in the low frequency regions.

Clearly, the regions constructed from the nonlinear parameter CR's would give a less conservative controller design more reflective of the actual parameter uncertainty associated with identification of the process.

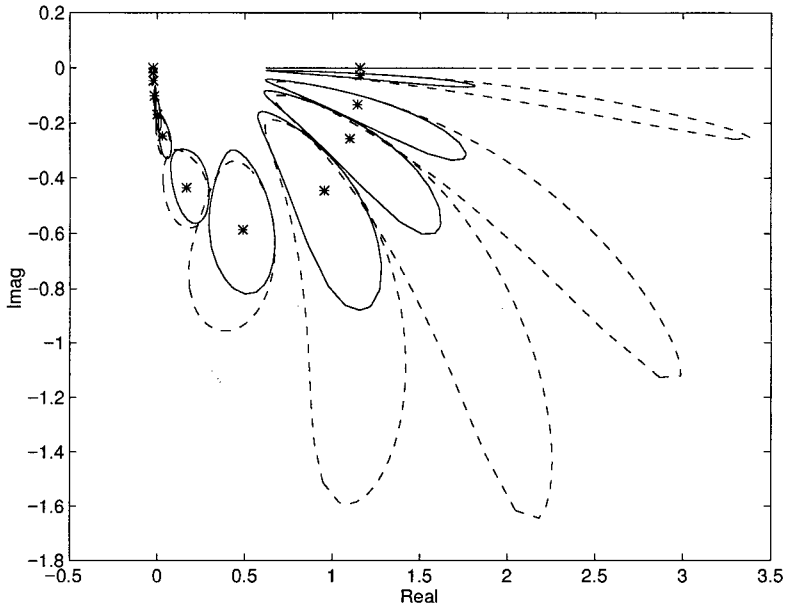

Figure 5.6: Representation of nonlinear (solid) and linear (dashed) 95% confidence bounds in the frequency domain. Points of the nominal Nyquist curve are shown by *'s.

5.4 Coverages of Confidence Intervals

The likelihood method for construction of (1-α)% confidence intervals for g(θ) provides (1-α)% coverage if the parameters enter into S(θ) and g(θ) linearly (Chen (1991)). However, identification and controller design using transfer function models most often involves nonlinear mappings of the parameters. The effects of such nonlinearities are tested in this section. As well, we examine the effect of finite data set lengths on confidence intervals for nonlinear functions.

To facilitate this, the Signed Root Deviance Profile (SRDP) is defined by Chen and Jennrich (1996) as,

$$\text{SRDP}(c) = \text{sign}\left(c - g(\hat{\theta})\right)\left[\frac{S(\hat{\theta}_c) - S(\hat{\theta})}{S(\hat{\theta})}\right]^{1/2} \tag{5.28}$$

where $g(\hat{\theta})$ is the nonlinear parametric function (e.g. controller robustness functions of Equations 5.5 and 5.6) evaluated at the maximum likelihood parameter estimates and $\hat{\theta}_c$ is defined by Equation 5.13. When plotted against $g(\theta)$, the SRDP function provides valuable information regarding nonlinearities present in the expectation surface. It is analogous to the Profile-t Function of Bates and Watts (1987) when $g(\theta)=\theta_i$, a single parameter (Chen and Jennrich (1996)). For a model which is linear in the parameters, a plot of the SRDP over the response space of $g(\theta)$ is a straight line. Comparison of the actual and approximate linear (or "reference") SRDP's gives a continuous measure of nonlinearity across the response space. This can provide insights into appropriate linearizing parameter transformations, should they be necessary. We note that, unlike contour plots which are limited to two dimensions, profiling can be applied to situations involving any number of parameters.

The reference line is normally constructed as a straight line passing through $(g(\hat{\theta}),0)$ with slope $\left[\nabla_\theta g(\hat{\theta}) \bullet \text{Cov}(\hat{\theta}) \bullet \nabla_\theta^T g(\hat{\theta})\right]^{1/2}$ as this coincides with the SRDP when it is linear. However the slope of the reference line will be zero for functions where $\nabla_\theta g(\hat{\theta})=0$. This occurs for the J_{perf} function of Equation 5.5 as was noted in Section 5.2.4. In such cases, the slope can be approximated by $\left[E_\theta(\Delta\text{Perf}(\hat{\theta}))\right]^{1/2}$. Chen (1993, Theorem 3.3.2) has shown that for general $g(\theta)$, the reference line is not necessarily tangent to the SRDP at $g(\hat{\theta})$.

In this and subsequent examples, "coverage" is calculated via 500 Monte-Carlo simulations. It is reported as the percentage of confidence intervals which encompass the true value. Coverages can be determined for either joint confidence regions of the model parameters ("parameter coverage") and/or nonlinear functions of the parameters, such as the robust control criteria of Equations 5.5 and 5.6 ("controller coverage"). Our interest is ultimately in the latter although there appears to be a close correspondence between the two.

Consider again the first-order example of the previous section. SRDP functions were determined for two different identification inputs, the control relevant optimal AR=-0.965 and non-optimal AR=-0.5. It is seen in Figure 5.7 that they are markedly different from one another and deviate considerably from their respective linear approximations. The vertical drop lines indicate the 95% confidence bounds and the superiority of the linear approximation in the AR=-0.965 case is evident. This superiority is mostly a reflection of the particular local conditions around which the linearization was taken. However, since a control-oriented optimal input does ensure small confidence regions there is some assurance that the 95% confidence bound is relatively close to the point of linearization. The corresponding coverages of the nominal 95% confidence regions for the normalized robust control criterion of Equation 5.12 are given in Table 5.2 but do not reflect the severity of the observed differences between the SRDP's and their respective linear reference lines. Hence, the linearization or "reference" line may not be the most appropriate for indicating deviations from nominal coverage.

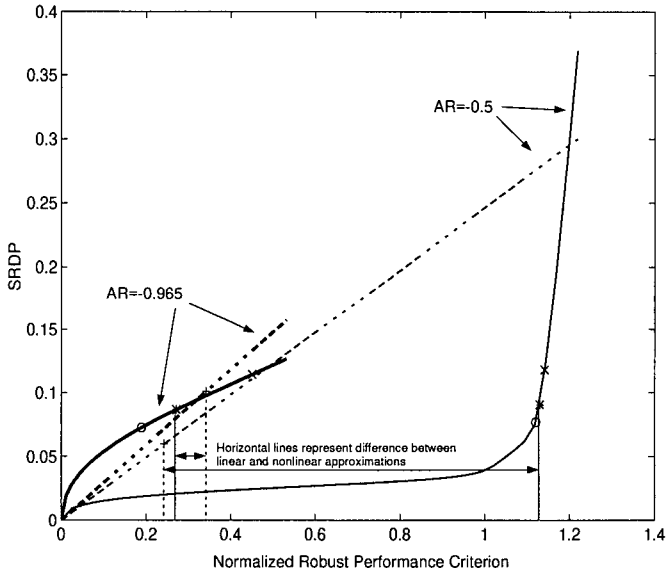

Figure 5.7: Signed Root Deviance Profile functions (Eqn. 5.28) for the first-order example with different input signal frequency contents. N_{ID}=500.
Solid lines: Signed Root Deviance Profiles (SRDP)
Dashed lines: Linear approximations
o, * and x: 90, 95 and 99% Confidence bounds
+: Approximate 95% linear bounds

Input (AR Parameter of Eqn. 27)	Controller Coverage by 95% CR's
-0.965	91.6
-0.5	89.6

Table 5.2: Controller coverages for various input signals applied to the first-order example of Section 5.3. N_{ID}=500.

From Figure 5.7, it is also possible to assess the increasing degree of conservatism introduced by specification of a higher probability level. When the profile plot is relatively flat in the neighbourhood of the (1-α)% critical point a great deal of conservatism can be introduced into the upper control bound specification with the requirement of 99% confidence. However, for the case with input AR=-0.5, we see that there is virtually no penalty associated with increasing the confidence level and it may be possible to satisfy

effectively a requirement of "hard" upper bounds on the performance (i.e. 100% certainty on the performance specification). Thus, careful inspection of the SRDP provides a means of setting reasonable performance expectations on the controller for problems of any dimensionality.

In Figures 5.8 and 5.9 we see the effect of increasingly short datasets on the efficacy of the confidence regions. For the essentially asymptotic case (N=10,000) both parameter and controller coverages are quite accurate, with some additional nonlinearity introduced in the controller criterion. Controller confidence bounds based on the linearization given in Equation 5.20 are overly conservative. As the number of observations in the data set is reduced, coverage drops and does so severely for N<500. The difference between parameter and controller coverages remains constant with the number of observations indicating that the nonasymptotic degradation in accuracy is associated with the parameter estimation stage.

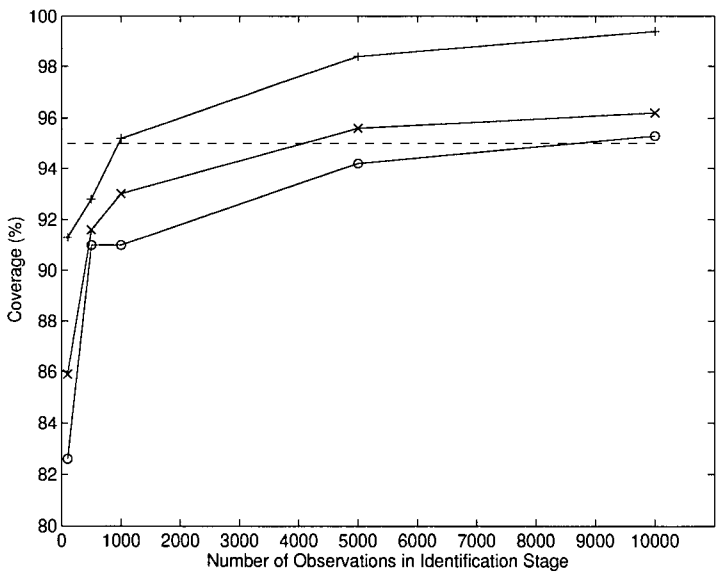

Figure 5.8: Non-asymptotic parameter and controller coverages for first-order example.
x: Parameter coverage based on nonlinear CR's
o: Controller coverage based on nonlinear CR's
+: Controller coverage based on approximate linear CR's

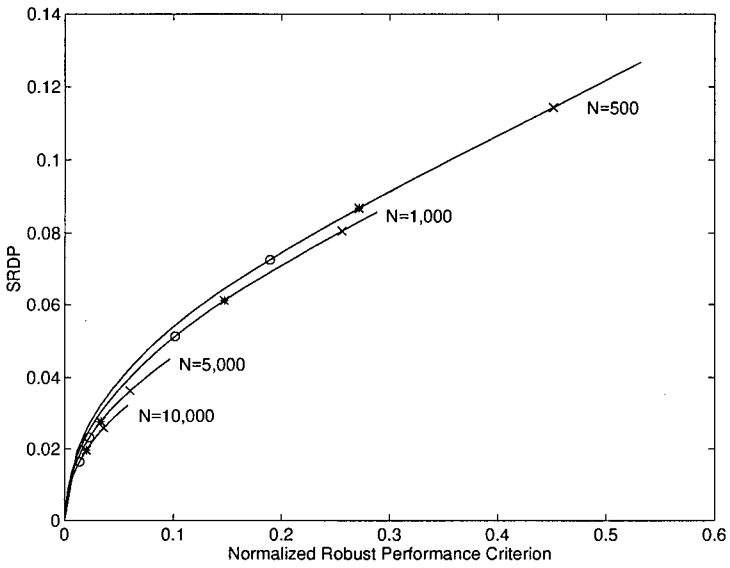

Figure 5.9: SRDP functions for first-order example with non-asymptotic model identification. Corresponding 90, 95 and 99% controller confidence bounds are shown as the points 'o', '*' and 'x' respectively.

5.5 Confidence Intervals, Validation and Undermodelling

Much emphasis has recently been put on the role of model validation and its connection to the size of uncertainty specifications on identified models. The basic result of Guo and Ljung (1994) is that for models which have passed a model validation test on the cross-correlation between residuals and past inputs, the error due to uncertainty in the process transfer function parameter estimates is larger than that due to inadequacy in the form of the model. Such a result is in line with the classical notion of model validation tests as part of the model building process (e.g. Box and Jenkins (1976)), and has been stated more recently by Ljung and Guo (1996) as "obtain an unfalsified model: reduce it if necessary".

Recent efforts in the system identification literature have abandoned this classical iterative approach and opted instead to determine uncertainty bounds on models of order less than that of the actual underlying process. A common approach is to fit an additional set of terms which represent this undermodelling simultaneously with the model parameters resulting in,

$$y(t) = \tilde{G}_p(z^{-1},\theta)u(t) + G_\Delta(z^{-1},\theta)u(t) + \xi(t) \tag{5.29}$$

where upon comparison with Equation 5.7, $G_p(z^{-1},\theta) = \tilde{G}_p(z^{-1},\theta) + G_\Delta(z^{-1},\theta)$. The unmodelled dynamics $G_\Delta(z^{-1},\theta)$ typically assume a Finite Impulse Response model, which is less parsimonious and more generic in form than $\tilde{G}_p(z^{-1},\theta)$.

In order to conduct tests for the magnitude of the parametric uncertainty associated with $\tilde{G}_p(z^{-1},\theta)$ and $G_\Delta(z^{-1},\theta)$ some a priori assumptions are placed on the undermodelling component. Wahlberg and Ljung (1992) specify an overbound on the sum of residual errors, β, which leads to "hard" (i.e. 100% coverage) bounds for the true process dynamics. The resulting uncertainty regions are given by:

$$(\theta - \hat{\theta})^T \mathrm{Cov}(\hat{\theta})(\theta - \hat{\theta}) \leq \beta \tag{5.30}$$

where θ is associated with both $\tilde{G}_p(z^{-1},\theta)$ and $G_\Delta(z^{-1},\theta)$. Only the case in which θ entered into the model linearly was treated. Nonlinear cases could be handled by the techniques discussed previously in this chapter. Goodwin et al. (1992) treat the observed $G_\Delta(z)u(t)$ as a realization of a stochastic process with conditions on the rate at which its impulse response decays. In both cases a likelihood ratio test is applied to the set of parameters in $\tilde{G}(z,\theta)$ and $G_\Delta(z,\theta)$ in order to produce linearized frequency domain confidence regions. Larimore (1993) made use of the non-central F-distribution in forming approximate linearized confidence bounds for dynamic models. The non-centrality

parameter is related to the bias present (i.e. distance between expectation planes) but requires an estimate of the true process dynamics for its estimation. Thus application of the likelihood ratio test dictates estimation of the true process dynamics.

In all of the above methods for characterizing uncertainty of reduced order models, it is also necessary to obtain a model of the 'true' process dynamics. The methodology for producing uncertainty regions presented earlier in this chapter relies on the assumption that the true process model is known and, in fact, produces uncertainty regions for this true process. It is presumed that these regions could subsequently be mapped to corresponding ones for reduced order models if deemed necessary for controller design. The important advantage here is that a more parsimonious model form for the true process dynamics is sought thereby avoiding problems of overfitting (i.e. capturing noise effects through fitting models parameters in addition to those required to completely describe the process dynamics).

To further illustrate these points the following example is given. Consider a second-order system,

$$y(t) = \frac{0.0172z^{-1}}{1 - 1.7236z^{-1} + 0.7408z^{-2}}u(t) + \xi(t) \qquad (5.31)$$

with σ_ε=sqrt(0.002). The input is a clipped (±1) realization of 1st order autoregressive process,

$$u(t) = \frac{0.01z^{-1}}{1 - 0.99z^{-1}}a(t) \qquad (5.32)$$

where a(t) is a unit variance white noise process independent of $\xi(t)$. A first-order transfer function model was fit to the data with varying orders, s, of the disturbance model.

$$G(z,\hat{\theta}) = \frac{\hat{b}z^{-1}}{1+\hat{a}z^{-1}}$$
$$H(z,\hat{\theta}) = \frac{1}{1+\hat{d}_1 z^{-1}+\ldots+\hat{d}_s z^{-s}} \tag{5.33}$$

Five hundred simulations of each case were performed and results are given in Table 5.3. Coverages for the true process model were calculated as the percentage of cases in which:

$$S(\theta_o) \le S(\hat{\theta}_{mod})\left[1+\frac{p_{mod}}{N-p_{mod}}F_{\alpha;p_{mod},N-p_{mod}}\right] \tag{5.34}$$

where the subscript 'mod' indicated the fitted model. The residuals were subjected to tests of autocorrelation (R_{AC}) and cross-correlation (R_{xc}) which are explained in Appendix C. Critical values at the 95% confidence level against which R_{XC} and R_{AC} should be compared are shown in brackets.

s	Mean Process Transfer Function Parameters		R_{xc} (M=20)	R_{AC} (M=20)	95% Model Coverage
	$\hat{a}$	$\hat{b}$			
0	0.0634	-0.9397	46.1 (28.9)	1550 (31.4)	100
1	0.0595	-0.9437	2.50 (28.9)	79.9 (30.4)	100
2	0.0527	-0.9520	0.80 (28.9)	34.5 (28.9)	89.2
3	0.0519	-0.9545	0.60 (28.9)	22.1 (27.6)	67.6
5	0.0509	-0.9546	0.50 (28.9)	19.1 (26.3)	61.2

Table 5.3: Results of undermodelling simulation.

For an inflexible disturbance model (s=0) the confidence bounds based on the sum of squared prediction errors are very large due to the large amount of bias present in the

identified model (i.e. the nominal sum of squared prediction errors is large). This is reflected in the validation statistics and the model would be rejected at the 95% confidence level. The autocorrelation function (ACF) for realizations of this case are shown in Figure 5.10 in which the model inadequacy is obvious. With increasing s, more of the residual dynamics are captured by the disturbance transfer function and the model bias is reduced. Correspondingly, a reduction in the validation statistics results to the point where the model is validated. The ACF for the s=3 case is shown in Figure 5.11. However, application of the likelihood ratio test to the validated identified models does not result in good coverages. This is a direct consequence of the overmodelling which has made the residual vector smaller than the true residuals.

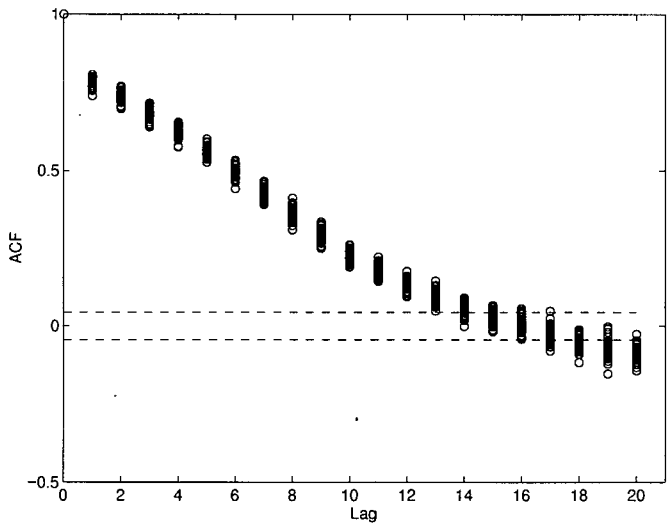

Figure 5.10: Auto-correlation function for undermodelling example with s=0.

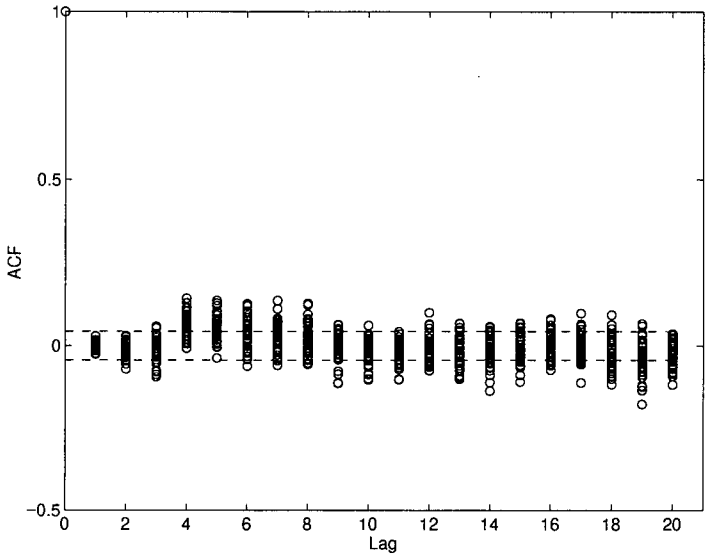

Figure 5.11: Auto-correlation function for undermodelling example with s=3.

The conclusion to be drawn from this illustration is that validation of a model does not guarantee confidence intervals will provide good coverage. In order to obtain good coverage a parsimonious model representative of the true process dynamics must be used. This emphasizes the need for a process models based on fundamental physical and chemical knowledge.

5.6 Application to Wet End Chemistry

This section applies the linear experimental design techniques developed in Section 5.2.4 to the problem of designing control relevant test sequences for the paper machine wet end chemistry system. The idea of designing and applying perturbation signals to the system might seem at odds with developing a detailed first principles simulation model. Indeed, part of the motivation for developing the simulation was to avoid the limitations of empirical models which are effective only in the range over which the data was taken.

However, as seen in Chapter 4, with incomplete knowledge of certain key model parameters, process data is required to determine values for these parameters. This was seen most clearly in Section 4.2.1 where an approximate fitting of model parameters was made to step response data. The purpose of the examples given here is to impart desirable frequency characteristics into the test signals so that they are relevant to anticipated closed-loop control requirements. The role of a previously developed simulation in designing these input sequences will also be noted, along with some practical aspects of their implementation. Hahn (1984) has noted the desirability of predicting process behaviour before implementing test signals into systems, in order that previously held perceptions are challenged in an objective manner. This prior prediction is done using the wet end chemistry simulation.

Test sequences were designed for both LMW cationic and HMW anionic polymers. Each sequence was designed to be 2 hours in duration. It was decided to overlap the sequences by commencing the HMW anionic sequence 1 hour after the start of the LMW test. This overlap was designed in order to show interactions between these two effects. However, it is noted that the signals are not specifically designed to account for these interactions.

The response of wire drainage to LMW cationic changes was used for design purposes, while the flume solids consistency response was paired with HMW anionic polymer. The closed-loop objective was the normalized robust performance criterion of Equation 5.12 subject to a square wave (closed-loop) command signal with fundamental frequency ω=0.0094. The results for the LMW cationic case will be shown as an example. Special considerations with regard to the rate of HMW anionic addition are also discussed.

From the simulated step response of Section 4.2.2, an approximate first-order transfer function model was identified for the LMW cationic (LMWC) ⇔ Wire Water Retention (WWR) response. The model is,

$$\mathrm{WWR}(t) = \left[\frac{-0.0213z^{-1}}{1-0.9814z^{-1}}\right]\mathrm{LMWC}(t) \tag{5.35}$$

The model following controller design procedure from Section 5.3 was again used so that the closed-loop response matches the open-loop response according to Equation 5.27.

The linear input design procedure of Section 5.2.4 was then applied to determine an optimal value of the AR parameter in the first-order time series of Equation 5.24, with results shown in Figure 5.12. The original and clipped time series realization implemented as the test signal for LMW cationic polymer are shown in Figure 5.13. It is noted that there are some high frequency switches in the proposed LMW cationic flowrate. These are ignored in the final proposed implementation of the signal as it would be impractical for operational staff to make these changes.

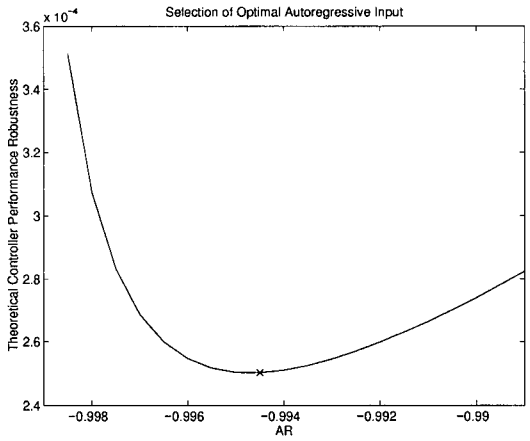

Figure 5.12: Selection of optimal input signal parameter for LMW cationic polymer test sequence

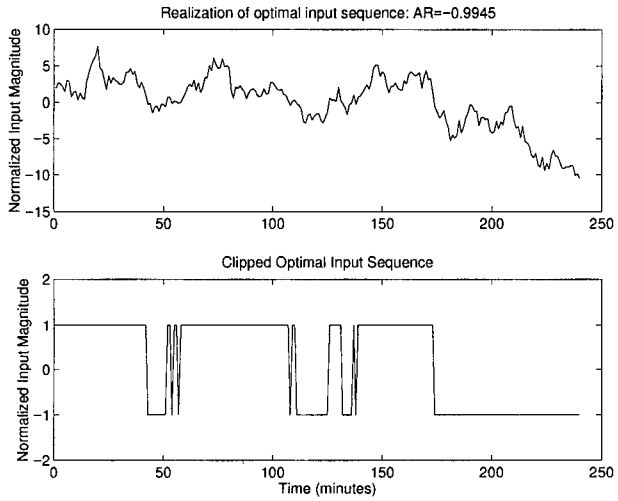

Figure 5.13: Clipped and non-clipped input realizations for LMW cationic polymer test sequence

The robustness of the anticipated controller using both the optimal input signal (AR=-0.9945) and a non-optimal test signal (AR=-0.8) are compared in Figure 5.14. The optimal test input's improved anticipated performance robustness is clearly illustrated by its much smaller confidence region volume. Worst case performance is indicated by the location of the 'x's on the corresponding confidence region boundaries, and where they lie on the control performance surface (dashed contours). In this case we see that the optimal input provides an anticipated three fold improvement in performance. Chapter 6 will explore whether these anticipated gains are realized in practice.

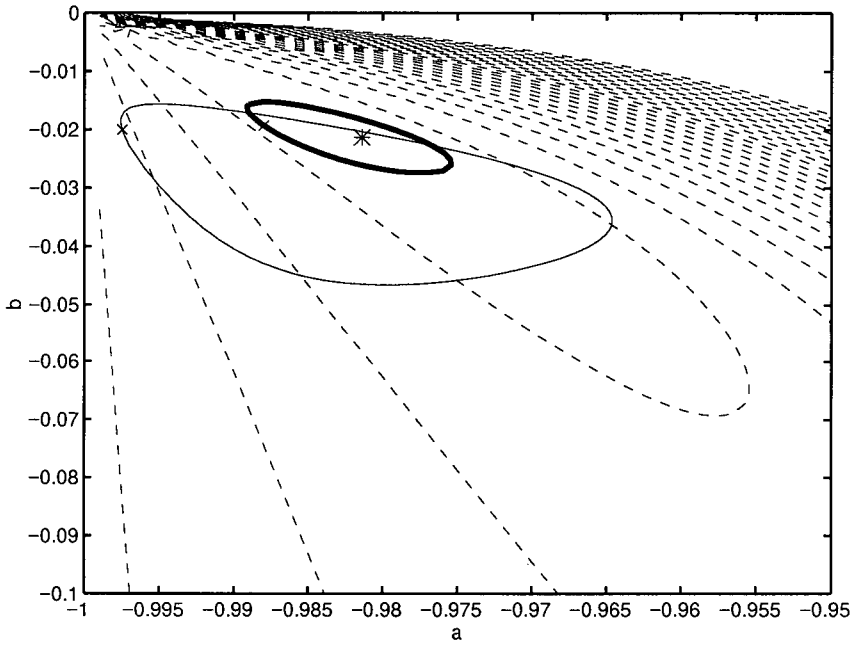

Figure 5.14: Controller robustness and identification plot for optimal and non-optimal input sequences in LMW cationic polymer test. Optimal Input (Thick contour), non-optimal input (thin contour).

For the case of the HMW anionic polymer test signal an additional constraint was imposed on the incremental rate of change to avoid a possible sheet break. After consultation with operating personnel a maximum rate of 0.6%/minute was determined. In order to incorporate this into the design procedure, the flume solids consistency response was restricted through choice of the desired closed-loop response, H_m, in a pole placement controller design (Aström and Wittenmark (1989)). In general, for second-order closed loop dynamics,

$$H_m(s) = \frac{1/\omega^2}{\omega^2 + 2\xi\omega + s^2} \tag{5.36}$$

where the parameters ξ and ω are chosen so that the maximal slope of the response is less than the above specified rate. The fact that, as a worst case scenario, there is essentially a straight open-loop gain relationship between input and output leads one to consider the

desired dynamics for both the input test signal and output closed-loop response to be expressed by H_m.

The resulting structure for H_m was found by choosing ω=0.4 and ξ=1, giving a discrete time transfer function representation,

$$H_m(z^{-1}) = \frac{\left(0.0616 + 0.0417z^{-1}\right)z^{-1}}{1.0 - 1.3406z^{-1} + 0.4493z^{-2}} \tag{5.37}$$

The input signal form was modified for the clipped time series according to the procedure shown in Figure 5.15.

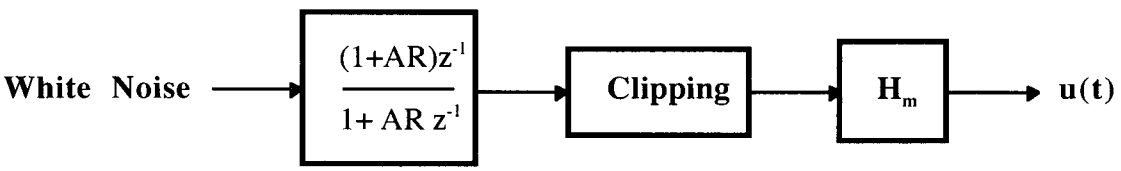

Figure 5.15: Modified procedure for obtaining input signal with second-order dynamics

In this way, the optimal parameter AR was chosen to account for the fact that both the identification input and the desired closed-loop response must follow suitably slow dynamics.

The designed test sequences and simulated responses are shown in Figures 5.16 and 5.17 respectively. Note that some simplifications were implemented by ignoring very short switches in the theoretical test signals. For the case of the HMW anionic test signal, ramped approximations are made in order to facilitate implementation of the signal in a DCS. Maximal test levels were agreed upon with operational staff to again ensure the

safety of the test. Due to a long term malfunction of the low consistency (retention) sensor electronics it was not possible to implement this test sequence during the course of this project.

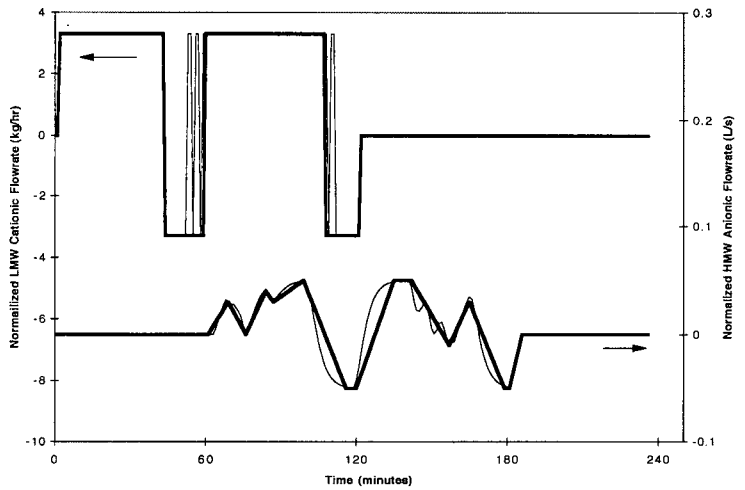

Figure 5.16: Multivariable input test sequence for LMW cationic and HMW anionic polymers

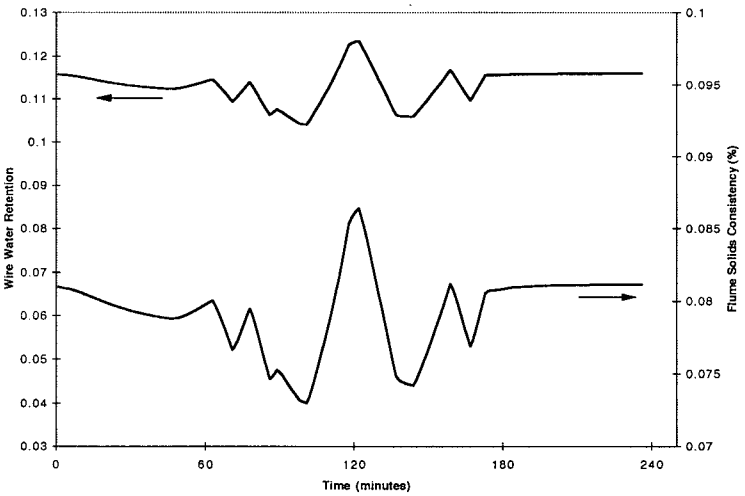

Figure 5.17: Simulated wire water retention and flume solids consistency responses to multivariable input test sequence.

5.7 Summary

The first part of this chapter has extended existing methodologies for producing bounds on the uncertainty associated with identified transfer function models used in the design of feedback control schemes. The result is that one can specify, with arbitrary probability, the anticipated uncertainty for any measure of closed-loop performance. The basic problem has been cast as an optimization of the controller robustness measure constrained by the model uncertainty, which is an application of a result due to Chen (1991). A constrained optimization approach has been suggested for determining the maximum and minimum expected robustness measures. As well, a procedure for representing the model uncertainty in the frequency domain has been given. The procedure also uses a constrained optimization approach as well as the fact that process transfer function frequency response is a nonlinear function of the parameters.

Parametric nonlinearities affecting both the modelling and control problems are accounted for by the above techniques. From the simple examples examined in this study, confidence bounds which account for such nonlinearity are found to be significantly more accurate than those based on linear approximations. The Squared Root Deviance Profile (SRDP), introduced in Chen and Jennrich (1996), was used to give a graphical summary of the nonlinearity in the constrained optimization problem. In this manner, trade-offs between the level of confidence in the bounds (i.e. conservatism) and controller robust performance could be analyzed.

The efficacy of the above confidence intervals has been determined by the statistical concept of "coverage" -- the probability that a confidence interval encompasses the true value. While confidence intervals based on likelihood regions are exact in shape they are approximate in the probability level, α, as their development is based on an analogy to the

linear case. As well, identification carried out with finite datasets leads to small deviances of the coverages from their nominal level. An example was given showing, through use of the SRDP function, the relationship between the nonlinearities introduced by the above two approximations and the corresponding loss in coverage. This suggests the need for finding linearizing transformations to the sum of squares functions.

An application of control-relevant input signal design was given. Through consideration of the control objective in the input signal design, substantial reductions in the size of the closed-loop uncertainty bounds were realized for a typical modelling/control situation. This was accomplished by affecting both the size of the parameter uncertainty region and its orientation with the control objective function. The input design theory was based on a first-order linear approximation to the closed-loop robust performance function. Hamilton and Watts (1985) have suggested a nonlinear formulation to the experimental design problem based on higher-order Taylor series expansion.

A basic assumption of the above methodology is that one has identified the correct model form. Bounds on the uncertainty of an identified model that are based on classical statistical assumptions have come under a great deal of scrutiny in recent years. In particular, the reluctance to search for an assumed "true" underlying process has motivated alternative approaches in which the residuals in a lower order model contain both a stochastic component and unmodelled process dynamics. Bounds of the resulting uncertainty from such schemes are typically estimated by fitting a reasonably generic model form to the residuals and conducting hypothesis tests based on this approximate model. It has been argued here through the principle of parsimony, and shown by example, that identification of the true process leads to coverages of uncertainty regions closer to nominal levels. This holds even if model validation statistics have found no evidence of lack of fit.

Chapter 6
Identification of Wet End Chemistry Dynamics

The previous chapter introduced a methodology for conducting identification experiments which ensure good closed-loop performance when the system is linear. This chapter implements these methods in the wet end chemistry control problem using the nonlinear simulation model developed in Chapter 3. This is done in order to test the identification method's effectiveness in a more challenging setting. The overriding goal is to obtain reliable input-output models of the wet end dynamics in a form suitable for controller design.

To this end, the HMW Anionic Polymer $\Leftrightarrow$ White Water Consistency loop will be investigated. Addition of this polymer is the final manipulated variable which affects wet end operations (retention, drainage, etc.) and as such is extremely important. The simulated open-loop behaviour of this loop was discussed in Section 4.2.1 and an optimal input testing sequence was designed in Section 5.6, based on the simulation. Simulation results indicated that interactions between short and long white water recirculations leads to higher order dynamics. This chapter will further characterize such behaviour. As well, data from the on-machine polymer ramp increase (Section 4.3) will be used to characterize the disturbances acting on the system.

6.1 Implementation of Control Relevant Identification

6.1.1 Disturbance Modelling

The ramped step increase investigated in Section 4.3 is used to determine a disturbance data sequence. The residuals from the measured white water filler consistency and the simulated data from Case 4 are taken as the disturbance sequence, which is plotted in Figure 6.1.

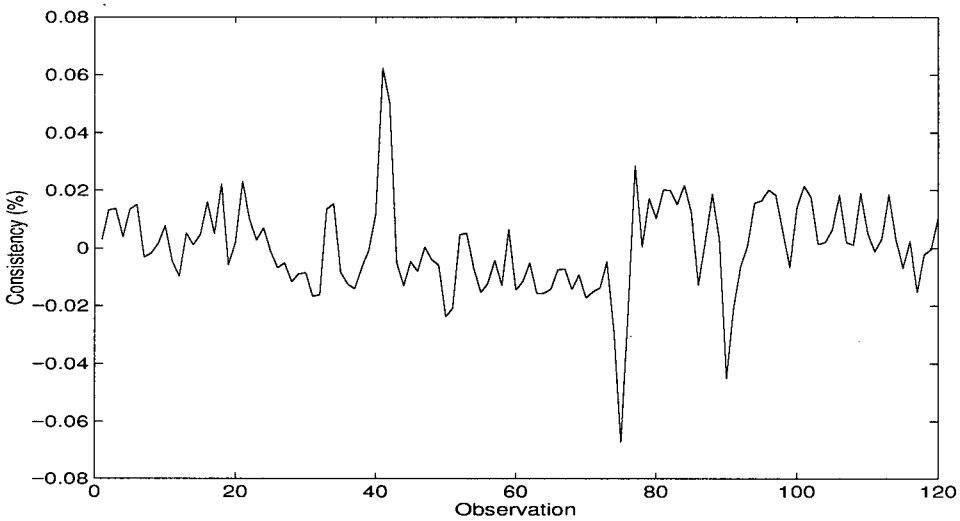

Figure 6.1: Additive disturbance sequence for white water filler consistency signal

A number of linear time series models were fit to the above sequence. These models are of the ARIMA (Autoregressive Integrated Moving Average) form represented by,

$$d(t) = \frac{c_o + c_1 z^{-1} + \ldots + c_r z^{-2}}{\nabla^l (1 + f_1 z^{-1} + \ldots + f_s z^{-1})} \xi(t) \qquad (6.1)$$

where, as in Chapter 5, $\nabla^l=(1-z^{-1})^l$ and $\xi(t)$ is a zero mean, normally distributed white noise process with variance σ_ξ^2. Inclusion of the differencing operator, ∇, accounts for low frequency drifting of the process.

Results from the model fitting by the method of maximum likelihood are summarized in Table 6.1. Models were partly judged by their ability to minimize the one-step ahead prediction error loss function. As well, the final prediction error (FPE) criterion indicates a trade-off between the amount of variation captured by the model and the complexity of the model. It can thereby be regarded as a measure of model predictive power (Priestly (1989)).

Structure	Loss Function ($x10^4$)	FPE ($x10^4$)
MA(1)	1.778	1.749
ARMA(1,1)	1.743	1.802
IMA(1,1)	1.749	1.778
IMA(1,2)	1.825	1.765
ARIMA(1,1,1)	2.069	2.140
ARIMA(1,2,1)	2.5720	2.661

Table 6.1 Results of fitting ARIMA time series to disturbance sequence

Most of the models have similar values for the loss function and FPE. To select the most appropriate model form the autocorrelation functions (ACFs) were examined. Figure 6.2 shows the ACFs for the IMA(1,1) and MA(1) cases. In the former, there is a significant correlation at lag 2 which led to an (unsuccessful) attempt at improving the model by second differencing. The MA(1) model has a significant correlation at lag 1. Surprisingly, addition of an AR parameter is not significant. The MA(1) model was chosen as it represents a stationary time series and the data suggest little evidence of the large drifts associated with non-stationary integrated forms. The fitted disturbance model is then:

$$d(t) = (1 + 0.6251z^{-1})\xi(t) \qquad (6.2)$$

with $\sigma_\xi^2=1.743x10^{-4}$. The standard deviation of the parameter is 0.0748.

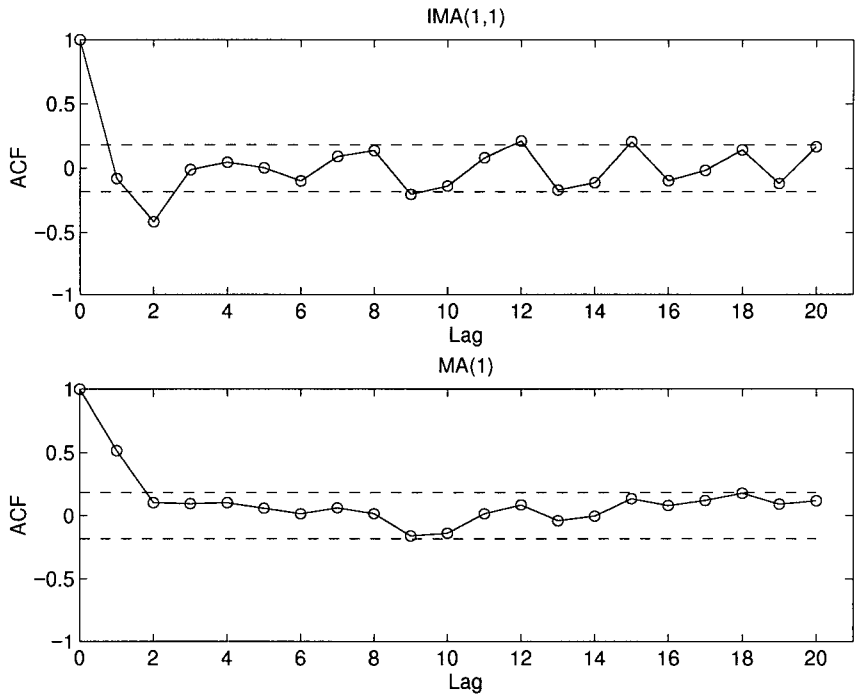

Figure 6.2: Autocorrelation functions of residuals from time series model fitting to disturbance sequence

6.1.2 Input Signal Implementation

Two input sequences were implemented in the simulated process manipulating HMW Anionic Polymer flowrate. The first is the 'control relevant' sequence shown in Figure 5.15. Design of this input sequence is discussed in Section 5.6 as well. The second input sequence is a square wave input signal with a switching time (1/2 period) of 30 minutes. This represents a simple test pattern that could be easily implemented in a mill and will be denoted as the 'ad-hoc' input. The ad-hoc input is also subject to a maximum rate of change constraint of 0.6%/minute. At each 30 minute interval the HMW Anionic flowrate is ramped to the next level and held at there until the next switching time. Both of these inputs are shown in Figure 6.3 below.

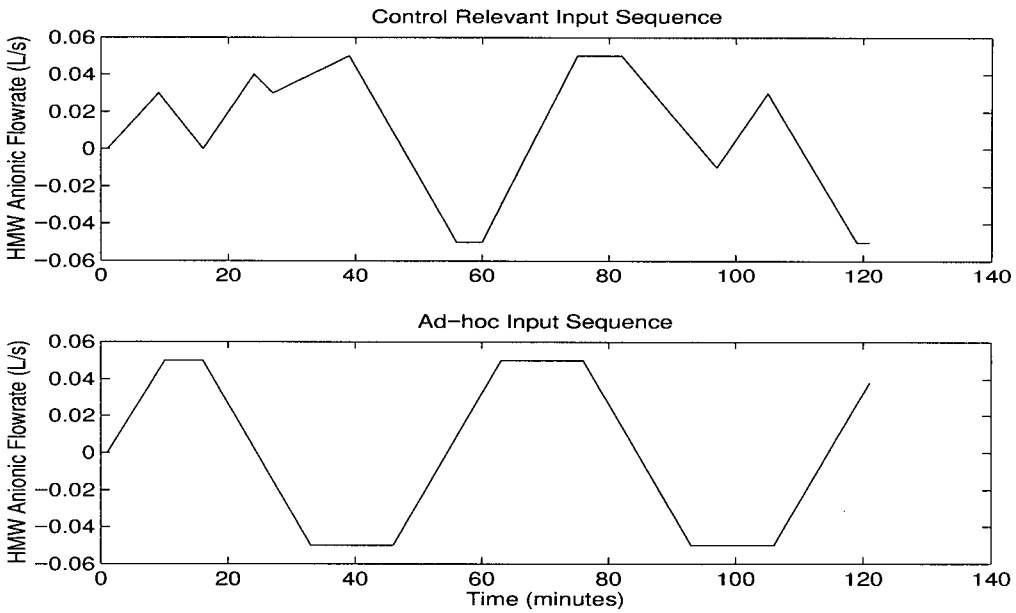

Figure 6.3: Control relevant and ad-hoc input sequences

Clearly the control relevant input sequence attempts to excite a broader range of frequencies than does the ad-hoc input. This is partly a reflection of the closed-loop requirements placed on the controller.

Upon implementation of these input sequences in the simulation model the white water filler consistency responses were generated and are shown in Figure 6.4.

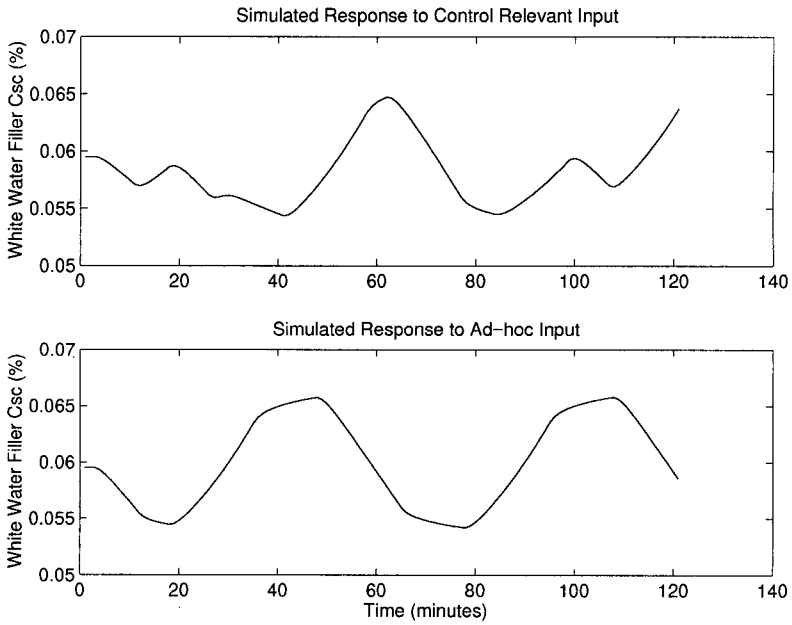

Figure 6.4: Simulated white water filler consistency responses to implementation of input sequences

6.1.3 Noise-free Identification of Linear Models

Linear transfer function models were first fit to the noise free responses using the data displayed in Figures 6.3. and 6.4. This provided a means to investigate the order of the true process dynamics without uncertainty introduced into the modelling process by the presence of noise. Furthermore, it is also possible to assess the frequency distribution of bias introduced if reduced order models are to be used for controller design.

The trade-off between model order and the squared prediction error loss function is shown in Figure 6.5. Note that there are separate curves corresponding to the two different input signals. This is due to the different frequency contents of the control relevant and ad-hoc inputs, with the former actually having a higher loss function for all model orders. As well, it is important to note that it was not possible to drive the loss function to zero even in

the noise free case. This indicates the presence of nonlinearities, the nature of which will be discussed in more detail later.

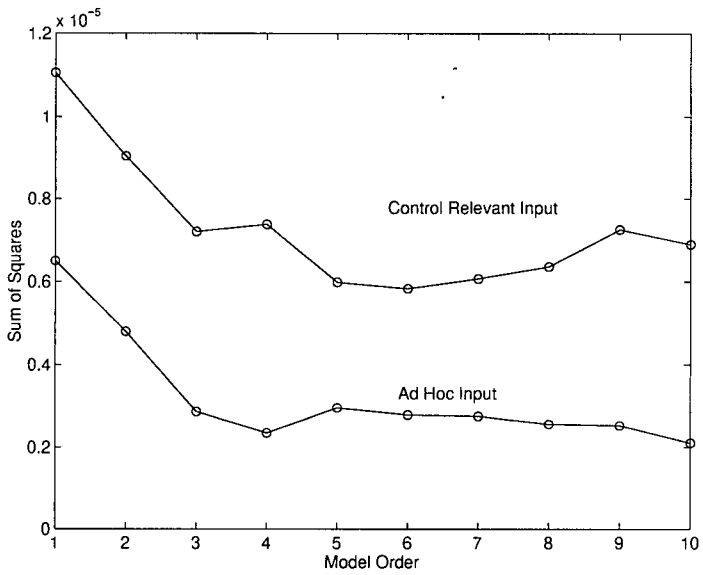

Figure 6.5: Loss function for noise free linear model fitting

The autocorrelation function for the 3rd and 5th order models identified using the control relevant input sequence are shown in Figure 6.6 by the thin and thick lines repectively. In the noise free case the ACF is an indication of model inadequacies indicated by linear correlation amongst lagged residuals. If the true system were linear then the ACF would be zero for lags > 0. Clearly the 5th order model does a reasonable job of capturing most of the linear effects present while there is some inadequacy indicated for the third order model.

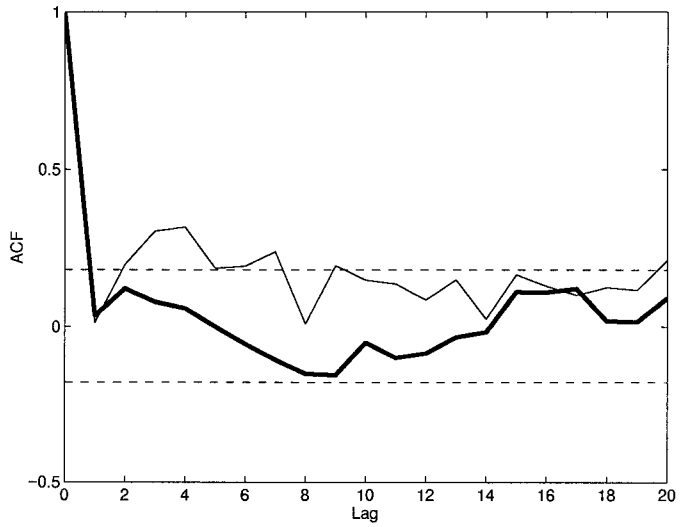

Figure 6.6 Autocorrelation function of fifth (thick) and third (thin) order models from fits to noise free data

If the set of possible models is restricted to those which are linear, the loss function curves demonstrate that there is little penalty to be paid for choosing a third-order approximation to the (unknown) true model. This is further illustrated in Figure 6.7 where Nyquist plots for fifth and third-order linear models are compared. Plots are shown for models identified with both the control relevant and ad-hoc inputs, along with the theoretical spectral densities of these inputs. Since the fundamental frequency of the square wave input is 1/60 minutes=0.0167 minutes^{-1} the ad-hoc input gives rise to excellent frequency matching in this region. The control relevant input, which excites a broader range of frequencies, has better mid-frequency matching with the higher order (linear) model.

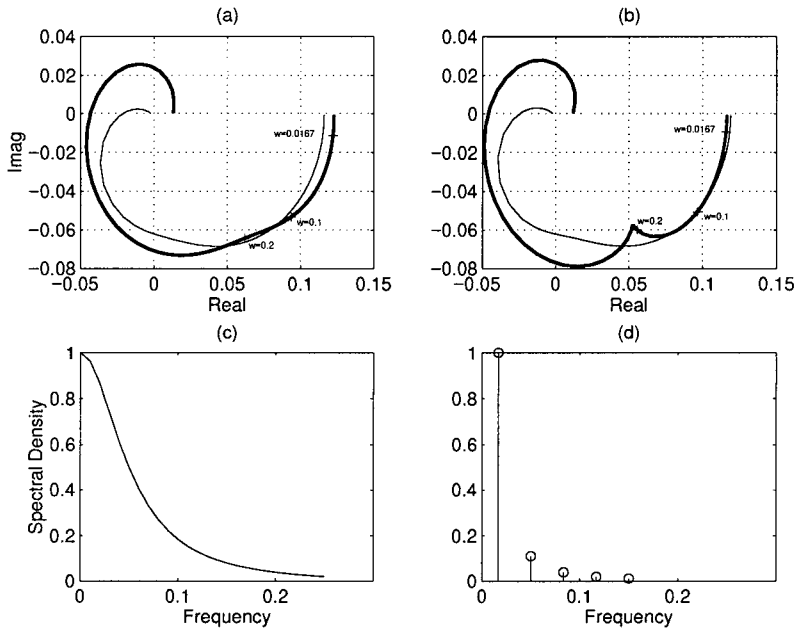

Figure 6.7: Nyquist plots and input spectra for noise free linear identification.

(a) Third (thin) and fifth (thick) order Nyquist plots, control relevant input

(b) Third (thin) and fifth (thick) order Nyquist plots, ad-hoc input

(c) Control relevant input spectral density (normalized)

(d) Ad-hoc input spectral density (normalized)

6.1.4 Identification of Linear Models in Presence of Noise

In order to test the efficacy of the control relevant methodology for this example, five realizations of an additive disturbance were generated according to the MA(1) model identified in Section 6.1.1 and added to the noise free simulated responses. The four parameters of the 3rd order model,

$$G(z,\hat{\theta}) = \frac{b_o z^{-1}}{1 + a_1 z^{-1} + a_2 z^{-2} + a_3 z^{-3}} \tag{6.3}$$

were identified for each of the 10 cases (5 for control relevant input case, 5 for ad-hoc input case). The third-order model was used because it was simpler for controller design purposes. Figure 6.7 also showed that bias introduced by using this lower order approximation is not too severe, particularly in the frequency ranges of interest.

Nyquist diagrams of the fitted models are shown in Figure 6.8 along with the noise free Nyquist plots for the 5th and 3rd order approximations. The variation in the models identified with the control relevant input is clearly much greater than that from application of the ad-hoc input. This is especially true at lower frequencies which is the result of the lower frequency content of the ad-hoc input signal. In order to achieve better closed-loop robustness one would expect models identified with the control relevant input to demonstrate reduced variability as was seen in Chapter 5. The reasons for this discrepancy will be discussed further in Section 6.1.6.

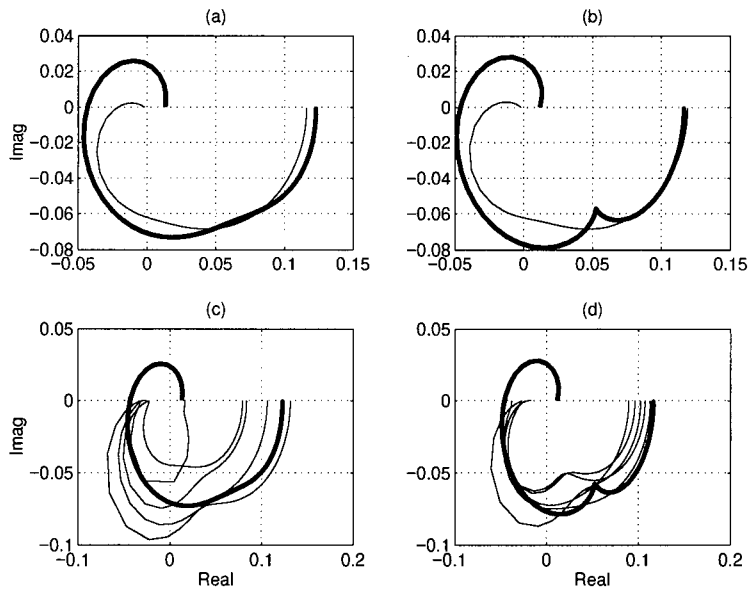

Figure 6.8: Nyquist diagrams of fitted third-order models with noisy data
(a) Control relevant input, noise free, 5th order (thick), 3rd order (thin)
(b) Ad-hoc input, noise free, 5th order (thick), 3rd order (thin)
(c) Control relevant input, noisy realizations (thin lines)
(d) Ad-hoc input, noisy realizations (thin lines)

6.1.5 Closed-loop Performance

Pole placement controllers were designed based on the third-order models identified from the noise free responses. A pole placement procedure was chosen as it allowed explicit specification of the closed-loop response and analytical determination of the controller transfer function, which was convenient for the input design procedure. This represents a slight re-design of the controller used to calculate the input signal in Section 5.6. The previous design was calculated "in the field" prior to completion of the simulation model.

First the desired closed-loop response was modelled with a 3rd order transfer function fitted to the HMW Anionic Polymer flowrate signal from the ramp test of Section 4.3. This higher-order representation was determined to satisfy causality conditions in the controller design. The resulting model normalized to unity gain is:

$$H_m(z^{-1}) = \frac{-0.1578z^{-1}}{1 - 1.0146z^{-1} + 0.3280z^{-2} - 0.1556z^{-3}} \tag{6.4}$$

Following Aström and Wittenmark (1990) the servo design problem is to find coefficients of the polynomials $R(z^{-1})$, $S(z^{-1})$ and $T(z^{-1})$ such that,

$$\frac{BT}{AR + BS} = \frac{B_m}{A_m} \tag{6.5}$$

where B/A is the process transfer function of Equation 6.3 and $B_m/A_m = H_m$. From this the resulting control law is:

$$R(z^{-1})u(t) = T(z^{-1})y_{sp}(t) - S(z^{-1})y(t) \tag{6.6}$$

The orders of the design polynomials R,S and T are subject to causality conditions specified in Aström and Wittenmark (1990). Some further design requirements are:

1. No cancellation of process zeros.
2. High gain at low frequencies. This is achieved by requiring $(1-z^{-1})$ to be a factor of R thereby introducing integral action into the controller.
3. Low sensitivity to measurement noise. This was achieved by proper selection of the observer polynomial $A_o(z^{-1})$.

With the above specifications, the algebraic design problem is then to solve the Diophantine equation:

$$(1 - z^{-1})A(z^{-1})R_1'(z^{-1}) + B^-(z^{-1})S(z^{-1}) = A_o(z^{-1})A_m(z^{-1}) \qquad (6.7)$$

where,

$$B(z^{-1}) = B^+(z^{-1})B^-(z^{-1}) = (1)b_o z^{-1}$$

$$R(z^{-1}) = (1-z^{-1})\,B^+(z^{-1})\,R_1'(z^{-1}) = (1-z^{-1})\,B^+(z^{-1})(1+r_1 z^{-1}+r_2 z^{-2})$$

$$S(z^{-1}) = s_o+s_1 z^{-1}+s_2 z^{-2}+s_3 z^{-3}$$

$$A_o(z^{-1}) = (1-a_{obs}z^{-1})^3$$

For all cases, a_{obs} was chosen as -0.5 as this value best attenuated high frequencies. The six polynomial coefficients r_1, r_2, s_o, s_1, s_2, s_3 and s_4 were determined for each case based on the identified model.

The expected performance of the controller was first (qualitatively) judged by examining the closed-loop response with the identified linear model as the true model. Both the servo and disturbance rejection performance were examined with a typical result (control relevant case) shown in Figure 6.9 and the corresponding loop gain transfer function Bode diagram in Figure 6.10. The servo performance is quite good with smooth controller action. The controller is able to (partially) reject low frequency disturbances but is still somewhat sensitive to higher frequency measurement noise. This sensitivity is seen in the Bode diagram in which the amplitude ratio does not roll off strongly. In practice it would be desirable to introduce filtering into the measurement feedback loop.

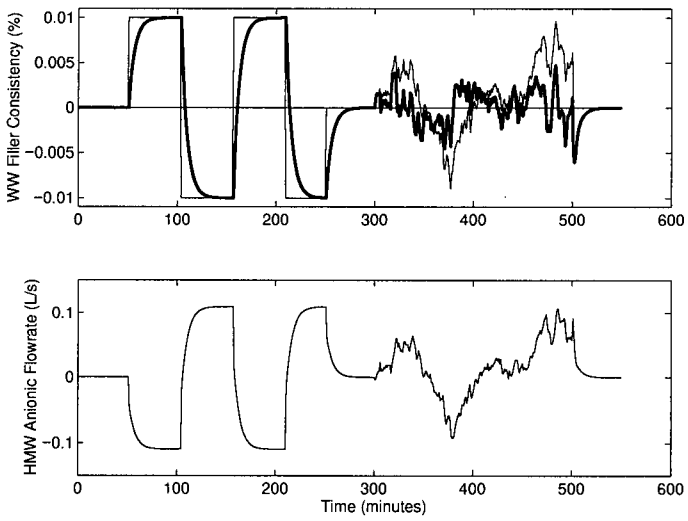

Figure 6.9: Simulated controller performance based on identified third-order linear model.

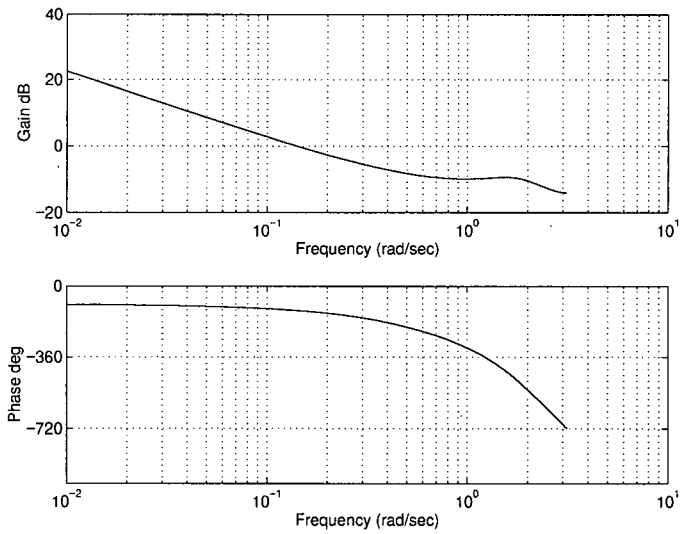

Figure 6.10: Bode diagram of loop gain transfer function for controller based on 3rd order linear model

These controllers were then implemented in the wet end chemistry simulation and the servo responses tested. Ten cases were simulated using the five models identified from both the control relevant and ad-hoc input sequences. For each of the ten cases, deviations from nominal H_2 performance were calculated as $\sum (y - y^{NF})^2$ where the nominal performance,

y^{NF}, was taken from a controller designed based on the noise free parameters. Results are shown in Table 6.2.

Realization	Control Relevant ($x10^3$)	Ad-hoc ($x10^3$)
1	1.137	0.804
2	7.788	5.795
3	77.024	3.764
4	31.445	11.094
5	7.190	6.502

Table 6.2: H_2 performance deviations for controllers designed based on noisy data

In all cases the controllers designed using models identified with the ad-hoc input gave superior robust servo performance. This is not surprising given the variation in the identified models seen in Figure 6.8 which resulted from excitation in frequency regions where apparent nonlinearities exist.

6.1.6 Identification of Nonlinear Behaviour

Difficulties were encountered in previous sections when attempting to fit linear dynamic models to data generated from the simulation model. The unreliable nature of models estimated from data generated using the control relevant input was attributed to excitation of frequencies at which nonlinearities were present. In order to examine this further, the simulation was excited at individual frequencies and the response examined. In general the responses were found to be nearly sinusoidal for all frequencies tested. Hence, approximate amplitudes and phase angles could be determined between the HMW Anionic

Polymer input and the White Water Filler Consistency output. These 'true' responses were then plotted on the Nyquist plane and are shown in Figure 6.11.

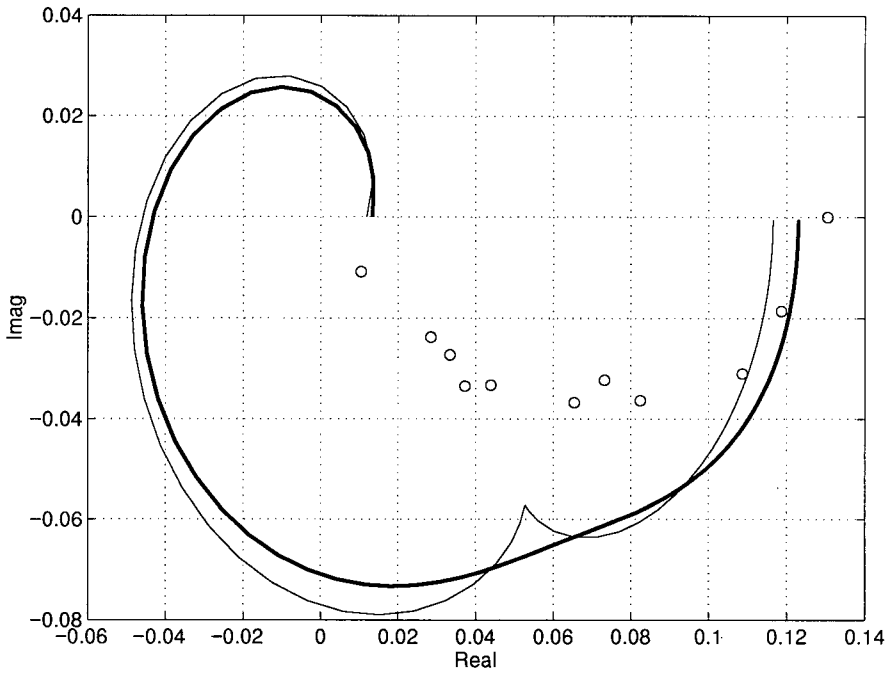

Figure 6.11: Frequency response from simulation model ('o') at various frequencies versus 5th order linear models identified using the control relevant (thin line) and ad-hoc (thick line) inputs.

Low frequency matching of the true and linear model responses is good. However, at higher frequencies there is considerable bias present. This agrees with the observations and results from previous sections. Since the control relevant input signal attempted to excite both low and high frequencies it introduced considerable bias into the modelling at these higher frequencies. The ad-hoc input, on the other hand, excited only the low frequency region and as such introduced little bias into the estimation.

To characterize this nonlinear behaviour further, the steady-state response of White Water Filler Consistency to HMW Anionic Polymer addition rate was examined over the normal operating range. This is shown in Figure 6.12 where a nearly linear relationship is evident

over the entire range. The close matching of the linear models and the simulation response in the low frequency range seen in Figure 6.11 is consistent with this result.

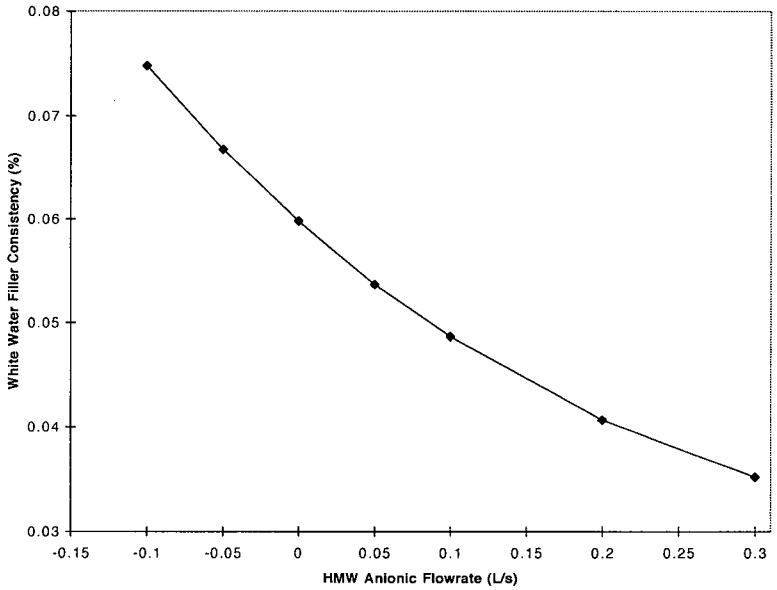

Figure 6.12: Steady-state response of White Water Filler Consistency to HMW Anionic Flowrate.

A nonlinear difference equation was fit to the noise free data giving a model of the form:

$$y(t) = -a_1 y(t-1) - \ldots - a_r y(t-r) + b_0^1 u(t-1) + \ldots + b_s^1 u(t-s) + b_0^2 u^2(t-1) + \ldots + b_1^1 u^2(t-1) \tag{6.8}$$

This maintains the form of a linear regression so that the ARX procedure in the Matlab System Identification Toolbox (The Mathworks (1995)) could be used. The sum of squared errors loss function for increasing model orders (r=s=l) is shown in Figure 6.13 and can be directly compared with the loss functions from linear model fitting of Figure 6.5. For both the control relevant and ad-hoc inputs the overall loss functions are consistently lower for all model orders. More importantly, it is possible to drive the loss function close to zero, indicating that the input nonlinear model form of Equation 6.8 is

capable of describing the process dynamics. Alternative models forms may provide more parsimonious representations but will not be explored here.

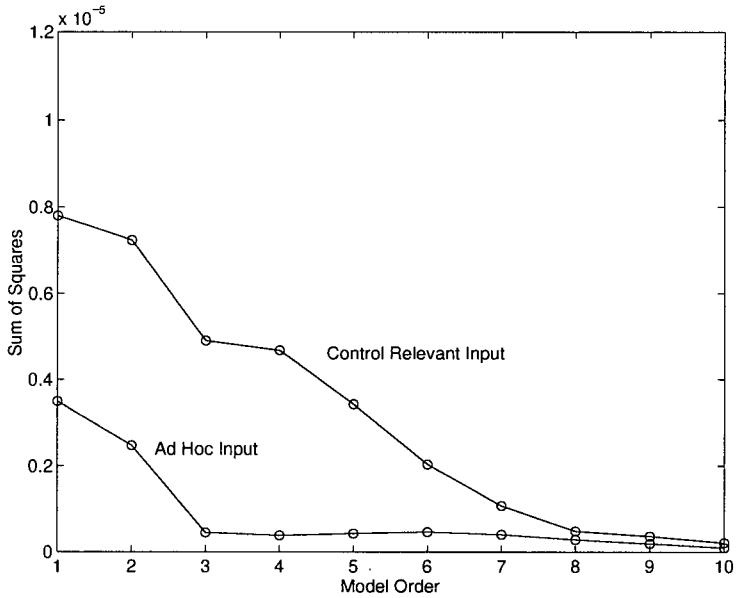

Figure 6.13: Loss functions for noise free nonlinear model fitting

6.2 Summary

One of the primary purposes of this chapter has been to test the control relevant identification methodology developed in Chapter 5 in a more challenging problem. Through use of the wet end chemistry simulation as the real plant, two different input signals were tested for their ability to identify dynamic models for the HMW Anionic Polymer/White Water Filler Consistency loop. Because of the presence of strong nonlinearities in the higher-order dynamics, the control relevant input failed to give models which were more robust than those from a low frequency ad hoc input when implemented into pole placement servo controllers. This indicates that the method itself may not be particularly robust to these types of nonlinearities. Thus it would seem appropriate to extend the control relevant identification methodology to include the presence of

nonlinearities. Knowledge of the presence and nature of nonlinearities could be furnished when an accurate process simulation is available. Without this level of a priori knowledge it is more appropriate to utilize input design techniques which are robust to model bias. Ljung (1987, Chapter 13) discusses design of input signals which account for the possibility of linear bias. Techniques for input design in the presence of nonlinear biases appear not to have been discussed in the literature.

Knowledge of the form of the process nonlinearity may aid in design of higher performance controllers for this loop. Rantala et al. (1993) have previously attempted adaptive control of the HMW Anionic Polymer / White Water Filler Consistency loop based on continuous identification of a linear ARX process model. The need for adaptation may be tailored by the operating range (i.e. gain scheduling) according to Figure 6.12 or by the frequency at which controller actions are demanded.

The value of an accurate process simulation has been underscored both in the identification and control stages. Most importantly, noise free identification can be carried out and potential biases in any proposed model can be identified prior to either input signal or controller design. Precise or control relevant models are not needed in order to develop the simulation model but rather follow from it.

Chapter 7

Conclusions and Future Work

7.1 Summary and Conclusions

The problem of identification and eventual control of chemical phenomena in papermaking is formidable. As seen in this and other works the presence of multivariable, nonlinear and often poorly understood effects in addition to difficult on-line measurements of key chemistry variables present major challenges. This work has attempted to increase the understanding of papermaking wet end chemistry such that reliable quantitative predictions of process performance are available. The primary end-use of the model developed here has been for eventual on-line control.

In order to accomplish the above, a large-scale dynamic simulation of the wet end chemistry system was developed encompassing the entire paper machine wet end. The model was based on the Prince Albert fine paper mill. Where possible, first-principles models were used and simulated responses were validated against on-line process data. Tools were developed for characterization and minimization of uncertainty in linear dynamic process models identified from noisy data. These techniques account for anticipated closed-loop requirements when the models are to be used in linear feedback control schemes. Finally, such control relevant identification techniques were applied to the wet end chemistry system to test their effectiveness using the previously developed simulation as the actual process.

The two main response variables studied were white water silo consistencies and wire drainage. The simulation model was able to predict variations in these two variables in a directionally correct manner thereby fulfilling the minimum requirement set out at the beginning of this work. This success was judged by comparison against on-line process data as well as the experience of paper mill personnel. Furthermore, it was demonstrated that the model is flexible enough such that calibration against on-line data leads to accurate predictions as well.

The on-line control of pH in the wet end was found unnecessary due to its control in the bleach plant. However, the wet end of a fine paper machine is sensitive to pH variations in the normal operating range even in the presence of calcium carbonate filler. If pH variations do occur either process solutions or better control in the pulp mill should be sought.

Development of the wet end chemistry simulation was accomplished by first building a 'physical' model of furnish component flows throughout the wet end. To this, modules were added describing refining, drainage, polymer adsorption and particle flocculation processes. The focus of these models was on their relationship to wet end chemistry phenomena. In particular, faithful tracking of fines production and recirculation throughout the wet end was maintained as this was found to have a major impact on retention and drainage phenomena as expected from previous studies.

Surface area production in hardwood and softwood refiners was modelled using experimental Canadian Standard Freeness data collected over a range of refiner specific energies. By assuming additional surface area is the result of fines production, the post-refiner fines level for various specific energies was determined. An element by element wire drainage model was also developed based on filtration theory and Kozney-Carman

analysis of the specific filtration resistance. This allows study of the effects of operator moves in vacuum levels. The effects of sheet forming characteristics are accounted for through the furnish composition, degree of flocculation and basis weight. The amount of water chemically bound to furnish particles was determined experimentally for each furnish component. In order to accomplish this a modification of the standard technique for determining water retention values was developed for filler particles. The water retention values obtained for precipitated calcium carbonate and chalk were 0.84±0.12 g/g and 0.22±0.03 g/g respectively. Due to the corresponding four fold difference in surface areas between precipitated calcium carbonate and chalk, these values suggest an electrostatic interaction mechanism for the binding of water to carbonate surfaces.

For the adsorption of polymers onto furnish surfaces the concept of *coverage* - the fraction of particle's surface covered by a polymer - played a central role. The degree of coverage directly affects the chance of successful collisions between particles in the flocculating process and was therefore tracked throughout the wet end by the chemistry simulation modules running parallel to the above physical process. The assumption of complete polymer adsorption onto furnish particles in proportion to their surface areas was supported by time scale calculations. A model for deactivation of polymer components was also implemented into the simulation based on polymer charge decay experiments reported in the literature. Coverages were adjusted to reflect the loss of electrostatic interaction potential of polymer components as they recirculated through the wet end. Second-order bridging flocculation kinetics were assumed with rate constants computed as the product of Smoluchowski rates of particle collisions. Empirical constants were selected to calibrate the model against process data.

Calibration of the simulation involved comparison against steady-state and dynamic process data. Equally important was the experience of mill technical personnel through whom the mechanisms leading to observed process responses could be confirmed. Initially, furnish component levels were set according to steady-state process data with assumed levels of retention and drainage. Modules added for these effects were calibrated against this steady-state data and then against dynamic responses. The main calibration parameters are the four rate constants in the bridging flocculation model and a single parameter which affects the (overall) calculated mat compaction factor thereby affecting drainage rate.

The simulation model is useful for control analysis and design, evaluation of process alternatives as well as operator training. The modular, object oriented manner in which it has been implemented allows for a "plug and play" approach to process/control analysis. The major drawback of the simulation is its speed which is 2-3 times faster than real time. Since the time constants in wet end chemistry can be in the order of an hour, lengthy simulation runs occur. This inhibits the simulation's usefulness in control analysis.

Reliable on-line data is required to further validate the simulation model and for future control schemes. As this project was carried out in an operating paper mill, the challenges and realities of obtaining such data were encountered. Mill personnel need assessments of the potential economic benefits to be expected from on-line sensors in order to justify their implementation and maintenance. An accurate process simulation has the potential to allow mill personnel to evaluate the economic benefits of implementing wet end sensors and control.

A method for producing confidence regions of specified probability for closed-loop robustness measures was proposed. It is based on optimization of closed-loop robustness criteria in terms of identification variables where the identified model/controller parameters

are constrained to lie within confidence regions. The procedure accounts for parametric nonlinearities and was shown to provide considerably more accurate confidence bounds than those based on linear approximations. A constrained optimization approach was also used to produce $(1-\alpha)\%$ frequency domain confidence regions for the open-loop system. The ability of the above procedure to provide $(1-\alpha)\%$ coverage was found to be affected by the degree of parametric nonlinearity and the number of observations in the dataset used for identification. The use of the Signed Root Deviance Profile function was useful in determining this degree of nonlinearity. A control relevant input signal design procedure was developed from a linearization of the closed-loop objective function in terms of identification variables. In the case where the true process was linear, considerable improvement in closed-loop robustness resulted when identification was carried out using such control relevant input signals.

Application of the control relevant methodology to the wet end chemistry simulation highlighted some limitations of such identification methods as well as exposing interesting process behaviour. The HMW Anionic Polymer $\Leftrightarrow$ White Water Filler Consistency loop was found to have nonlinear (in the inputs) dynamic behaviour. Surprisingly, the static gain of this loop is not strongly nonlinear. Because of this nonlinear behaviour, the input design methodology failed to produce better closed-performance when compared to a low frequency square wave input.

Throughout this work the value of a high fidelity simulation based on first principles models has been seen. Details of the mechanisms during (simulated) step response experiments could be tracked without the need to perturb the process. As well, identification of process behaviour was done in a noise free environment. From this, the frequency distribution of bias from approximation of a higher order system could be

evaluated as well as identification of nonlinearities. Models from such an identification could then be used to better design validation experiments. In this way the a priori information available to the experimenter is increased.

7.2 Future Work

Study of wet end chemistry through the simulation model can proceed in two distinct paths: either through incorporating further physical and chemistry models into the simulation or further analysis of the dynamics for control design. Considerable scope exists in both areas. Ideally they should proceed simultaneously.

Several specific additional units/phenomena that should be implemented into the simulation are listed below. In most cases they can be incorporated as separate modules and added without disruption of the existing simulation.

1. Physical Modules: Simons IDEAs objects based on first-principles dynamic models for the slice lip opening, shoe vacuum, saveall, presses and dryers need developing.
2. Fibre Properties: A method for representing fibrillated fiber needs to be included rather than ascribing increased surface area due refining to fines. This could possibly be accomplished by introducing a separate component and an attached parameter to represent the degree of refining/fibrillation. Secondly, it may be advantageous to expand the distribution of fibre lengths rather than just representing it by long and fine fibre fractions. However, this may require large amounts of memory in the simulation and would also require characterization of this distribution throughout the wet end.

3. Chemical Effects: Laboratory experiments to determine maximal adsorption of polymers onto furnish components (Γ^{Max}) should be carried out for this system. This would provide accurate parameters for the simulation model rather than relying on approximate values from the literature. Fibre deswelling by polymers should be further studied and implemented into the simulation if found significant. Laboratory experiments may support this effort. Inclusion of fiber surface and/or total stock charge effects would be beneficial to include into the simulation model. This would allow for study of charge reversal due to overdosing of polymers. Better characterization of the effects of organic substances which interfere in retention and drainage processes ("anionic trash") could also be accomplished with a charge model. Reliable on-line measurements of zeta potential would facilitate its development. Finally, other chemical additives should be included into the model including sizing agents and biocides.
4. Operating Scenarios: Currently, the production of broke is assumed to occur on a continuous basis. In a mill, the majority of broke production is during discrete sheet break events (approximately 2 times per day). These situations clearly place higher demands on the broke handling system and cause variations in the white water systems. It would be of great benefit to develop the flexibility to simulate these situations. The other common operating scenario which has a large effect on the wet end is during transition from slush to baled pulp in either hardwood or softwood. Some development would be required in order to efficiently handle such a change in the simulation.
5. Transportation Times in Pipes: Inclusion of transportation times in piping networks would increase the accuracy of the simulation model and allow more reliable evaluation of dead times in control loops.

An efficient method for determination of the Kinetic Rate Constants (k_i's) of Equation 3.32 needs to be determined such that resulting white water consistencies can be affected individually for each component. This may be possible by a multivariable analysis using singular value decomposition based techniques such as Principal Component Analysis. A goal would be to find the minimum number of tuning parameters for the simulation model.

Further analysis of the magnitude and nature of disturbances present in the wet end needs undertaking. This could be accomplished through examination of residuals from comparison of simulated and measured responses. For example, comparison of simulated changes in stock composition with on-line freeness and drainage measurements could indicate changes in incoming fibre characteristics.

Characterization of the interactions between the basis weight and ash control loops should be carried out as strong coupling was observed in the simulation model. The first step is to obtain actual time delays and tuning constants. Then the need for decoupling control in response to wet end chemistry disturbances could be determined.

Finally, the need for extensions to the linear (in the inputs) control relevant identification techniques was clear in Chapter 6. Two avenues need exploring: extension to nonlinear systems and development of the multivariable case. Either of these forms a significant undertaking.

References

Aström, K.A. and Wittenmark, B. (1990) Computer-Controlled Systems, Prentice Hall, Englewood Cliffs, NJ.

Bates, D.M.; Watts, D.G. *Nonlinear Regression Analysis and its Applications;* Wiley: New York, 1988.

Bernier, J. and Begin, B. (1994) "Experience of a Microparticle Retention Aid System", Tappi Journal, 77, 11, 217-224

Blixt, T. (1995) "Chalk", TAPPI Dyes, Filler and Pigments Short Course, TAPPI Press, Atlanta

Box, G.E.P.; *Some Theorems on Quadratic Form Applied in the Study of Analysis of Variance Problems 1. Effect of Inequality of Variance in the One-Way Classification*; Annals of Mathematical Statistics, **1954**, 25, 290-302

Box, G.E.P.; Jenkins, G.W. *Time Series Analysis: Forecasting and Control;* Holden Day: San Francisco, 1976.

Boyce, W.E. and DiPrima, R.C. (1992) Elementary Differential Equations and Boundary Value Problems, Wiley, New York

Branion, R.M.R. et al. (1978) "A Current State of Drainage Theory Up to January 1978: A Monograph", Omni Continental Ltd., New Westminister, B.C., Canada

Brewster, D.B. and Rogers, J.H. (1985) "Analysis of On-line Drainage Testers", Pulp and Paper Canada, 86, 7, T186

Britt, K.W. (1975) "The Fines Fraction of Paper Stock", In Retention of Fine Solids During Paper Manufacture, Ch. 8, Tappi Press, Atlanta

Brown, A.J. (1996) "Ground Calcium Carbonate Fillers for High Ash Content, High Strength Papers", Proc. TAPPI Papermakers' Conference, Philadelphia

Bussiere, S. et al. (1988) "Analysis and Control of the White Water Recirculation in an Integrated Newsprint Mill: A Dynamic Simulation Approach", Process Simulation Symposium, CPPA Technical Section, Quebec, 91-94

Casey, J.P. ed. (1981) Pulp and Paper: Chemistry and Chemical Technology, Chapter 16, Wiley, New York

Chen, J.S. *Confidence Intervals for Parametric Functions in Nonlinear Regression,* Ph.D. Thesis, University of California, Los Angeles, Dept. of Mathematics, 1991

Chen, J.S. and Jennrich, R.I. *The Signed Root Deviance Profile and Confidence Intervals in Maximum Likelihood Analysis*, Journal of the American Statistical Association, **1996**, 91, 993-998

Doucette, J.A. (1988) "White Water And Savealls", TAPPI Stock Preparation Short Course, Chicago, 107-116

Duff, I.S. (1977) "A Survey of Sparse Matrix Research", Proc. IEEE, 64, 4, 500-535

Eklund, D. and Lindström, T. (1991) Paper Chemistry: An Introduction, DT paper Science Publications, Finland

El-Hosseiny, F. and Yan, J.F. (1980) "Analysis of Canadian Standard Freeness: Part I. Theoretical Considerations: Part II. Practical Implications", Pulp and Paper Canada, 81, 6, 61-70

Gallant, A.R. *Nonlinear Statistical Models*, Wiley, New York, 1987

Gear, C.W. (1971) "Simultaneous Numerical Solution of Differential-Algebraic Equations", IEEE Trans. Circuit Theory, CT-18, 1, 89-95

Godfrey, K.R. ed. *Perturbation Signals for System Identification*, Prentice-Hall, Englewood Cliffs, 1993.

Goodwin, G.C.; Payne, R.L. *Dynamic System Identification: Experiment Design and Data Analysis;* Academic Press: New York, NY, 1977.

Goodwin, G.C.; Gevers, M.; Ninness, B. Quantifying the Error in Estimated Transfer Functions with Application to Model Order Selection; IEEE Transactions on Automatic Control, **1992**, 37, 913-928.

Gregory, J. (1988) "Polymer Adsorption and Flocculation in Sheared Suspensions", Colloids and Surfaces, 31, 231-253

Guo, L. and Ljung L. *The Role of Model Validation for Assessing the Size of the Unmodelled Dynamics*, Proc. 33rd Conference on Decision and Control, **1994**, 3894-3899

Gupta, B. and Scott, W.E. (1995) "Interactions Between Cationic Starches and Papermaking fibers: The Effect of Starch Characteristics on Fiber Surface Charge and Starch Retention", Proc. Tappi Papermakers Conference, 85-95

Hahn, G.J. (1984) "Experimental Design in the Complex World", Technometrics, 26, 1, 19-31

Hamilton, D.C.; Watts, D.G. A Quadratic Design Criterion for Precise Estimation in Nonlinear Regression Models; Technometrics, **1985**, 27, 241-250

Han, S.T. (1962) "Drainage in a Vacuum Former", Tappi Journal, 45, 4, 292-295

Harris, E.J. (1995) "Modelling and Optimising Process Water Flows and Quality in a Paper Mill", PhD Thesis, UMIST, United Kingdom

Hedborg, F.A. (1992) "Chemical Aspects of the Adsorption, Retention and Sizing Processes in Fine Paper Stocks Containing Calcium Carbonate", PhD Thesis, Royal Institute of Technology, Stockholm

Helmicki, A.J.; Jacobson, C.A.; Nett, C.N. Control Oriented System Identification: A Worst-Case/Deterministic Approach in H_∞; IEEE Transactions on Automatic Control, **1991**, 36, 1163-1176.

Hjalmarson, H. and Ljung, L. *A Unifying View of Disturbances in Identification*, IFAC Symposium on System Identification, Copenhagen, **1994**, 383-388

Htun, M. and de Ruvo, A. (1978) "The Implication of the Fines Fraction for the Properties of Bleached Kraft Sheet", Svensk Papperstidning, 16, 507-510

Humphrey, K.C. (1986) "A Dynamic Simulation of an Aspect of Wet-End Chemistry", PhD Thesis, UMIST, United Kingdom

Ingmanson, W.L. and Andrews, B.D. (1959) "The Effect of Beating on Filtration Resistance and its Components of Specific Surface and Specific Volume", Tappi Journal, 42, 1, 29-35

Jeppson, R.W. (1977) Analysis of Flow in Pipe Networks, Ann Arbor Science, Ann Arbor

Kamiti, M. and van de Ven, T.G.M. (1995) "Impinging Jet Studies of the Kinetics of Deposition and Dissolution of Calcium Carbonate Particles", PGRLR 601, Pulp and Paper Center, McGill University, Montreal, Canada

Kedem, B. *Binary Time Series*, Dekker, New York, 1980

Koethe, J.L. and Scott, W.E. (1993) "Polyelectrolyte Interactions with Papermaking Fibers: The Mechanism of Surface-Charge Decay", Tappi Journal, 76,12, 123-133

Kortelainen, H. (1992) "Tools for Successful Wet-End Chemistry Control", Tappi Journal, 75, 12, 112-117

Kortelainen, H. et al. (1989) "Application of a New Fiber and Filler Retention Monitoring System at a Fine Paper Mill", Proc. TAPPI Papermakers' Conference, Washington, D.C.

Kaunonen, A. (1988) "Studies on On-line Retention and Cationic Demand Measurement and Their Utilization on a Paper Machine", PhD Thesis, Tampere University of Technology, Finland

Larimore, W.E. *Accuracy of Confidence Bands Including the Bias of Model Under-Fitting*, Proc. American Control Conference, **1993**, 1995-1999

Laufmann, M. (1992) "Woodfree Alkaline Papermaking 1991", Proc. Technicelpa, Portugal

Lee, L. and Poola, K. *Statistical Testability of Uncertainty Models*, , IFAC Symposium on System Identification, Copenhagen, **1994**, 189-194

Lindström, T. (1992) "Chemical Factors Affecting the Behaviour of Fibres During Papermaking", Nordic Pulp and Paper Research Journal, 7,4, 181-192

Lindström, T. (1989) "Some Fundamental Chemical Aspects on Paper Forming", in Fundamentals of Papermaking: Transactions of the Ninth Fundamental Research Symposium , Volume 1, Cambridge, 311-412

Ljung, L. *System Identification: Theory for the User;* Prentice Hall; Englewood Cliffs, NJ, 1987.

Ljung, L. and Guo, L. *Estimating the Total Error from Standard Model Validation Tests*, 13th IFAC World Congress, **1996**, 133-138

Luyben, W.L. (1990) Process Modelling, Simulation and Control for Chemical Engineers, McGraw-Hill, New York

MacGregor, J.F.; Harris, T.J.; *The Exponentially Weighted Moving Variance*, Journal of Quality Technology, **1993,** 25, 2, 106-116

MacGregor, J.F.; Harris, T.J.; Wright, J.D. *Duality Between the Control of Processes Subject to Randomly Occurring Deterministic Disturbances and ARIMA Stochastic Disturbances*, Technometrics, **1984**, 26, 389-397

Maciejowski, J.M. (1997) "Reconfigurable Control using Constrained Optimization", European Control Conference, Brussels, 107-130

Marton, J. (1980) "The Role of Surface Chemistry in Fines - Cationic Starch Interactions", Tappi Journal, 63, 4, 87-91

Marton, J. (1974) "Fines and Wet End Chemistry", Tappi Journal, 57, 12, 90-93

Meincer, W.P. (1992) "High-Fidelity Real Time Dynamics Process Simulation with Object-Oriented Programming, Part 1: The Tool", Proc. Control Systems '92, Whistler, 163-170

Miyanishi, T. (1995) "On-line Zeta Potential Analysis of a Fine Paper Machine and Newsprint Paper Machine", TAPPI Journal, 78, 3, 85-91

Miyanishi, T. et al. (1988) "Dynamic Simulation for Efficient Paper Machine Grade Change", Tappi Journal, 71, 1, 49-56

Ninness, B. and Goodwin, G.C. *Estimation of Model Quality*, Automatica, **1995**, 31, 1771-1797

Ödberg, L. et al. (1993) "Kinetic Aspects of the Adsorption of Polymers on Cellulosic Fibres", Nordic Pulp and Paper Research journal, 1, 8, 6-9

Orccotoma, J.A. et al. (1996) "Transient Fines Distribution During Broke Recirculation in an Integrated Newsprint Mill", 82nd Annual Meeting, CPPA Technical Section, A353-A357

Page, D.H. (1989) "The Beating of Chemical Pulps - The Action and the Effects", Transactions of the 9th Fundamental Research Symposium, Cambridge, U.K., 1-38

Pantelides, C.C. and Barton, P.I. (1993) "Equation-Oriented Dynamic Simulation: Current Status and Future Perspectives", Proc. European Symposium on Computer Aided Process Engineering - 2, S263-S285

Pelssers, E.G.M. et al. (1989) "Kinetic Aspects of Polymer Bridging: Equilibrium Flocculation and Nonequilibrium Flocculation", Colloids and Surfaces, 38, 15-25

Press, W.H. et al. (1988) Numerical Recipes in C, Cambridge University Press, U.K.

Rantala, T. et al. (1994) "Practical Experiences of Improvements on Board Machine by Wet End Monitoring and Controls", Proc. TAPPI Papermakers' Conference, 299-305

Rantala, T. et al. (1993) "Retention Modelling and Control in the Paper Machine Wet End", IFAC World Congress, Sydney, Vol. 6, 61-66

Rivera, D.E.; Morari, M. Control-Relevant Model Reduction Problems for SISO H_2, $H\infty$, and μ-Controller Synthesis; International Journal of Control, **1987**, 46, 505-527

Roberts, J.C. (1996a) The Chemistry of Paper, The Royal Society of Chemistry, Cambridge

Roberts, J.C. (Ed.) (1996b) Paper Chemistry: 2nd Edition, Blackie, London

Ryti, N. and Paulapuro, H. (1991) Pulp and Paper Manufacture, Volume 6, TAPPI, Atlanta, 112-157

St. Jacques, M. (1982) "Computerized Dynamic Material Balance of a Paper Machine Wet End", Proc. TAPPI Engineering Conference, 97-110

Sanders, N.D. and Schaefer, J.H. (1991) "high Precision, In-mill Measurement of Zeta Potential Distributions of Stocks and Furnish Aids Alkaline Performance", Proc. TAPPI Papermakers' Conference, 349-366

Sargent, R.W.H. and Westerberg, A.W. (1964) "SPEED-UP in Chemical Engineering Design", Trans. Inst. Chem. Eng. (London), 42,190-197

Scallan, A.M. and Carles, J.E. (1972) "The Correlation of the Water Retention Value with the Fibre Saturation Point", Svensk Papperstidning, 75, 17, 699-703

Scott, W.E. (1996) Principles of Wet End Chemistry, TAPPI Press, Atlanta

Shirt, R.W.; Harris, T.J.; Bacon, D.W. Experimental Design Considerations for Dynamic Systems; Industrial and Engineering Chemistry Research, **1994**, 33, 2656-2667.

Smith, C.A. and Corripio, A.B. (1985) Principles and Practice of Automatic Process Control, Wiley, New York

Spriggs, D.R. (1992) "pH Control: Therefore and the Why", Papier, Carton et Cellulose, 41, 1, 44-50

Stone, J.E. et al. (1968) "Influence of Beating on Cell Wall Swelling and Internal Fibrillation", Svensk Papperstidning, 71, 19, 687-694

Swerin, A. et al. (1990) "Deswelling of Hardwood Kraft Pulp Fibers by Cationic Polymers", Nordic Pulp and Paper Research Journal, 4, 188-196

Syberg, O. and Wild, N.W. eds. (1992) "Introduction to Process Simulation", Tappi Press, Atlanta

Tappi (1996) Tappi Test Methods, Tappi Press, Atlanta

Tarjan, R. (1972) "Depth-first Search and Linear Graph Algorithms", SIAM J. Numerical Analysis, 2, 345-365

Taylor, G.I. (1958) "Drainage at a Table Roll and a Foil", Pulp and Paper Magazine of Canada, 59, 172-176

The Mathworks Inc., *Optimization Toolbox*, **1995**, Natick, Massachusetts

The Mathworks Inc., *System Identification Toolbox*, **1995**, Natick, Massachusetts

Tulleken, H.J.A.F. *Generalized Binary Noise Test Signal Concept for Imporved Identification - Experiment Design*, Automatica, **1990**, 26, 37-49

Unbehend, J.E. (1991) Pulp and Paper Manufacture, Volume 6, TAPPI, Atlanta, 112-157

Van Den Hof, P.M.J. and Schrama, R.J.P. *Identification and Control - Closed-loop Issues,* Automatica, **1995**, 31, 1751-1770

van de Ven, T.G.M. (1993) "Particle Deposition on Pulp Fibers", Nordic Pulp and Paper Research Journal, 1, 8, 130-147

van de Ven, T.G.M. (1984) "Theoretical Aspects of Drainage and Retention of Small Particles on the Fourdrinier", Journal of Pulp and Paper Science, 10, 3, 57-63

Wahlberg, B.; Ljung, L. Hard Frequency-Domain Model Error Bounds from Least-Squares Like Identification Techniques; IEEE Transactions on Automatic Control, **1992**, 7, 900-912.

Westerberg, A.W. et al. (1979) Process Flowsheeting, Cambridge University Press, London

Wise, B.M. (1994) PLS Toolbox, Version 1.4 (for use with MATLAB), Eigenvector Technologies, West Richmond, Washington

Woodard, B. and Wheeler, M. (1992) "Monitoring and Control of the Drainage Process", TAPPI Engineering Conference, Boston

Appendix A

Water Retention Value of Fillers

Tappi Useful Method 256 describes the standard procedure for measuring Water Retention Value (WRV) of pulp samples. In it, a pad of pulp is formed in a Buchner funnel and transferred to a 100 mesh screen suspended in a specially fitted centrifuge tube. Due to the very small particle size of filler material it is not possible to form and retain a pad consisting of solely filler. The method described here is a slight modification of the standard procedure such that filler material is retained on a preformed pulp pad which has known WRV. D. Barzyk (Weyerhaeuser) originally suggested the calculation procedure. The conditions of centrifuging (30 minutes at 900g) remain the same as in the standard procedure.

The following steps were performed:

1) Using a single sample of pulp (refined Kraft softwood), 8 repeat measurements of WRV were performed using Tappi UM 256. This yielded an overall $WRV_{Pulp} = 1.64 \pm 0.08$ g/g.

2) Measure out the equivalent of 2 o.d. grams of the above pulp slurry, dilute with distilled water to approximately 1% consistency and put through a Buchner funnel to form a pulp pad.

3) From a slurried sample of filler, the equivalent of approximately 8 o.d. grams of filler was measured out and diluted with distilled water to less than 10% consistency so it is easily suspended. This is slowly poured over the fiber pad in the Buchner funnel such that the filler is retained on top of the pad. It was observed that very little filler passed through with the filtrate.

4) The fiber/filler pad is then divided into 4 pieces and put in the specially fitted centrifuge tubes as in the standard procedure. These are then balanced and centrifuged for 30 minutes at 900g.

5) After centrifuging, the fiber/filler samples are transferred to preweighed crucibles each with markings capable of withstanding an ashing furnace (e.g. etching). The sample plus crucibles are weighed, oven dried and then reweighed as in the standard procedure to determine the total bound water (BW_{Total}).

6) The oven dried sample is then ashed according to Tappi Method T211 to determine the filler content.

7) Denoting the mass of pulp and filler in each sample W_{pulp} and W_{filler} respectively we have,

$$BW_{Filler} = BW_{Total} - W_{Pulp} \bullet WRV_{Pulp} \quad (A.1)$$

$$WRV_{Filler} = BW_{Filler}/W_{Filler} \quad (A.2)$$

Using this procedure for 8 repeat samples of each filler type, precipitated calcium carbonate was found to have a WRV of 0.84±0.12 g water/g PCC and chalk had a WRV of 0.22±0.03 g water/g chalk. We note that the use of significantly larger quantities of filler in relation to pulp in Steps 2 and 3 of this procedure helps to reduce the impact of measurement uncertainty in Step 1.

It is not clear what effect the chemical environment has on the above results. The amount and nature of the various ions adsorbed onto the filler surface could possibly alter the amount of water associated with the filler particles. Scallan and Carles (1968) discuss various other factors affecting the validity of results from the water retention value method. In particular, there is evidence that the mass of each sample in may affect the compression of the pulp pad during centrifuging. Thus it would be useful to vary the amount of filler and pulp used. Ideally, one would like to use the minimum amount of pulp required to retain the filler.

Appendix B

IDEAs Process Flowsheets

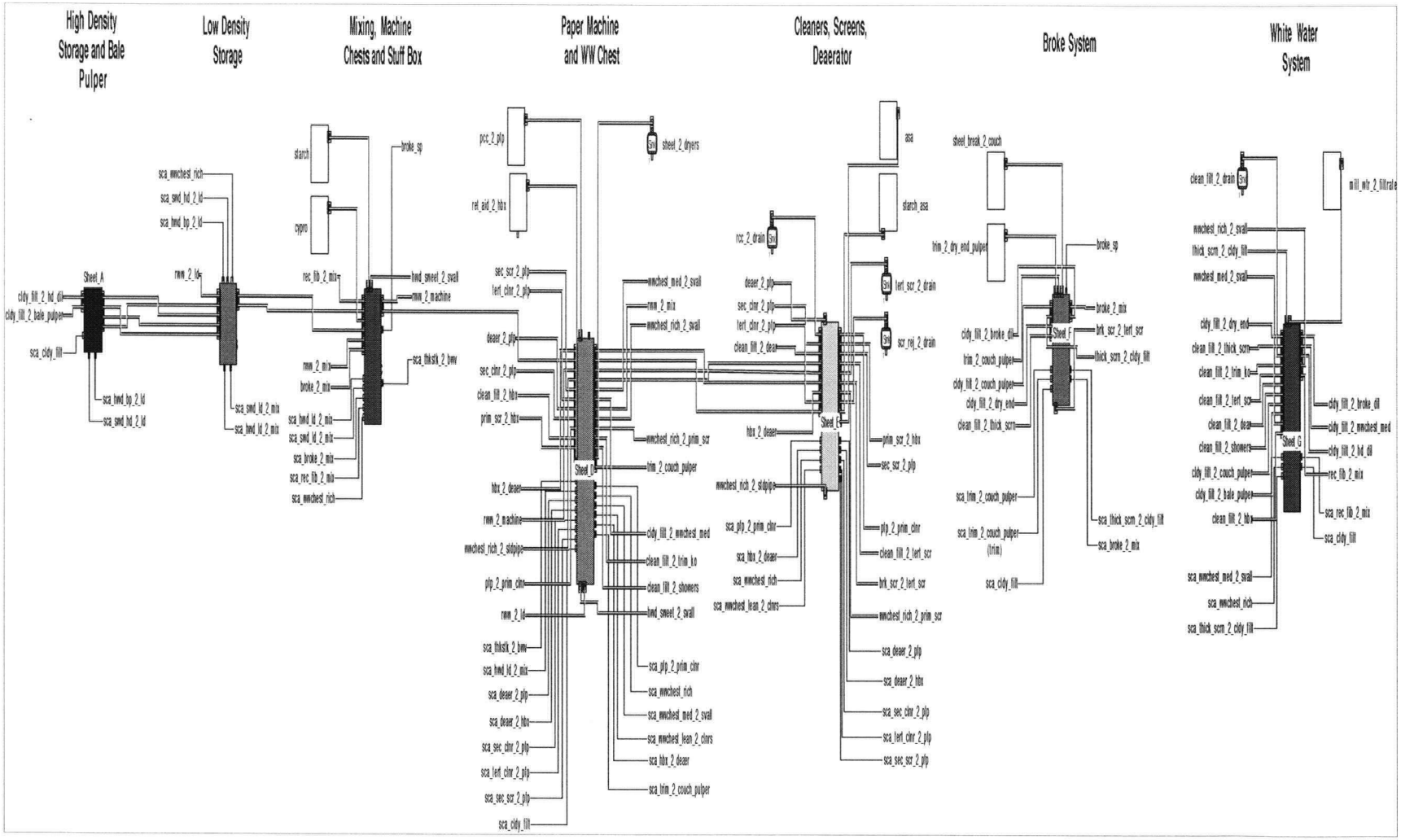

Figure B1: Major Areas of Paper Machine Model

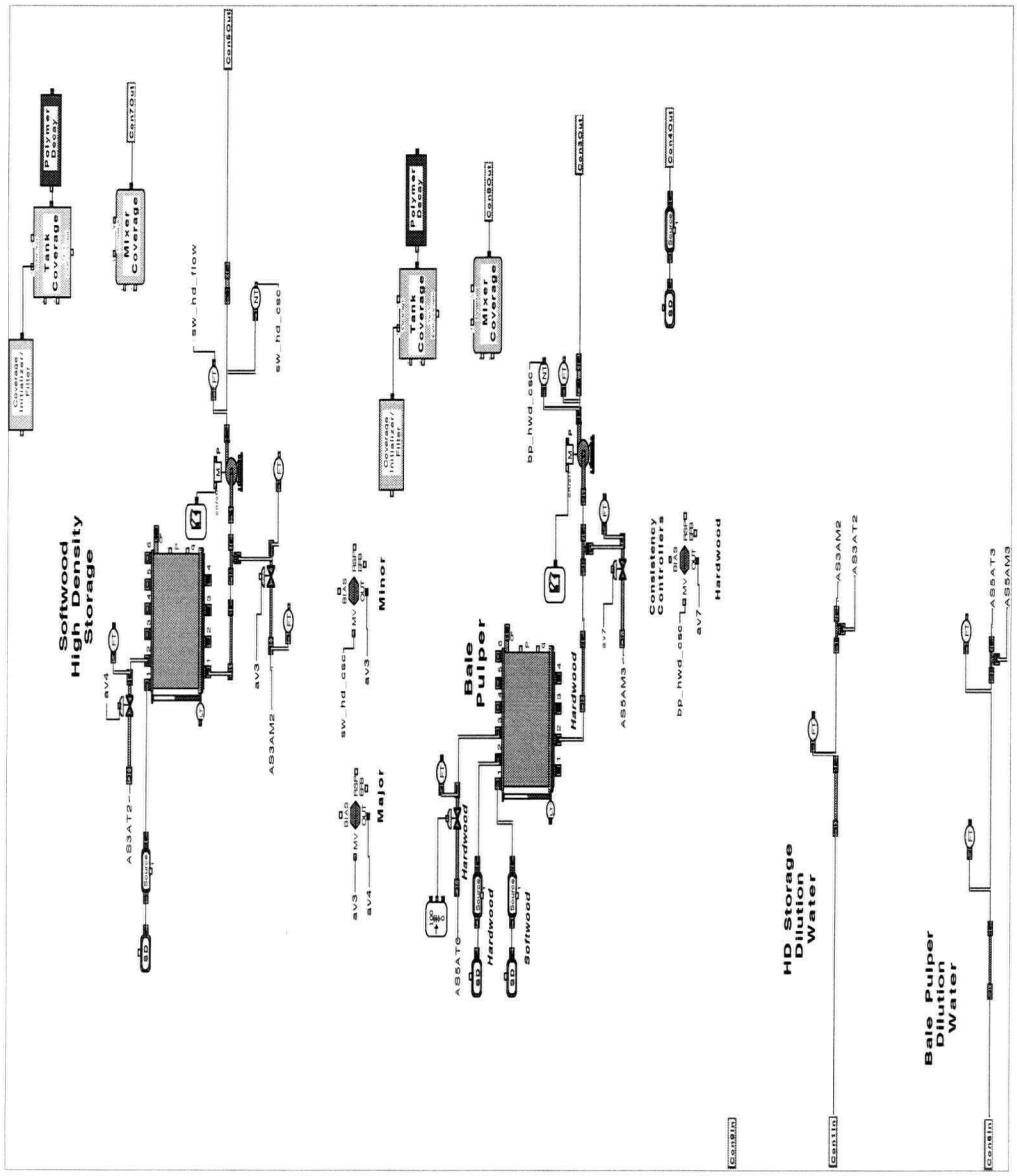

Figure B2: High density storage area flowsheet

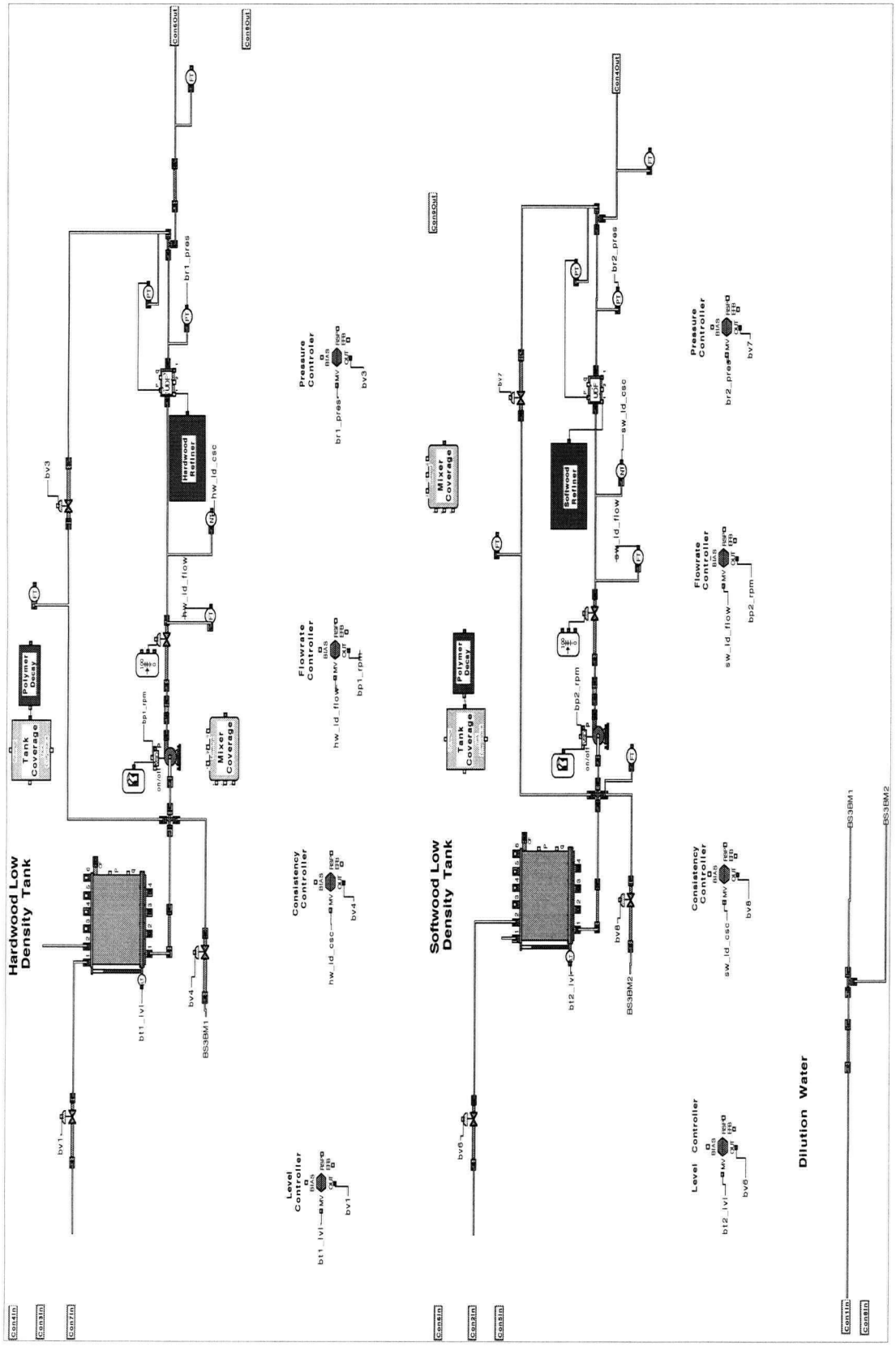

Figure B3: Low density storage area flowsheet

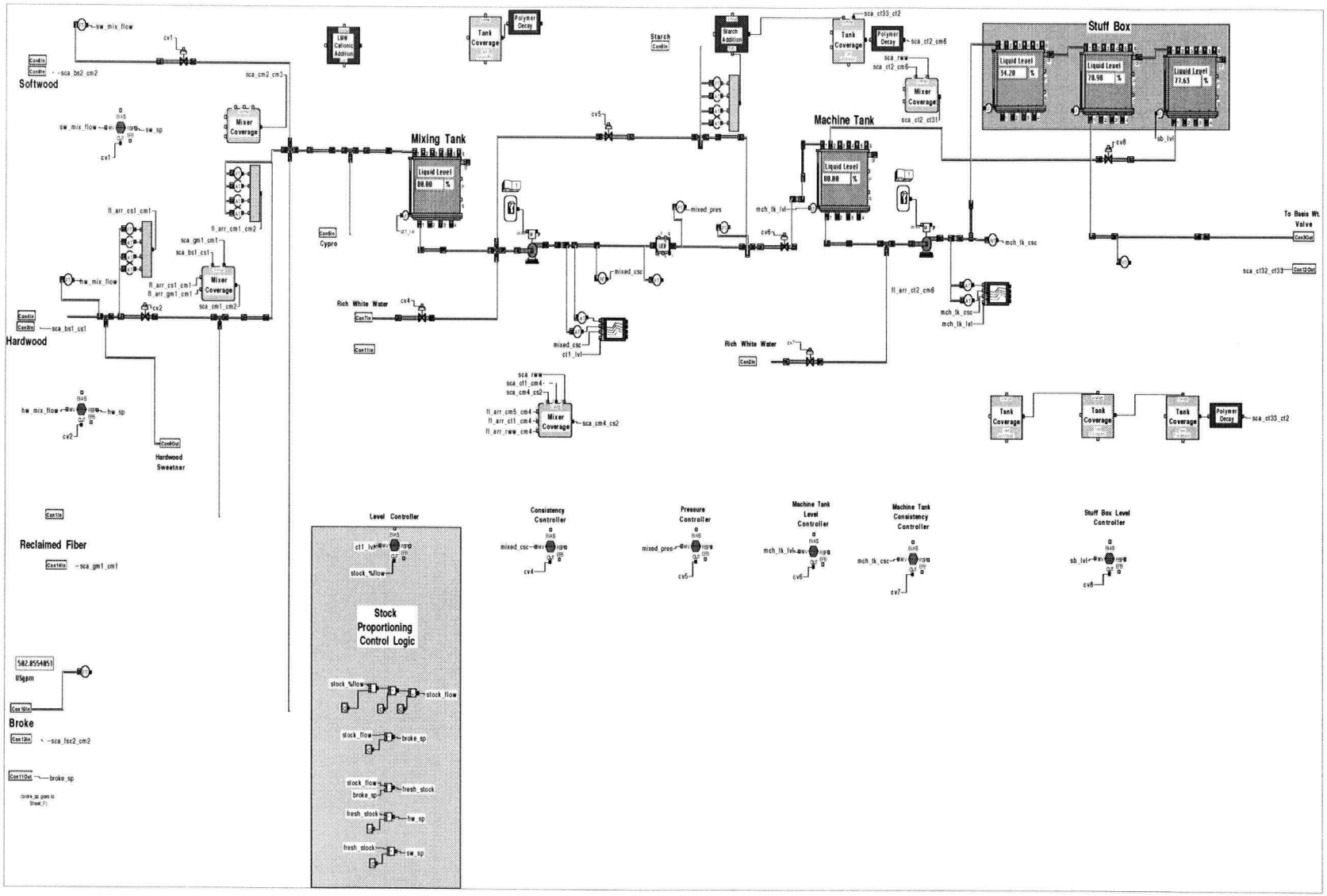

Figure B4: Mixing and machine chest flow diagram

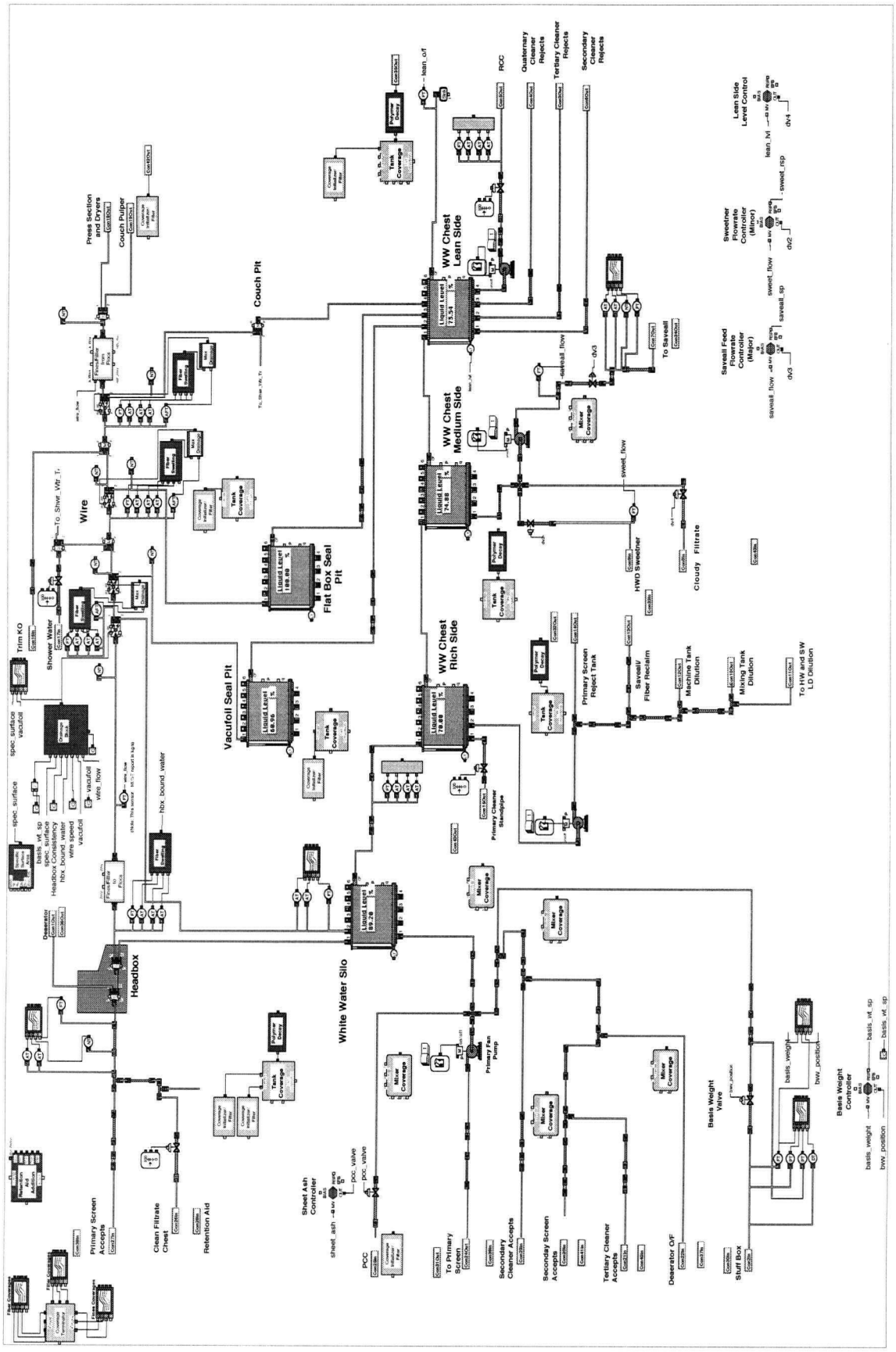

Figure B5. Paper machine flow diagram

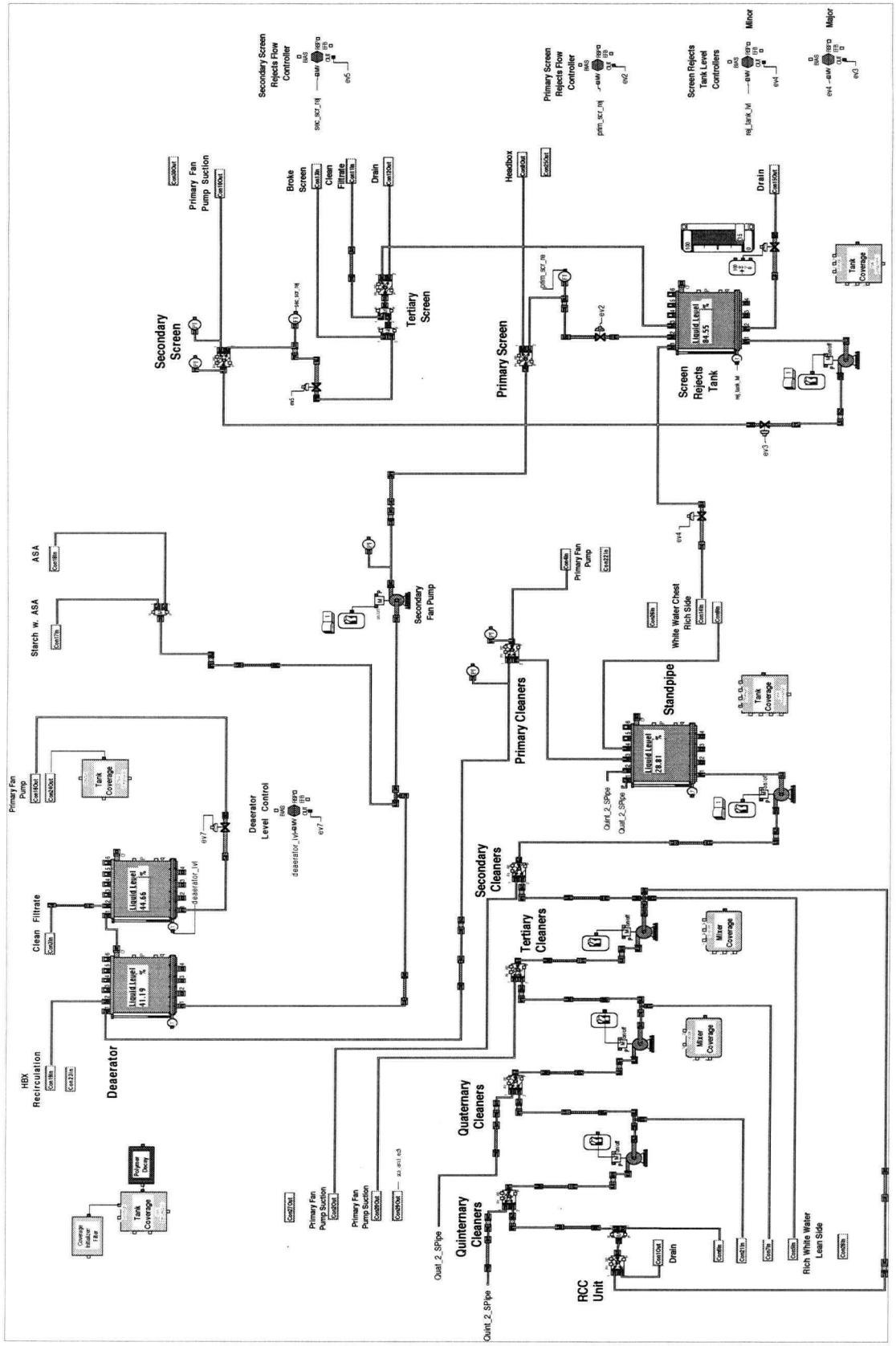

Figure B6. Screening and cleaners area flow diagram

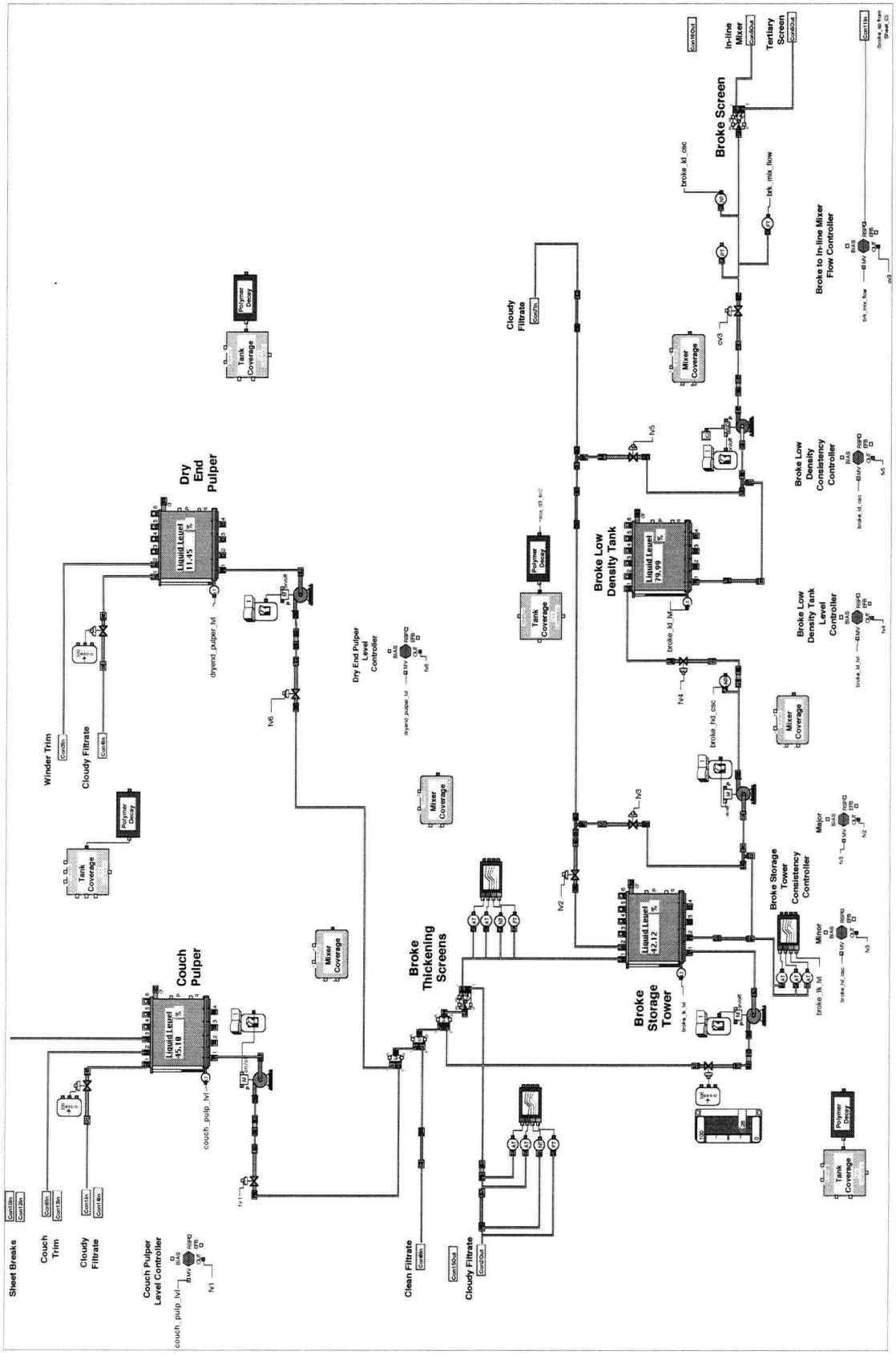

Figure B7. Broke system flow diagram

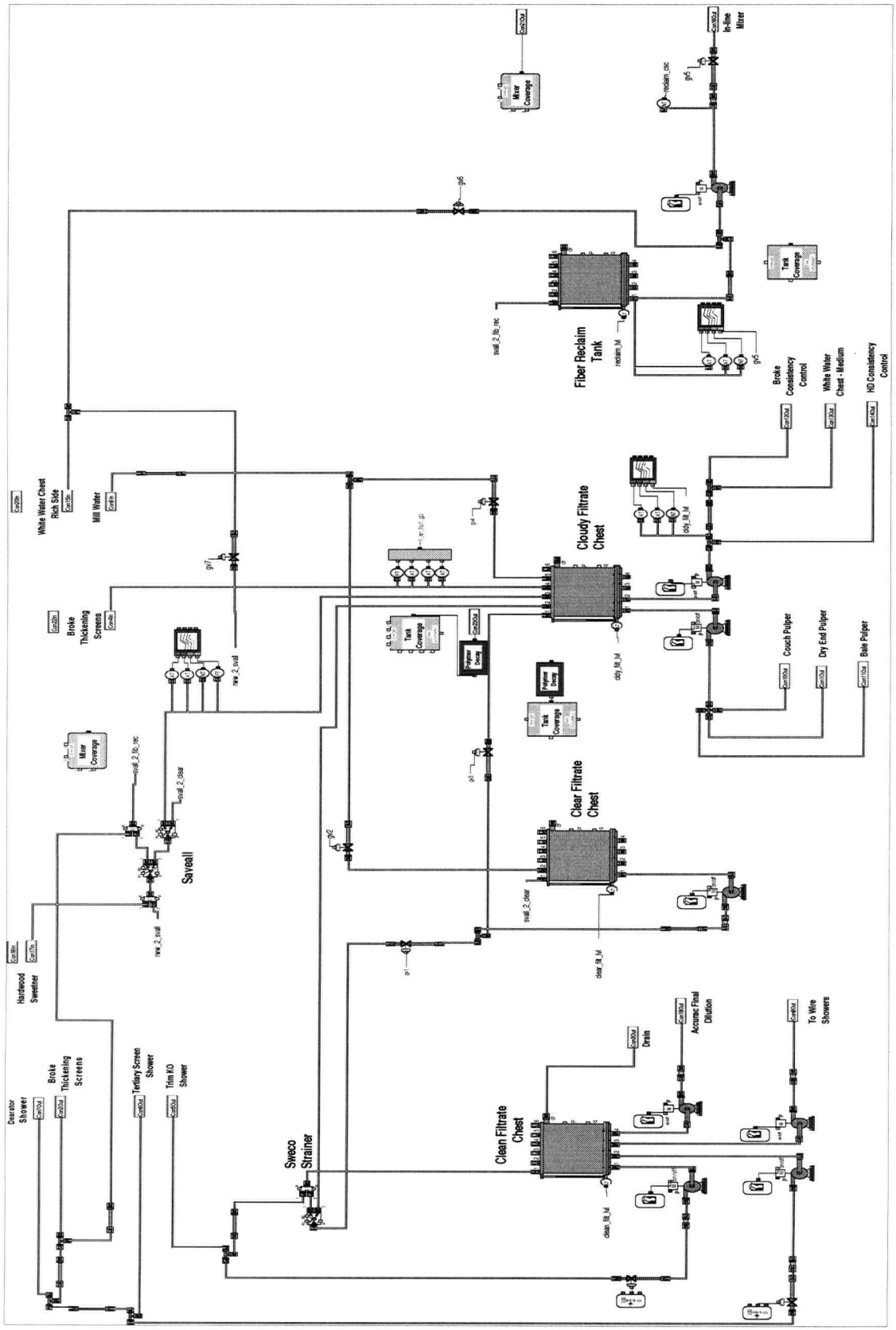

Figure B8. White water system flow diagram

Appendix C

Tests of Residuals

Model validation tests are applied to the residual vector, e_o. The cross-correlation test is,

$$R_{XC} = \frac{1}{\hat{r}_{ee}(0)} \hat{r}_{eu}^T \hat{R}_u^{-1} \hat{r}_{eu} \tag{C.1}$$

where

$$\hat{r}_{eu}(\tau) = \frac{1}{\sqrt{N}} \sum_{t=1}^{N} e(t)u(t-\tau) \tag{C.2}$$

$$\hat{r}_{eu} = [\hat{r}_{eu}(0),...,\hat{r}_{eu}(M)] \tag{C.3}$$

$$\hat{R}_u = \frac{1}{N} \sum_{t=1}^{N} \varphi_u(t)\varphi_u^T(t) \tag{C.4}$$

$$\varphi_u(t) = [u(t),...,u(t-M)] \tag{C.5}$$

and the auto-correlation test is,

$$R_{AC} = \frac{1}{\hat{r}_{ee}^2(0)} \hat{r}_{ee}^T \hat{r}_{ee} \tag{C.6}$$

$$\hat{r}_{ee}(\tau) = \frac{1}{\sqrt{N}} \sum_{t=1}^{N} e(t)e(t-\tau) \tag{C.7}$$

$$\hat{r}_{ee} = [\hat{r}_{ee}(0),...,\hat{r}_{ee}(M)] \tag{C.8}$$

M is the maximum lag to which the tests are applied. Both R_{AC} and R_{XC} can be compared against a chi-squared distribution with $M+1-p_{\text{Disturbance Model}}$ and $M-p_{\text{Process Model}}$ degrees of freedom respectively.